Sentinel-6 MF validation and cross calibration activities

2025 Annual Report

CLS

Reference : CLS-ENVP-RP-26-0101
Issue : 1/ 2
Date : June 18, 2026

EUMETSAT
Eumetsat-Allee 1, D-64295 Darmstadt, Germany
Tel: +49 6151 807-7
Fax: +49 6151 807 555
http://www.eumetsat.int

Document Reference:	CLS-ENVP-RP-26-0101
Date:	June 18, 2026
Issue	1.2

Project:	MISSION PERFORMANCE SERVICE FOR SENTINEL-6 MISSION	
Title:	Sentinel-6 MF validation and cross calibration activities 2025 Annual Report	
	Name	**Company**
Author(s):	B. Courcol T. Krzemien M. Alves F. Ehlers E. Ferrer O. Gassot A. Mangilli E. Mazaleyrat T. Moreau L. Rodet	CLS CELAD CLS CLS CLS CLS CLS CLS CLS CLS
Approved by:	M. Raynal	CNES
Application authorized by :	S. Dinardo	EUMETSAT

Change Log

Version	Date	Changes
1.0	03/04/2026	First Draft
1.1	06/05/2026	CNES review taken into account
1.2	12/06/2026	EUMETSAT review taken into account

Acronyms

AMR	Advanced Microwave Radiometer
CLS	Collecte Localisation Satellites
CMEMS	Copernicus Marine Service
CNES	Centre National d'Etudes Spatiales
DUACS	Data Unification and Altimeter Combination System
DV	Default Value
ECMWF	European Centre for Medium-range Weather Forecasting
EUMETSAT	European Organisation for the Exploitation of Meteorological Satellites
ESA	European Space Agency
GIM	Global Ionosphere Maps
GDR	Geophysical Data Record
GMSL	Global Mean Sea Level
HR	High Resolution Mode, also called Synthetic Aperture Radar (SAR) or Delay Doppler Altimetry (DDA)
HRMR	High Resolution Microwave Radiometer
LR	Low Resolution Mode (=LRM)
LUT	Look-Up Table
MLE	Maximum Likelihood Estimator
MQE	Mean Quadratic Error
MSS	Mean Sea Surface
NASA	National Aeronautics and Space Administration
NOAA	National Oceanic and Atmospheric Administration
NR	Numerical Retracker
NTC	Non Time Critical
PB	Processing Baseline
RMC	Range Migration Correction
SAMOSA	SAR Altimetry MOde Studies and Applications
SSH	Sea Surface Height
SSHA	Sea Surface Height Anomaly(=SLA)
SLA	Sea Level Anomaly(=SSHA)
SSB	Sea State Bias
STD	Standard Deviation
SWH	Significant Wave Height
VWM	Vertical Wave Motion
WTC	Wet troposphere Correction

Table of Content

List of Figures

List of Tables

1 Introduction

Sentinel-6 / Michael Freilich is a collaborative Copernicus mission, implemented and co-funded by the European Commission, ESA, EUMETSAT and the USA through NASA and NOAA.

EUMETSAT is responsible for the Sentinel-6 operations as part of the Copernicus component of the EU Space Programme. The Sentinel-6 Quality Assessment reports are generated by CNES as per EUMETSAT CNES agreement in the context of Copernicus.

This document presents the synthesis report concerning validation activities of Sentinel-6 data for the year 2025.

1.1. History

Sentinel-6 satellite was successfully launched on the 21th of Novembre 2020. On November 30th, its Poseidon-4 altimeter was switched on, and since December 17th 2020, Sentinel-6 is on its operational orbit to continue the long term climate data record on the primary TOPEX, Jason-1, Jason-2 and Jason-3 ground track.

To calibrate both altimeters, POS4 was switched to its redundant side (POS4-B) on the 14th of September 2021. It remains in this configuration from this date onwards.

Up until April 7, 2022, Sentinel-6 MF and Jason-3 operated in tandem flight, maintaining a separation of only 30 seconds. Following this period, Jason-3 was transferred to the same interleaved orbit previously utilized by TOPEX between 2002 and 2005, Jason-1 from 2009 to 2012, and Jason-2 from 2016 to 2017.

After the tandem phase with Jason-3, Sentinel-6 MF has become the reference mission in the CMEMS multi-missions Ocean topography products.

A second tandem phase between Jason-3 and Sentinel-6 MF took place from January 30 to June 2, 2025.

During 2025, the most significant development for Sentinel-6 MF processors was the update of the processing baseline to version G01, implemented on April 8, 2025, and applied to non-time-critical data from March 14, 2025. The main improvement introduced in this version is the transition from GDR-F to GDR-G standards for MDT, MSS, ocean tide, and load tide models, as well as from POE-F to POE-G for the orbital solution. It also includes LUT updates for the LR MLE4 retracker in Ku-band and the MLE3 retracker in C-band, computed to align LR MLE4 values with LR NR. The last important improvement is the application of the vertical wave motion correction at 20 Hz to both HR SAMOSA and HR NR.

Since the beginning of the mission, Sentinel-6 data is monitored on a cyclic frequence to assess its products' quality. Cyclic reports are available through Eumetsat website. Please note that analyses are done over ocean only, no assessment is done over hydrological targets. This encompasses several points, which are either part of Cal/Val routine activities or following mission events:

- mono-mission validation and monitoring,
- accuracy and stability of SLA measurements check,
- specific studies and investigations.

1.2. Overview

The present document assesses Sentinel-6 data quality and mission performance over ocean. After an executive summary in the next page, dedicated sections of this report deal with:

- description of data processing,
- data coverage / availability,
- monitoring of rejected spurious data,
- analysis of relevant parameters derived from instrumental measurements and geophysical corrections,
- system performance via analyses at crossover points,
- system performance via along-track Sea Level Anomalies monitoring,
- GMSL analysis.

Over all these parts, the document also presents some Sentinel-6 MF/Jason-3 cross-calibrations.

2 Executive Summary

Sentinel-6 MF onboard altimeter (POS4) allows for simultaneous low and high resolution observations due to its innovative design. This is referred as **interleaved mode** in which hence the instrument acquires data at same time in :

- Low Resolution Mode, hereafter "LR", which is the historical mode used by previous altimeters in the Topex/Jason satellites.
- High Resolution Mode, hereafter "HR", commonly called Synthetic Aperture Radar (SAR) or Delay Doppler Altimetry (DDA), and already used on Cryosat-2 and on the Sentinel-3 satellites.

Over the year 2025, POS4 altimeter operated in Range Migration Correction and open loop tracking for most of the globe.

In April 2025, the Sentinel-6 MF processing baseline was upgraded from version F09 to G01, with the new version applied to data from March 14, 2025 onward. G01 major improvements include:

- Upgrade to GDR-G standards for the following models:
  - Ocean and load tides solution 2 (FES): FES14 => FES22 (new barotropic tide model for global ocean).
  - MSS solution 1: Hybrid CNES-CLS2022/Scripps/DTU => Hybrid CNES-CLS2023/Scripps/DTU (more informations on [22]).
  - MSS solution 2: DTU2018 => DTU2021.
  - MDT: CNES-CLS MDT 2018 => CNES-CLS MDT 2022 (new global MDT combining drifters, hydrography profiles and high frequency radar data).
- Addition of C-band Complex Echoes to L1A ALT Products.
- Instrumental Look-Up Tables update for LR MLE retrievals.
- Removal of the MLE3 variables in the Ku-band L2 LR products.
- Vertical Wave Motion correction applied at 20Hz for both HR NR and SAMOSA.
- Wind Speed alignment to model thanks to sigma0 calibration biases update.
- POE-G orbit.

More details about the PB G01 can be found in the dedicated product notice ([7]).

Furthermore, as part of the deployment of the processing baseline G01, the MLE4 range LUT was updated and applied to data starting from April 12, 2025.

A full mission reprocessing was performed in late 2025. See the dedicated assessment report for further details ([8]).

Note also that the second tandem phase between Jason-3 and Sentinel-6 MF took place from January 30 to June 2, 2025. Jason-3 was moved to a different orbit prior to and after this phase, between January 7 and January 30, 2025, and between June 2 and June 18, 2025.

During each cycle, missing measurements were monitored and spurious data were edited (see section 4.2.). Relevant parameters derived from instrumental measurements and geophysical corrections were also analysed. Please note that this analysis is done **over ocean** only, no assessment is done over hydrological targets. This summary focuses on the performance over the year 2025.

1/ Data availability

In 2025, data availability over ocean was excellent for both Sentinel-6 MF LR and HR products (figure 1), with respectively 99.84 % and 99.55 % of available data. Over this year, **no important event impacting data availability occurred.**

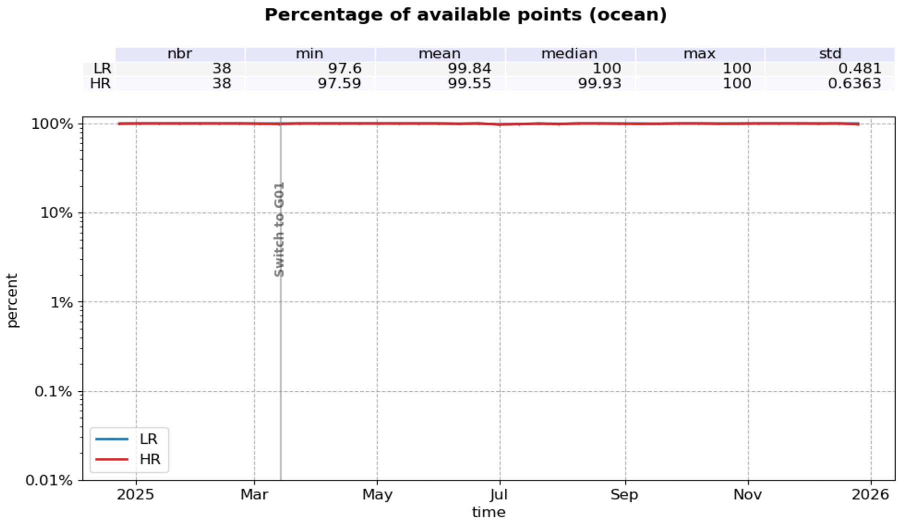

Figure 1: Percentage of available data over ocean for NTC Sentinel-6 MF LR (blue) and HR (red) per cycle over the year 2025.

2/ Sea Level Anomalies

In 2025 Sentinel-6 MF and Jason-3 SSHA followed identical seasonal cycles and variations (figure 2), with mean values of 5.3 cm for Sentinel-6 MF LR MLE4, 5.3 cm for LR NR, 3.9 cm for HR SAMOSA, 5.5 cm for HR NR and 5.3 cm for Jason-3. Excluding the Caspian Sea, Sentinel-6 MF SSHA daily standard deviation shows to be similar between all datasets.

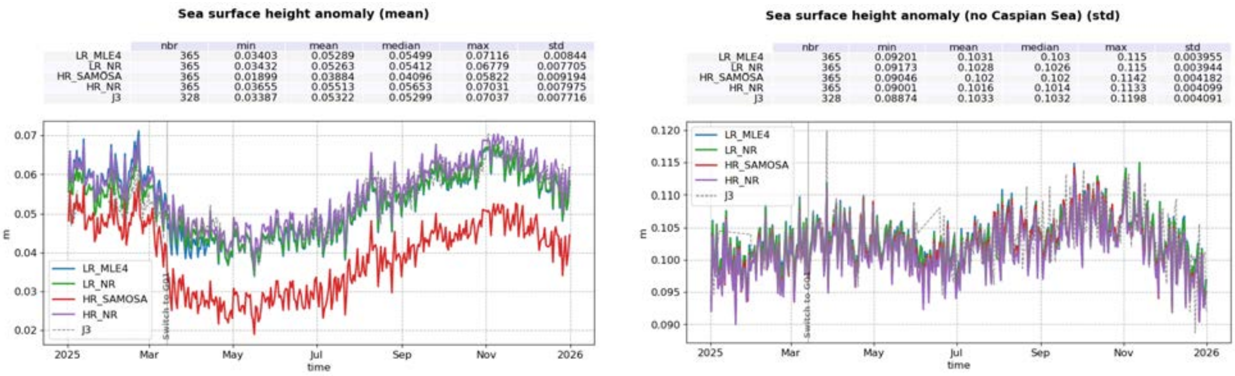

Figure 2: Mean (left) and standard deviation (right) SSHA by day for LR MLE4 (blue), LR NR (green), HR SAMOSA (red), HR NR (purple) and Jason-3 (black). Computed over the year 2025. The discontinuities in Jason-3 monitoring are due to orbit changes during its tandem phase with Sentinel-6 MF.

The comparison between LR MLE4 and LR NR SSHA, as shown in figure 3, shows that LR MLE4 is now fully consistent with LR NR thanks to the MLE4 LUT update. HR NR SSHA comparison to HR SAMOSA highlights a strong correlation to sea state, and initial investigations indicate that it is mostly due to the absence of skewness parameter in SAMOSA. This is under investigation.

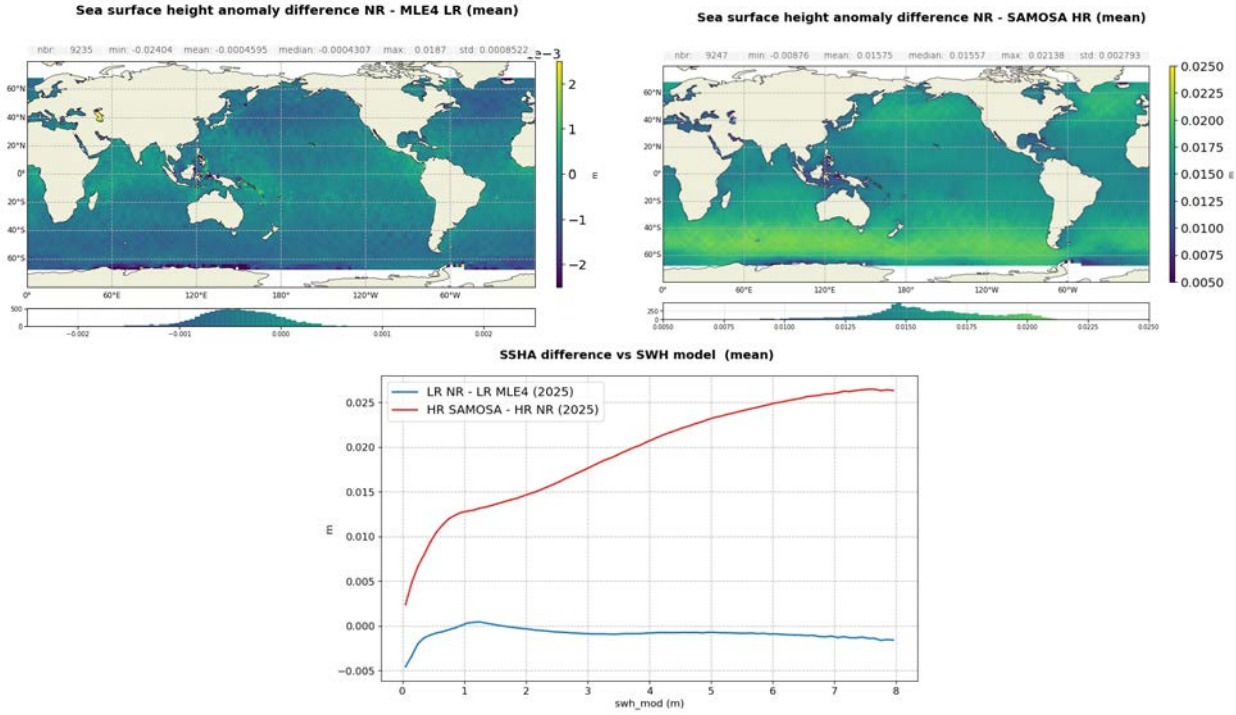

Figure 3: Maps of Sentinel-6 MF SSHA difference for LR NR - LR MLE4 (top left) and HR NR - HR SAMOSA (top right), and the corresponding mean as a function of ERA 5 model SWH (bottom).

3/ Performance at crossover points

Looking at SSH difference at mono-mission crossovers, mean values are well centered around 0 for all modes and retrackers (figure 4 left panel).

Concerning the SSH error at mono-mission crossovers ($STD\ /\ \sqrt{2}$), Sentinel-6 MF shows very good and stable performance with an error of 3.3 cm in LR and 3.2 cm in HR, which is similar to Jason-3 error (figure 4 right panel).

The degraded Jason-3 values observed around January and June 2025 are due to the orbit changes performed before and after the tandem phase with Sentinel-6 MF.

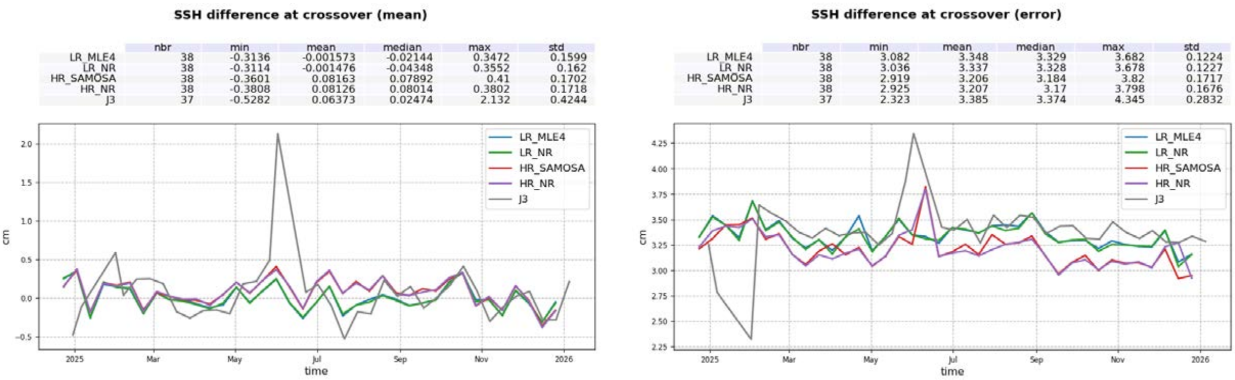

Figure 4: Monitoring of SSH difference at mono-mission crossover for Sentinel-6 MF LR MLE4 (blue), LR NR (green), HR SAMOSA (red), HR NR (purple) and Jason-3 (black). Mean (left) and error (right) per cycle are computed over the year 2025. Only data with |latitude| < 50 °, bathymetry < -1000 m and low oceanic variability were selected.

As shown in figure 5, the mean differences in sea surface height (SSH) at Sentinel-6 MF and Jason-3 crossover points exhibit consistent behavior across all four Sentinel-6 MF retrieval types throughout 2025. There is no evidence of drift or recurring patterns over the year. The observed mean SSH differences are minimal: -0.1 cm for LR MLE4, -0.1 cm for LR NR, 1.3 cm for HR SAMOSA, and -0.4 cm for HR NR. The PB G01 update is associated with a jump in SSH differences for all retrackers, with larger increases for LR MLE4 and HR SAMOSA (+1 cm relative to Jason-3) than for the NR retrackers (+0.5 cm).

The HR SAMOSA map (middle left panel) also highlights the absence of skewness parameter in the HR SAMOSA processing, leading to correlation with sea state conditions in the comparison with Jason-3. Thanks to the addition of this parameter to the HR NR processing, such patterns are not visible on the HR NR SSH comparison to Jason-3.

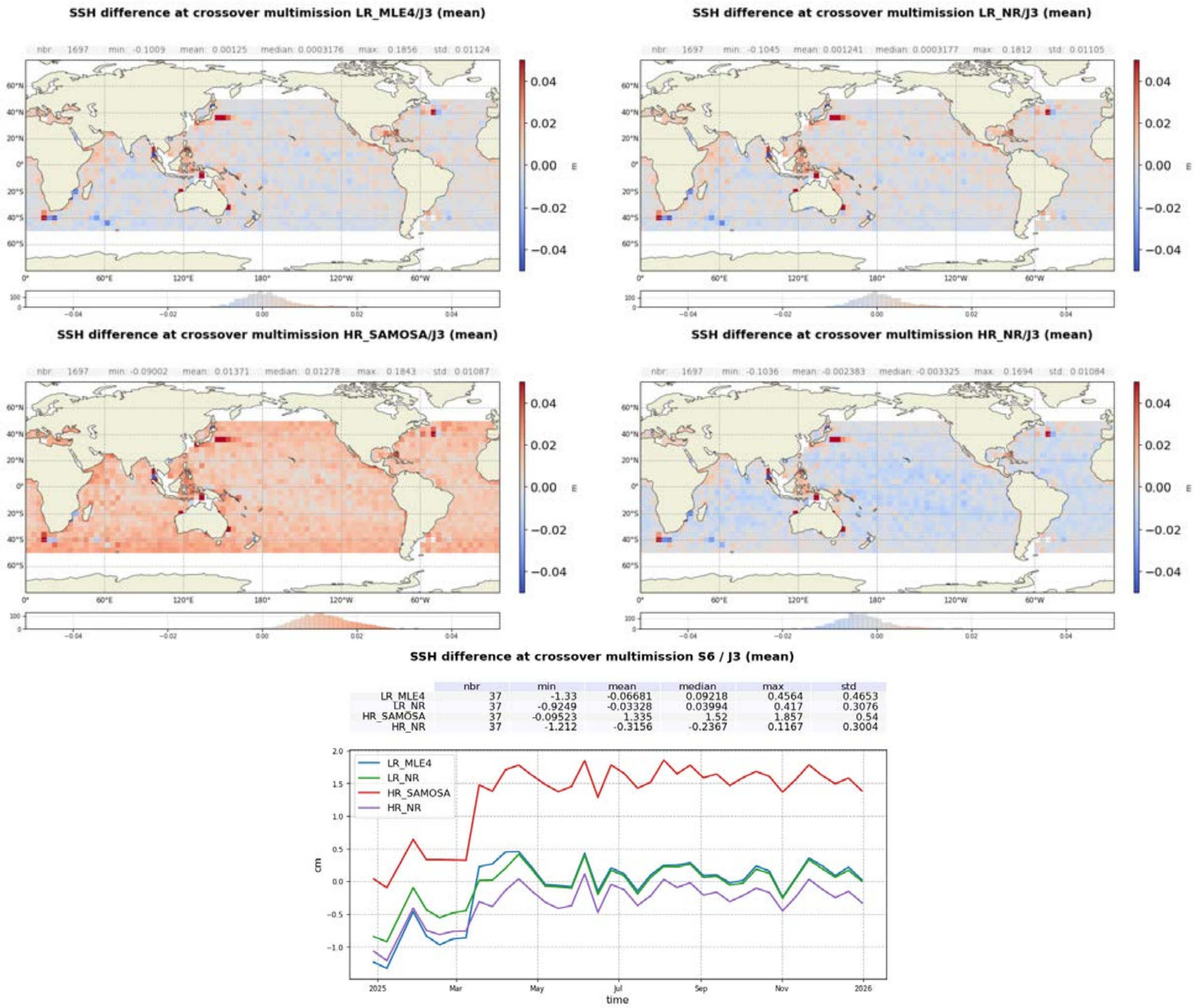

Figure 5: Sentinel-6 MF - Jason-3 SSH difference at crossover: maps over year 2025 for LR MLE4 (top left), LR NR (top right), HR SAMOSA (middle left) and HR NR (middle right), and corresponding cyclic monitoring (bottom). Only data with |latitude| < 50 °, bathymetry < -1000 m and low oceanic variability were selected.

4/ Contribution to Global Mean Sea Level

Regional and global biases between missions have to be precisely estimated in order to ensure the quality of the reference GMSL series as seen in Figure 6. For more details, see the dedicated section on AVISO+ website[1].

Sentinel-6 MF GMSL may be impacted by two known effects:

- The instrumental aging consisting of the evolution of the PTR shape in range direction. It impacts both range and SWH estimates in the analytical models as is the case of LR MLE4 and HR SAMOSA. Note that numerical models account for the in-flight instrument aging and hence are not affected by these impacts.
- In HR mode, the evolution of the PTR shape in azimuth direction has an impact on the range variations within a burst. It is corrected by the range walk correction introduced in PB F09.

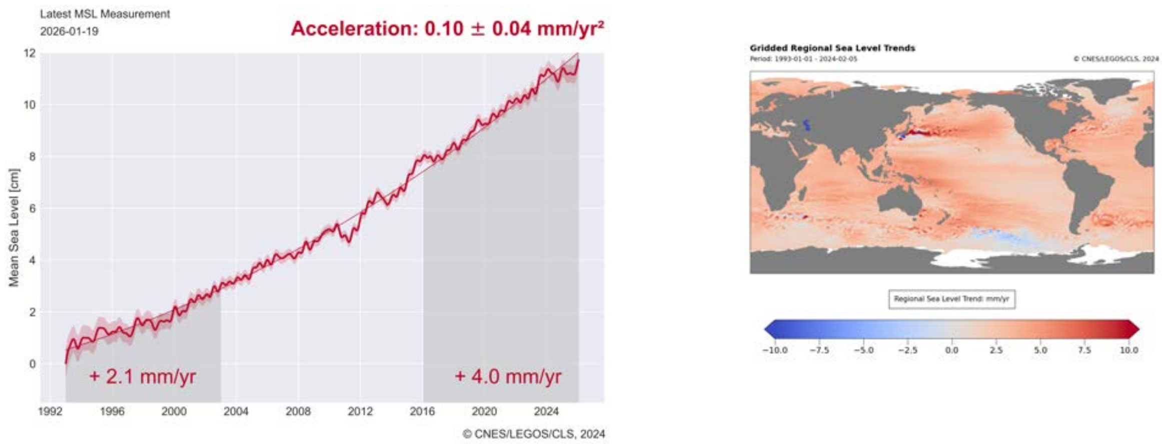

Figure 6: Global (left) and regional (right) MSL trends from 1993 onwards.

[1] https://www.aviso.altimetry.fr/en/data/products/ocean-indicators-products/mean-sea-level.html

3 Processing Status

3.1. Data used

Sentinel-6 MF

The metrics provided in this document are based on Sentinel-6 MF dataset over 2025 for L2 NTC 1Hz products. Additionally, some long-term monitoring includes data that encompasses the entire POS4-B period, starting from cycle 31 pass 109 (corresponding to September 14th, 2021), or the entire mission lifetime.

Sentinel-6 MF data processing has evolved over time. Initially, from the start of the mission on December 17, 2020 through October 5, 2023 (covering cycle 107, pass 7), all data were reprocessed using the original Processing Baseline (PB) F08. Following this, from October 5, 2023 to February 10, 2024 (up to cycle 119, pass 254), a patched version of PB F08 was used. The updated PB F09 was then used from February 10, 2024 to March 14, 2025 (up to cycle 160, pass 20). Beginning March 14, 2025, data have been processed with the PB G01. For further details about these processing baselines, please refer to section 3.4..

"Ocean" retrackers were used, being MLE4 and NR for LR mode and, for HR mode, SAMOSA and NR. A detailed description of the products can be found in the Sentinel-6 MF product notices for PB F08 [4], F09 [6] and G01 [7].

Jason-3

Comparison with Jason-3 uses L2 1 Hz GDR-F ([2]) products with MLE4 retracking on the same period as Sentinel-6 MF.

During 2025, the second tandem phase between Jason-3 and Sentinel-6 MF took place from January 30 to June 2. In this context, Jason-3 was moved onto the Sentinel-6 MF orbit from January 7 to January 30, 2025, and returned to its nominal orbit from June 2 to June 18, 2025.

Sentinel-6 MF F08, Sentinel-6 MF F09, and Jason-3 GDR-F share the same standard in terms of geophysical corrections: same tide models, same mean surface height, etc. (see [17] Appendix A for more details). In particular :

- for the wind speed, Collard algorithm is used on both missions
- for the sea state bias, Sentinel-6 MF processing uses sea state bias parametrization derived from Jason-3 GDR-F data, both in LR and in HR.

This is no longer true since PB G01 was applied to Sentinel-6 MF, while Jason-3 continues to use the GDR-F standard. See section 3.4. for more details.

3.2. List of events

The following table shows the major events that occurred over 2025.

Date start	Date end	Cycle	System	Event
06/01/2025 01:41:24	06/01/2025 01:41:24	153	AMR-C	AMR deep sky calibration
05/02/2025 16:23:48	05/02/2025 16:23:48	156	AMR-C	AMR deep sky calibration
07/03/2025 01:37:37	07/03/2025 01:37:37	159	AMR-C	AMR deep sky calibration
20/03/2025 07:36:00	20/03/2025 07:44:00	160	Platform	Station keeping maneuver
05/04/2025 19:40:18	05/04/2025 19:40:18	162	AMR-C	AMR deep sky calibration
04/05/2025 00:56:08	04/05/2025 00:56:08	165	AMR-C	AMR deep sky calibration
02/06/2025 18:51:43	02/06/2025 18:51:43	168	AMR-C	AMR deep sky calibration
16/06/2025 09:05:56	17/06/2025 13:38:48	169	Altimeter	OLTC Update (Step 1)
17/06/2025 10:01:00	17/06/2025 10:08:00	169	Platform	Station keeping maneuver
23/06/2025 07:53:14	24/06/2025 14:20:01	170	Altimeter	OLTC Update (Step 2)
30/06/2025 01:46:06	30/06/2025 01:46:06	170	AMR-C	AMR deep sky calibration
29/07/2025 19:47:39	29/07/2025 19:47:39	173	AMR-C	AMR deep sky calibration
31/08/2025 00:38:26	31/08/2025 00:38:26	177	AMR-C	AMR deep sky calibration
28/09/2025 16:36:00	28/09/2025 16:36:00	180	AMR-C	AMR deep sky calibration
14/10/2025 09:43:00	14/10/2025 09:49:00	181	Platform	Station keeping maneuver
28/12/2025 00:21:00	28/12/2025 00:21:00	180	AMR-C	AMR deep sky calibration

Table 1: Events on Sentinel-6 mission.

From 03/07/2025 23:07 to 16/07/2025 07:30 (cycle 171 pass 93 to cycle 172 pass 156), wildfires near Fairbank station caused a ground segment anomaly (UNS 12337), resulting in LR and HR data loss and missing platform mispointing.

3.3. Tracking and acquisition mode

Sentinel-6 MF altimeter, Poseidon-4, always operates in interleaved mode, which enables simultaneous measurements in :

- Low Resolution Mode, hereafter "LR", which is the historical mode used by previous altimeters on the Topex/Jason satellites. Please note that while Topex/Jason altimeters acquired data with a 2kHz PRF, the Sentinel-6 LR mode uses a 9kHz PRF.
- High Resolution Mode, hereafter "HR", commonly referred to as Synthetic Aperture Radar (SAR) or Delay Doppler Altimetry (DDA), already implemented on Cryosat-2 and Sentinel-3 satellites.

The LR and HR modes use separate retrackers (MLE4/NR and SAMOSA/NR respectively) and the resulting data are available in distinct products.
Please note that while LR products contain both Ku and C bands, there is no C band measurements in HRand therefore HR products contain only Ku band data.

Over the year 2025, POS4 altimeter operated in open loop.

3.4. Processing versions

From 2024/02/10 to 2025/03/14 (cycle 120 pass 1 to cycle 160 pass 20), Sentinel-6 MF NTC data were processed using the processing baseline F09. The main changes brought by this PB were :

- Numerical Retracking (NR) in HR mode, which includes skewness parameter set at 0.1. Please note that these new retracker outputs do not replace but complement SAMOSA-derived parameters: NR and SAMOSA retrievals are both included in HR products.
- Range walk correction in ALT L1 processing for HR mode for both SAMOSA and NR.
- Vertical Wave Motion (VWM) correction in ALT L2 HR products applied to NR Significant Wave Heights (SWH).

The first two updates listed above aimed at improving the long-term stability of the HR retrievals, the latter at improving the SWH [16].
Furthermore, PB F09 also included a correction in the computation of the HR backscatter coefficient ; a corrected definition of total power in LR MLE4, and an updated configuration parameter which improves LR NR in case of peaky waveforms and during maneuvers. More details on the PB F09 can be found in the associated product notice [6], on EUMETSAT user portal.

From 2025/03/14 (cycle 160 pass 21), Sentinel-6 MF NTC data were processed using the processing baseline G01. The main changes brought by this PB were :

- Addition of C-band Complex Echoes to L1A ALT Products.
- Instrumental Look-Up Tables update for LR MLE retrievals.
- External path delay and g scaling updates.
- Removal of MLE3 from Ku-band variables.
- Vertical Wave Motion correction applied at 20Hz for both HR NR and SAMOSA.
- Wind Speed alignment to model thanks to sigma0 calibration biases update.
- Orbit MOE/POE-G

A specific LUT update for range MLE4, along with geoid auxiliary files correction, was applied starting on 12/04/2025 at 01:08. PB G01 also included evolutions to GDR-G standards for the following models:

- Ocean and load tides solutions 2 (FES): FES14 => FES22.
- MSS solution 1 : Hybrid CNES-CLS2022/Scripps/DTU => Hybrid CNES-CLS2023/Scripps/DTU.
- MSS solution 2 : DTU2018 => DTU2021.
- MDT : CNES-CLS MDT 2018 => CNES-CLS MDT 2022.

More details on the PB G01 can be found in the associated product notice [7], on EUMETSAT user portal.

In 2025, a complete reprocessing of the mission was carried out using the PB G01 baseline. The analysis of this reprocessed dataset is not included in the present report and is instead documented in the dedicated processing report ([8]).

4 Data coverage and edited measurements

This section presents the monitoring results for the entire mission duration (shown on the left) and specifically for the year 2025 (shown on the right).

4.1. Missing measurements

4.1.1. Over land and ocean

Determination of missing measurements relative to the theoretically expected orbit ground pattern is an essential tool to detect missing telemetry or satellite events.

Figure 7 shows the percentage of available measurements for Sentinel-6 MF LR and HR modes for all surfaces observed. Global availability is excellent for both LR (99.00%) and HR (98.69%) over 2025.

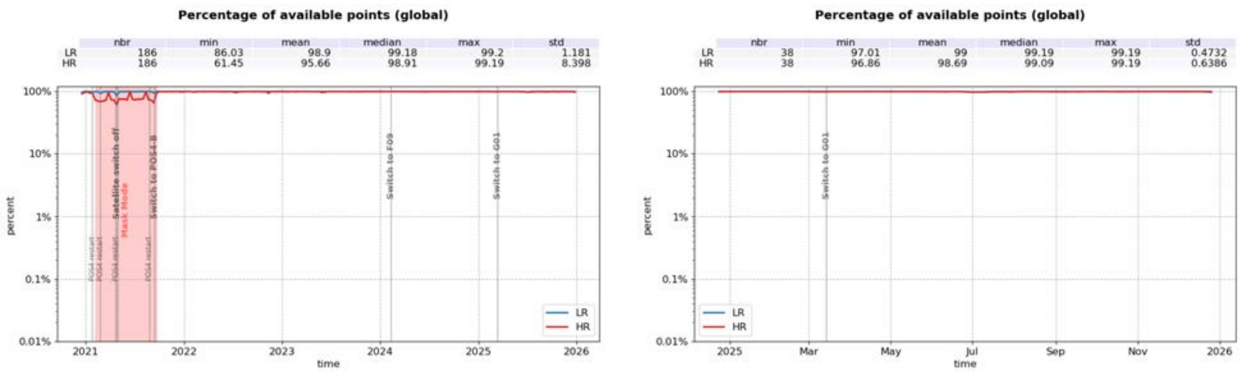

Figure 7: Percentage of available data over all surfaces for both LR (blue) and HR (red) per cycle over the entire mission lifetime (left) and 2025 only (right).

Table 2 and 3 give the list of fully missing passes for LR and HR respectively, along with related events.

Cycle	Pass	Date	Comment
169	180	2025-06-17 11:46:08 to 12:42:21	UNS 12257
169	181	2025-06-17 12:42:21 to 13:38:34	UNS 12257
171	249	2025-07-10 00:22:01 to 01:18:14	UNS 12337
171	250	2025-07-10 01:18:14 to 02:14:27	UNS 12337
171	251	2025-07-10 02:14:27 to 03:10:40	UNS 12337
171	252	2025-07-10 03:10:40 to 04:06:53	UNS 12337
171	253	2025-07-10 04:06:53 to 05:03:05	UNS 12337
171	254	2025-07-10 05:03:05 to 05:59:18	UNS 12337
172	1	2025-07-10 05:59:18 to 06:55:31	UNS 12337
172	2	2025-07-10 06:55:31 to 07:51:44	UNS 12337
172	3	2025-07-10 07:51:44 to 08:47:57	UNS 12337
172	4	2025-07-10 08:47:57 to 09:44:10	UNS 12337
172	5	2025-07-10 09:44:10 to 10:40:23	UNS 12337
174	99	2025-08-02 21:45:24 to 22:41:37	No relative event
174	145	2025-08-04 16:51:17 to 17:47:30	No relative event

179	9	2025-09-17 23:18:43 to 00:14:56	Undelivered orbit files
179	10	2025-09-18 00:14:56 to 01:11:09	Undelivered orbit files

Table 2: List of missing passes in LR over 2025

Cycle	Pass	Date	Comment
159	16	2025-03-03 22:21:40 to 23:17:53	UNS 11887
160	6	2025-03-13 10:58:02 to 11:54:15	UNS 11925
160	134	2025-03-18 10:53:31 to 11:49:44	UNS 11948
169	180	2025-06-17 11:46:08 to 12:42:21	UNS 12257
169	181	2025-06-17 12:42:21 to 13:38:34	UNS 12257
171	249	2025-07-10 00:22:01 to 01:18:14	UNS 12337
171	250	2025-07-10 01:18:14 to 02:14:27	UNS 12337
171	251	2025-07-10 02:14:27 to 03:10:40	UNS 12337
171	252	2025-07-10 03:10:40 to 04:06:53	UNS 12337
171	253	2025-07-10 04:06:53 to 05:03:05	UNS 12337
171	254	2025-07-10 05:03:05 to 05:59:18	UNS 12337
172	1	2025-07-10 05:59:18 to 06:55:31	UNS 12337
172	2	2025-07-10 06:55:31 to 07:51:44	UNS 12337
172	3	2025-07-10 07:51:44 to 08:47:57	UNS 12337
172	4	2025-07-10 08:47:57 to 09:44:10	UNS 12337
172	5	2025-07-10 09:44:10 to 10:40:23	UNS 12337
173	102	2025-07-24 02:35:31 to 03:31:44	UNS 12376
173	103	2025-07-24 03:31:44 to 04:27:57	UNS 12376
174	99	2025-08-02 21:45:24 to 22:41:37	No relative event
174	145	2025-08-04 16:51:17 to 17:47:30	No relative event
177	218	2025-09-06 07:10:32 to 08:06:45	UNS 12534
178	248	2025-09-17 09:15:30 to 10:11:43	UNS 12567
179	9	2025-09-17 23:18:43 to 00:14:56	Undelivered orbit files
179	10	2025-09-18 00:14:56 to 01:11:09	Undelivered orbit files
182	136	2025-10-22 16:13:33 to 17:09:46	UNS 12681
183	30	2025-10-28 10:53:20 to 11:49:33	UNS 12701
187	242	2025-12-15 09:53:04 to 10:49:17	UNS 12896
189	10	2025-12-26 04:00:12 to 04:56:25	UNS 12921
189	82	2025-12-28 23:27:39 to 00:23:52	UNS 12925

Table 3: List of missing passes in HR over 2025

4.1.2. Over ocean

Figure 8 shows the percentage of available measurements for Sentinel-6 MF LR and HR modes for ocean only. Availability over ocean is excellent for both LR (99.84%) and HR (99.55%) in 2025.

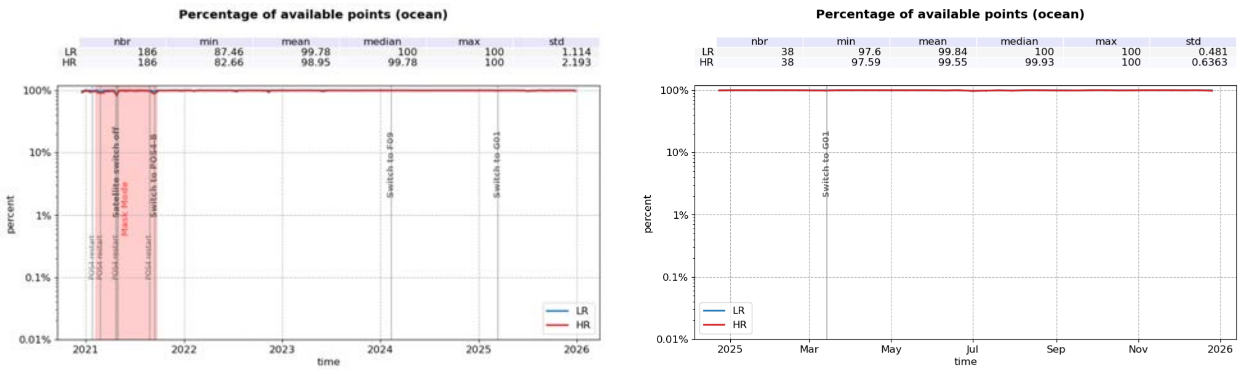

Figure 8: Percentage of available data over ocean for both LR (blue) and HR (red) per cycle over the entire mission lifetime (left) and 2025 only (right).

4.2. Edited measurements

4.2.1. Overview

The outlier detection or editing step of the Cal/Val process is applied to remove any measurement that is considered erroneous. Thus, it helps to refine the various metrics which are provided in the specific sections dedicated to the performance over the ocean. The definition of an erroneous measurement, and of the accepted error level on the final sea level anomaly is of course a trade-off between accuracy and data coverage. The monitoring of the percentage of valid and edited measurements also provides relevant information about the mission performance.

A series of editing criteria are used to detect outliers over ocean. This process is divided into 4 main parts:

- removal of all measurements over land using a land/water mask,
- removal of all measurements affected by sea-ice (section 4.2.2.),
- removal of all measurements which exceed defined thresholds on different parameters (section 4.2.3.),
- further checks on along-track SLA consistency (section 4.2.5.).

The percentage of edited data per day for HR and LR datasets over ocean in 2025 is monitored on figure 9. In average, slightly fewer data are edited in HR mode (10.0 % in SAMOSA and 10.0 % in NR) compared to LR (11.6 % in MLE4 and 11.5 % in NR).

An annual signal is visible : the total percentage of edited data is lower during March/April/May (6-7 %), then increasing during May to July and remains around 14-15 %, and start to slowly decrease in mid-September. This expected behaviour is related to sea ice coverage (see dedicated part 4.2.2.), and was already observed on previous altimetry missions such as Jason-3.

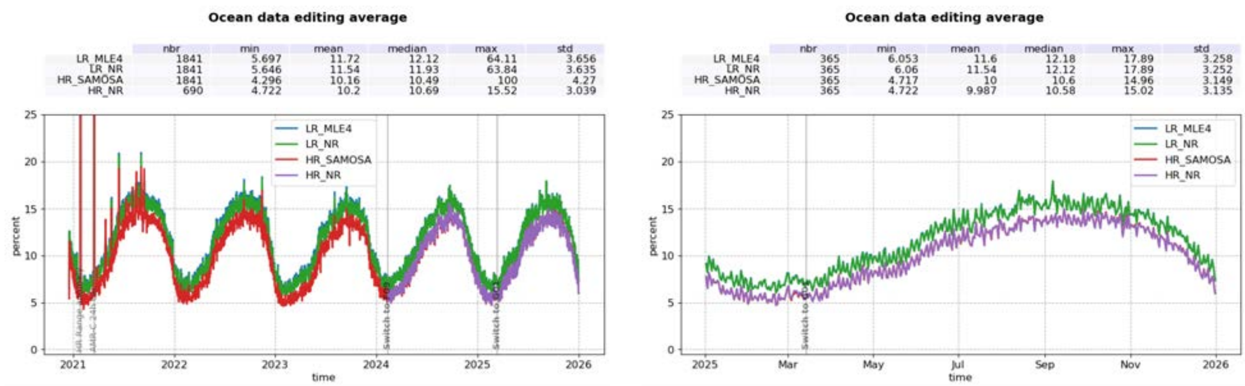

Figure 9: Percentage of edited data over ocean for LR MLE4 (blue), LR NR (green), HR SAMOSA (red) and HR NR (purple) per day over the entire mission lifetime (left) and 2025 only (right).

The maps of figure 10 represent the percentage of edited data for LR MLE4, LR NR, HR SAMOSA and HR NR, over the year 2025. Inter Tropical Convergence Zone (ITCZ) or zones with sea ice appear on the maps as regions with less valid data, as it is also the case for other altimeters: measurements are corrupted by rain or sea ice. They were therefore removed by editing. HR and LR maps are in line, except in wet zones where less HR data are edited. A potential explanation for such behaviour could be a better capability of HR processing to retrieve clean geophysical parameters over wet zones.

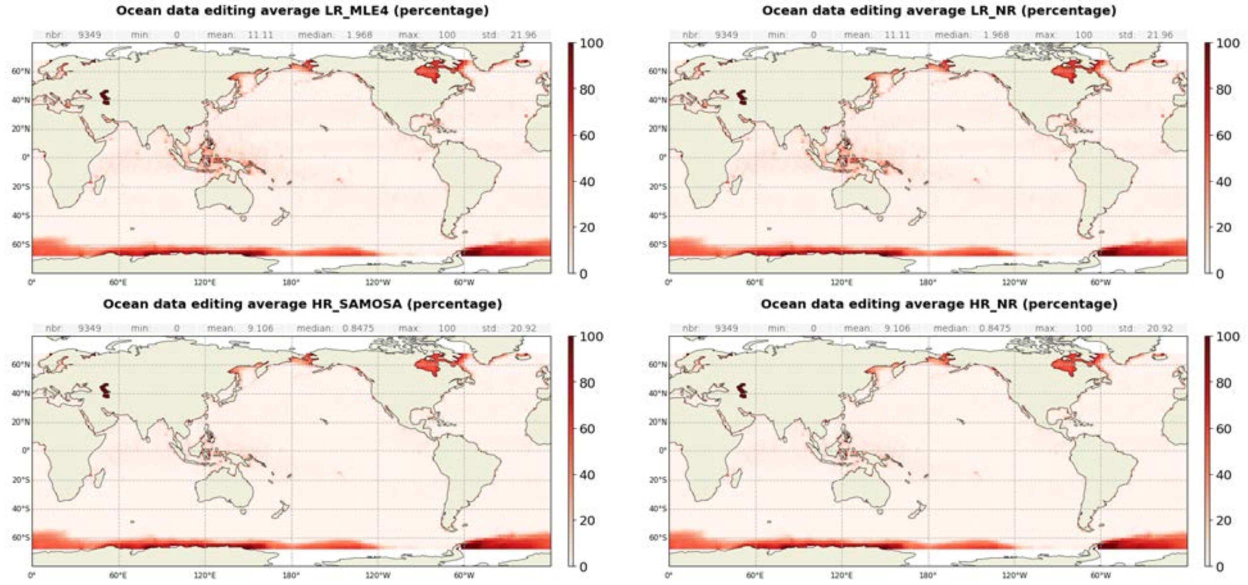

Figure 10: Maps of average percentage of edited ocean data for LR MLE4 (top left), LR NR (top right), HR SAMOSA (bottom left) and HR NR (bottom right), computed over 2025.

4.2.2. Flagging quality: ice

The first step of the editing process includes the removal of points where ice is detected. The ice flag (based on rad_sea_ice_flag in L2 products) is used to remove measurements affected by sea ice within the altimeter footprint.

The percentage of measurements edited on the ice flag criterium over ocean is monitored on the figure 11.

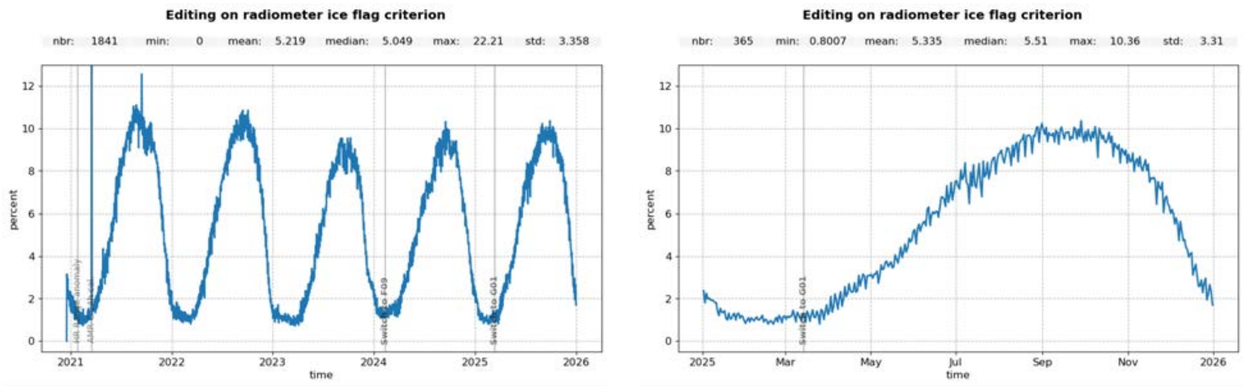

Figure 11: Percentage of data edited on ice criterion per day over the entire mission lifetime (left) and 2025 only (right).

Over the period shown, no anomalous trend is detected but the nominal annual cycle is visible. Indeed, the maximum number of points over ice is reached during the austral winter (i.e. July - September). As Sentinel-6 MF satellite has an inclination of $66°$, it does not detect thawing of sea ice (due to global warming), which takes place especially in Northern Hemisphere over $66°$.

Note that the percentage of edited data on ice criterion is lower for Sentinel-6 MF (5.2 % on average) than on Jason-3 (5.8 % on average [10]). Such a difference is due to the different definition of the ice flags used for this editing step. On Jason-3, the ice flag (ice-flag in L2 product) is computed using a combination of radiometer and altimeter parameters. On Sentinel-6 MF, the sea ice flag is derived from radiometer outputs only. We recommend updating the ice flag with a computation similar to Jason-3 to improve its robustness.

4.2.3. Thresholds

4.2.3.1. Overview

Once the measurements corrupted by sea ice surfaces are identified, the quality of the parameters retrieved by the altimeter, as well as that of the geophysical corrections are checked with respect to defined thresholds. These thresholds are detailed in table 4, with the corresponding percentage of detected outliers in LR MLE4, LR NR, HR SAMOSA and HR NR over 2025. These percentages are closely monitored cycle by cycle, day by day and pass by pass by CLS Cal/Val routines. A distinction is made between indicators at default value, and indicators out of bounds. For both cases, an individual measure may be edited by different criteria.

This allows detection of anomalies in the number of removed data, which could have instrumental, geophysical or algorithmic origins.

Parameters	Min thres.	Max thres.	Unit	% rejected			
				LR MLE4	LR NR	HR SAM.	HR NR
Sea surface height anomaly	-2	2	m	3.32	2.68	2.93	2.52
Sea surface height	-130	100	m	2.32	1.73	0.01	0.01
Nb measurements of range	10	N/A		0.16	0.00	0.00	0.00
Std. deviation of range	0	See (*)	m	2.59	1.05	0.95	1.10
Backscatter coefficient	7	30	dB	2.05	0.16	0.11	0.18
Nb measurements of sigma0	10	N/A		0.15	0.00	0.00	0.00
Std. deviation of sigma0	0	1	dB	3.92	2.57	0.77	0.99
Significant wave height	0	11	m	2.39	0.27	0.09	0.43
Altimeter wind speed	0	30	m.s-1	2.18	0.86	1.20	0.95
Sea State Bias	-0.5	0	m	2.02	0.01	0.00	0.00
Ionospheric correction filtered	-0.4	0.04	m	2.74	2.51	2.75	2.50
Square off nadir angle	-0.2	0.64	deg2	0.85	1.46	N/A	N/A
Equilibrium tide	-0.5	0.5	m	0.06	0.06	0.06	0.06
Combined atmospheric correction	-2	2	m	0.00	0.00	0.00	0.00
Dry tropospheric correction	-2.5	-1.9	m	0.00	0.00	0.00	0.00
Internal tide	-5	5	m	0.00	0.00	0.00	0.00
Ocean tide	-5	5	m	0.09	0.09	0.09	0.09
Pole tide	-15	15	m	0.00	0.00	0.00	0.00
Earth tide	-1	1	m	0.00	0.00	0.00	0.00
Radiometer wet tropospheric correction	-0.5	-0.001	m	0.09	0.09	0.09	0.09
Global statistics of edited measurements by thresholds				6.3	6.2	4.7	4.6

Table 4: Table of parameters used for editing and the corresponding percentages of edited measurements for each parameter for Sentinel-6 MF LR and HR.

(*) The maximum threshold for range standard deviation is set as function of significant wave height as follow:

- In LR:
  - for SWH $\leq$ 2m : 0.192
  - for SWH > 2m : 0.018 * SWH + 0.156
- In HR:
  - for SWH $\leq$ 2m : 0.087
  - for SWH > 2m : 0.033 * SWH + 0.121

The monitoring of edited data based on these thresholds criteria is shown in figure 12. On this monitoring, slightly different behaviours are observed between datasets. There is less data at default value in LR NR than in LR MLE4, as well as in HR NR than in SAMOSA. However, the opposite is true for criteria out of bounds. This indicates that more data are retrieved in NR (both LR and HR), but most of this additional data is of poor quality and then edited on threshold criteria. The total percentages of edited data based on the thresholds criteria are indeed almost identical between LR MLE4 and NR and between HR SAMOSA and NR.

Looking at data at default value (i.e. unavailable, bottom right panel), an annual signal is visible. Part of this signal can be linked to sea ice. Indeed, as stated above, Sentinel-6 MF radiometer sea ice flag definition does not allow to detect all measurements affected by sea ice. For the remaining measurements, MLE4, NR and SAMOSA retrackings failed to retrieve geophysical parameters, hence the default values detected here.

Looking at out-of-bound data (top right panel), fewer data are edited in HR SAMOSA (1.8 %) and HR NR (2.2 %) than in LR (3.1 % in MLE4 and 3.8 % in NR). All monitorings are stable in time, with a small annual signal of about 1 % amplitude.

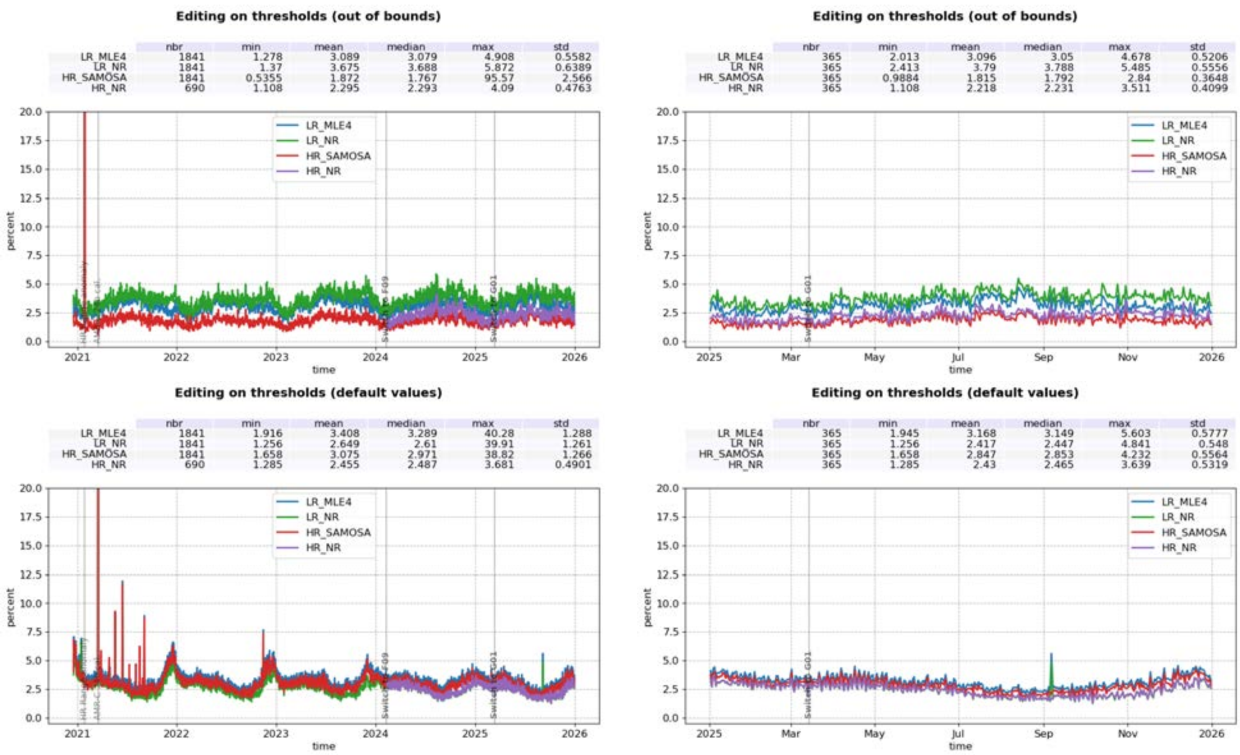

Figure 12: Percentage of data edited on threshold criteria for LR MLE4 (blue), LR NR (green), HR SAMOSA (red) and HR NR (purple) per day, for out of bounds (top) and default value (bottom) indicators over the entire mission lifetime (left) and 2025 only (right).

The overall percentage of edited data with this threshold step is of 6.3 % for LR MLE4, 6.2 % for LR NR, 4.7 % for HR SAMOSA and 4.6 % for HR NR (table 4). The difference is possibly caused by HR mode being less impacted by rain cells in wet zones.

4.2.3.2. Individual thresholds

20 Hz measurements number on range and sigma0

1 Hz range and sigma0 measurements computed with fewer than ten 20 Hz measurements are edited. Indeed, they are considered insufficiently consistent for computing range estimates at 1Hz resolution.

In LR, such situation usually occurs in regions with heavy rain, as shown on figures 14 and 16. Indeed, waveforms are distorted by rain cells, which makes them often meaningless for SSH calculation. As a consequence, edited measurements due to several altimetric criteria are often correlated with wet areas. Over 2025, the average percentage of range measurements removed using this criterion is 0.16 % for Sentinel-6 MF LR MLE4 compared with less than 0.01 % for LR NR and HR (figure 13). For the sigma0, the average percentage of measurements removed using this criterion is 0.15 % for Sentinel-6 MF LR MLE4 compared with less than 0.01 % for LR NR and HR (figure 15)

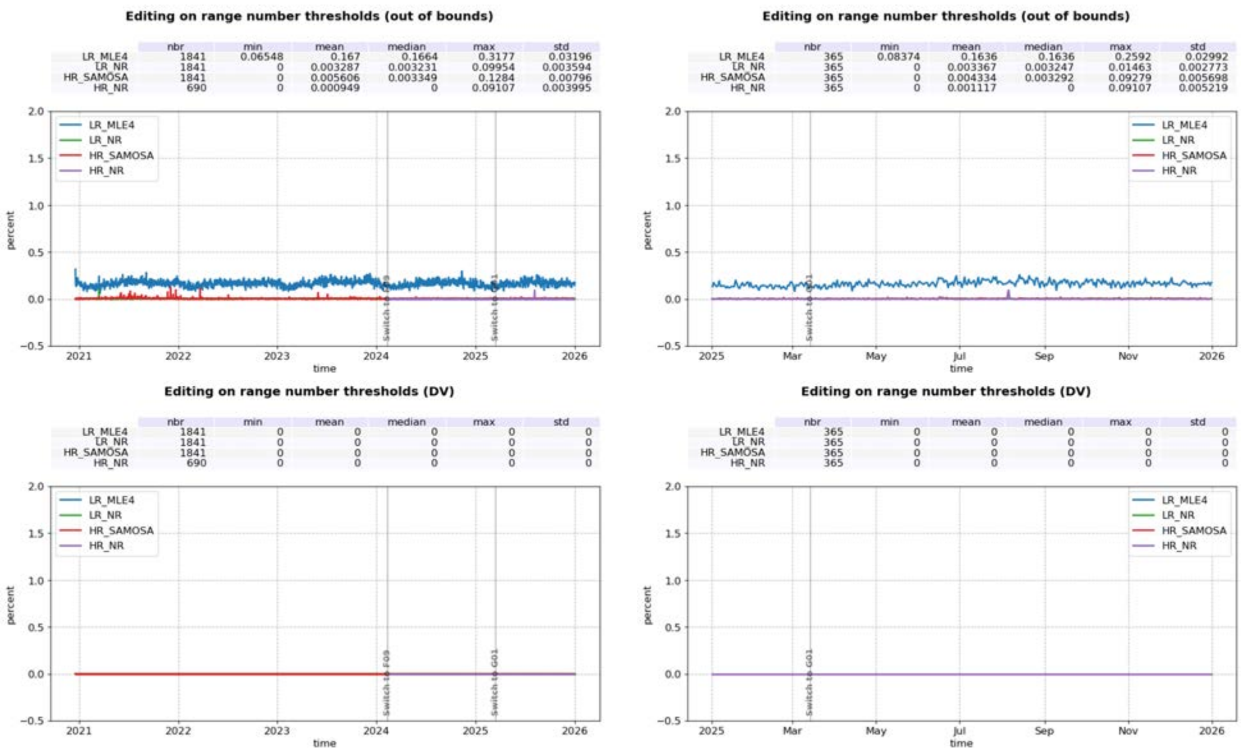

Figure 13: Percentage of data edited on range number threshold for LR MLE4 (blue), LR NR (green), HR SAMOSA (red) and HR NR (purple) per day, for out of bounds (top) and default value (bottom) over the entire mission lifetime (left) and 2025 only (right).

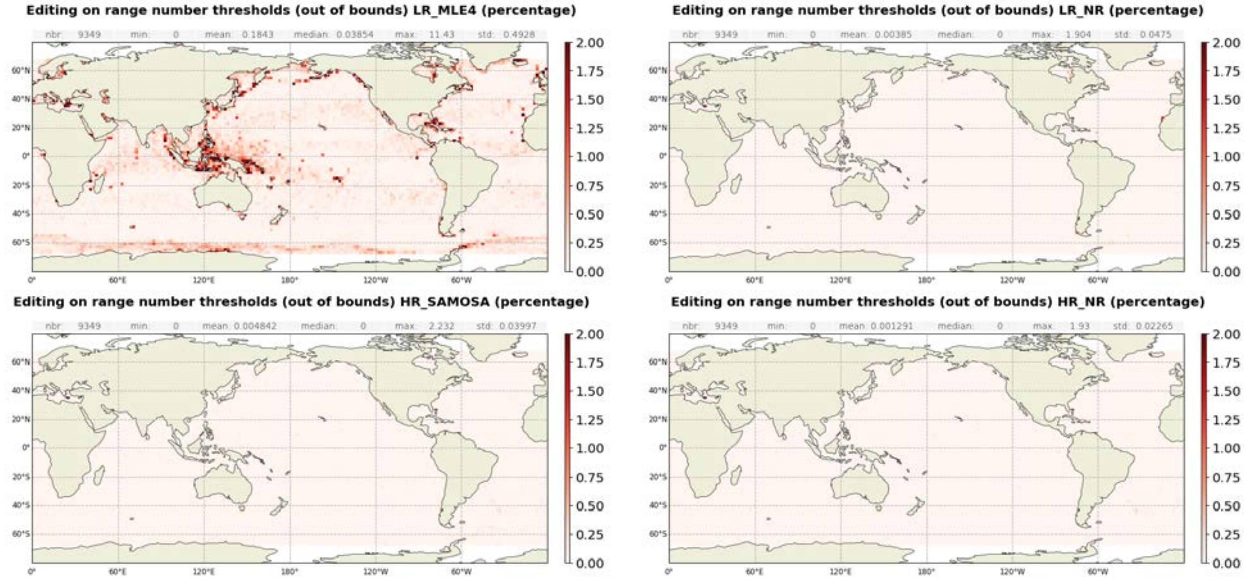

Figure 14: Maps of average percentage of data edited on range number threshold for both LR MLE4 (top left), LR NR (top right), HR SAMOSA (bottom left) and HR NR (bottom right), for out of bounds, computed over 2025.

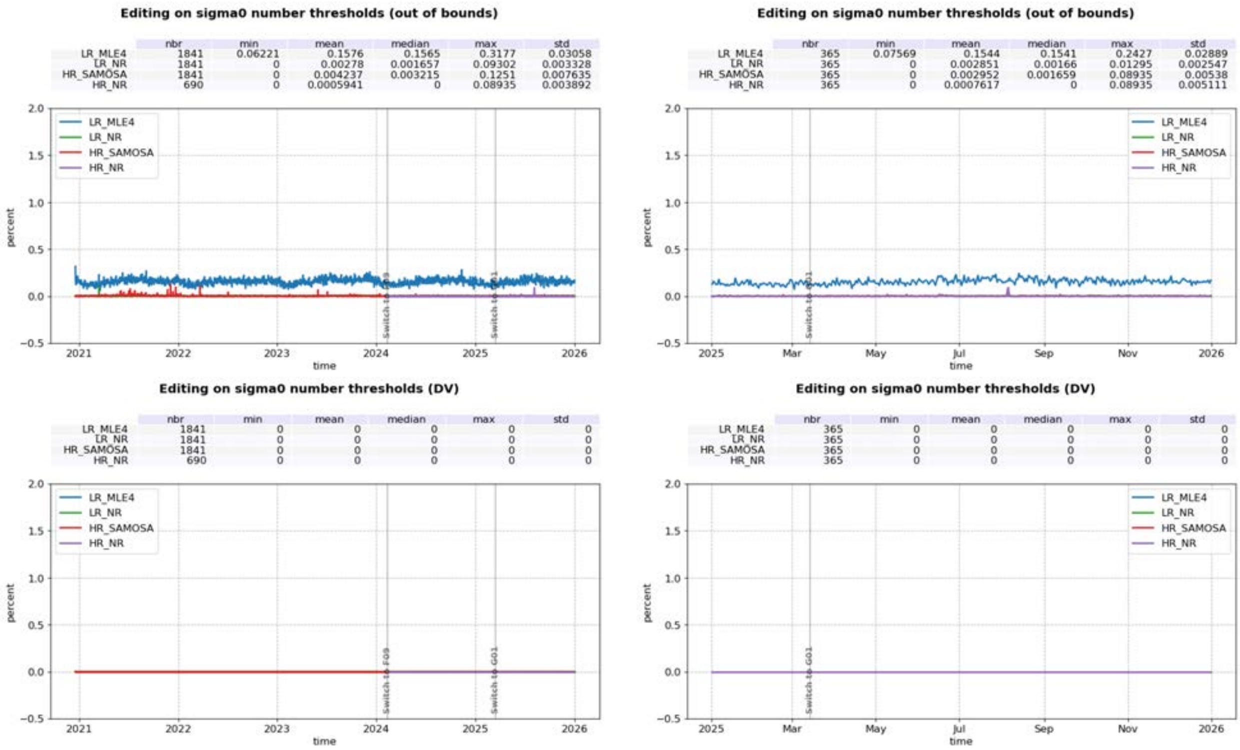

Figure 15: Percentage of data edited on sigma0 number threshold for LR MLE4 (blue), LR NR (green), HR SAMOSA (red) and HR NR (purple) per day, for out of bounds (top) and default value (bottom) over the entire mission lifetime (left) and 2025 only (right).

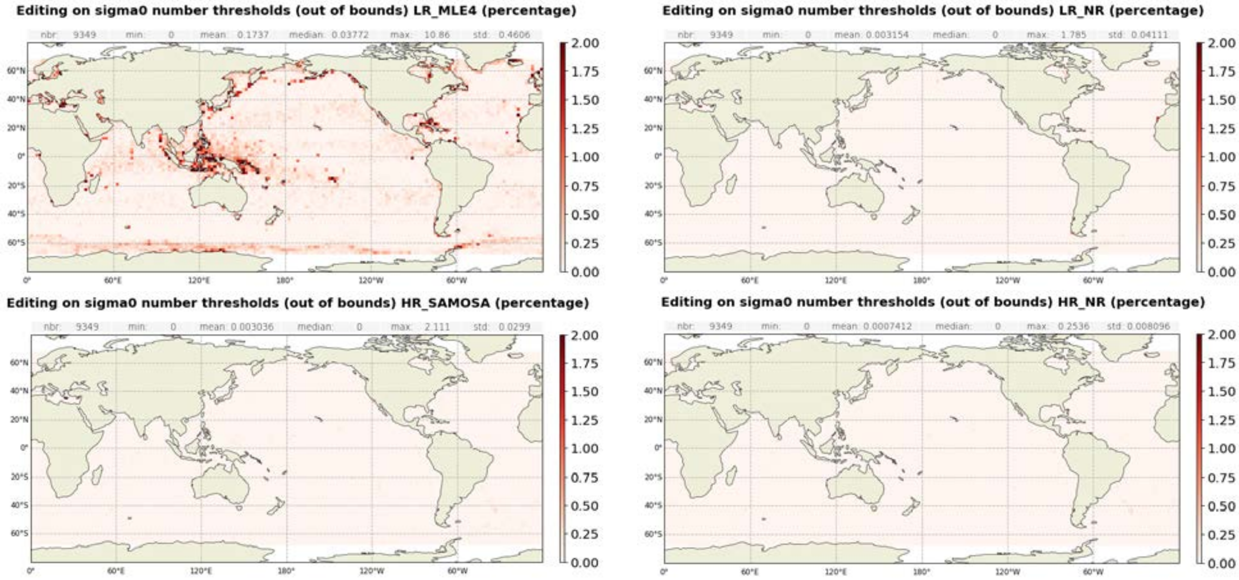

Figure 16: Maps of average percentage of data edited on sigma0 number threshold for both LR MLE4 (top left), LR NR (top right), HR SAMOSA (bottom left) and HR NR (bottom right), for out of bounds, computed over 2025.

20 Hz measurements standard deviation on range and sigma0

Using the threshold editing on 20Hz range measurements standard deviation (figure 17), 2.59 % of data are removed in average in LR MLE4, higher than in LR NR, HR SAMOSA and HR NR (1.05 %, 0.95 and 1.10 % respectively). This difference is explained by a higher percentage of range standard deviation set to Default Value for LR MLE4 (figure 17, bottom panel). It highlights the LR NR and HR processing capabilities to retrieve geophysical parameters on icy regions.
Additionally, an annual signal appears here for all processing. As for 20Hz range measurements number, edited measurements are correlated with wet areas (figures 18 and 19).

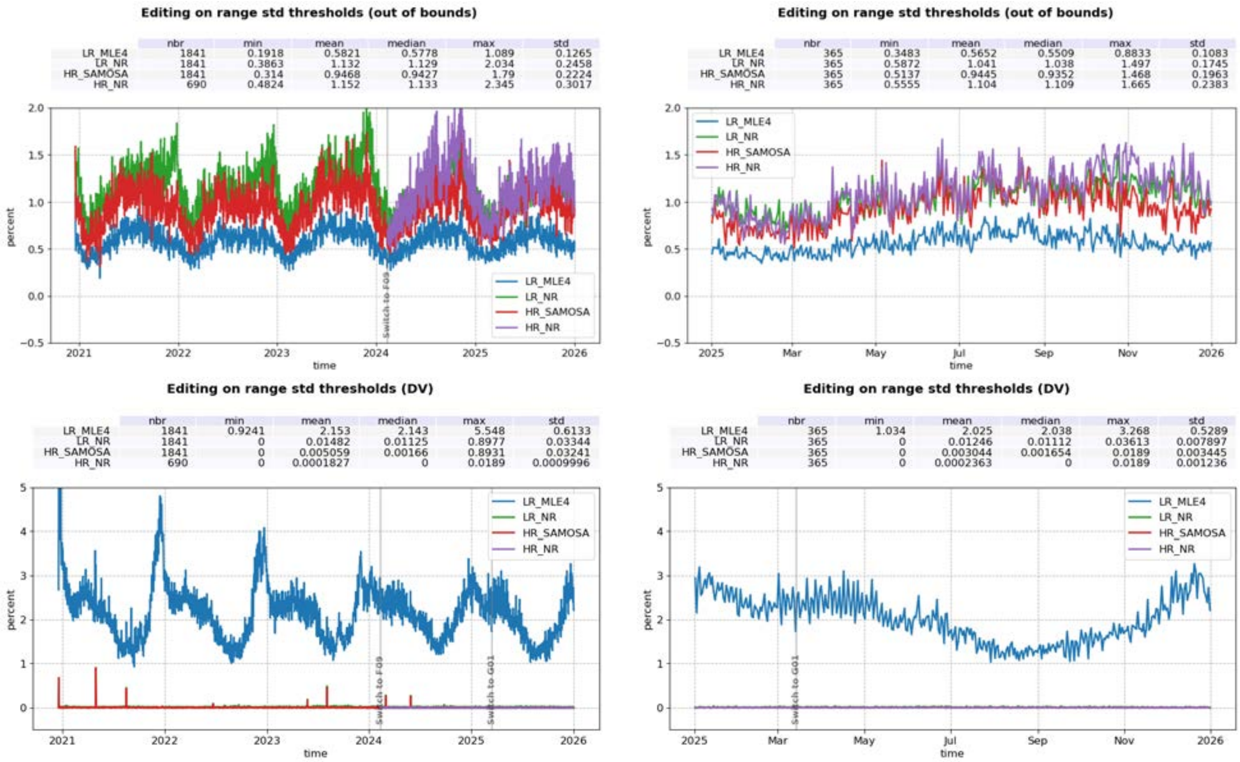

Figure 17: Percentage of data edited on range std threshold for both LR MLE4 (blue), LR NR (green), HR SAMOSA (red) and HR NR (purple) per day, for out of bounds (top) and default value (bottom) over the entire mission lifetime (left) and 2025 only (right).

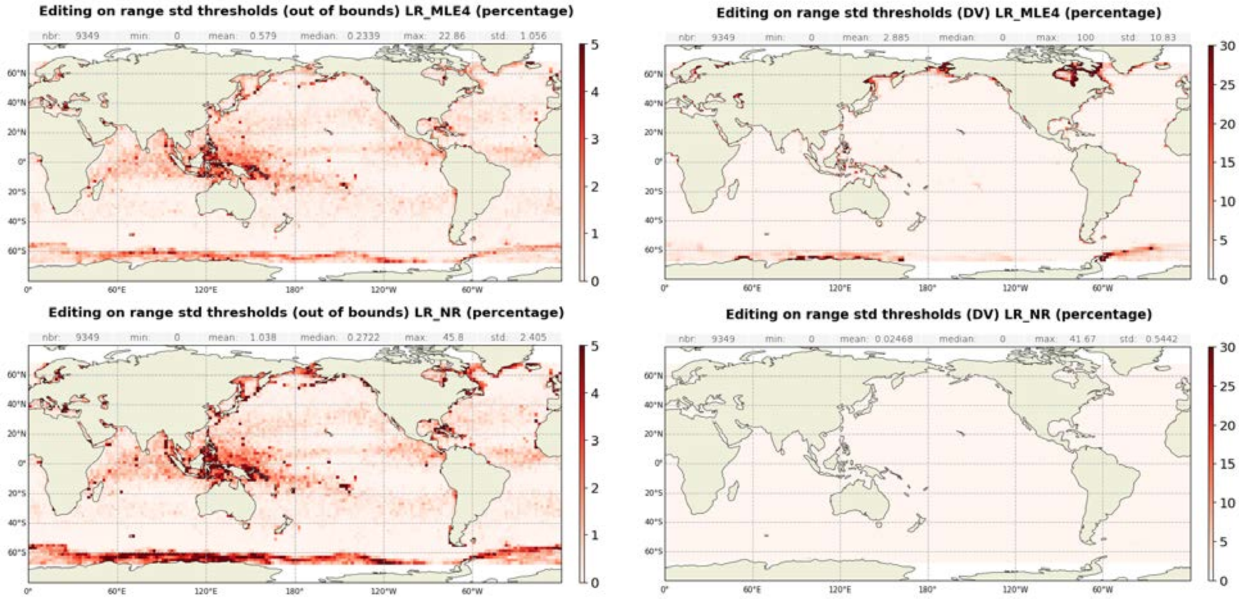

Figure 18: Maps of average percentage of data edited on range std threshold for both LR MLE4 (top) and LR NR (bottom), for out of bounds (left) and default value (right), computed over 2025.

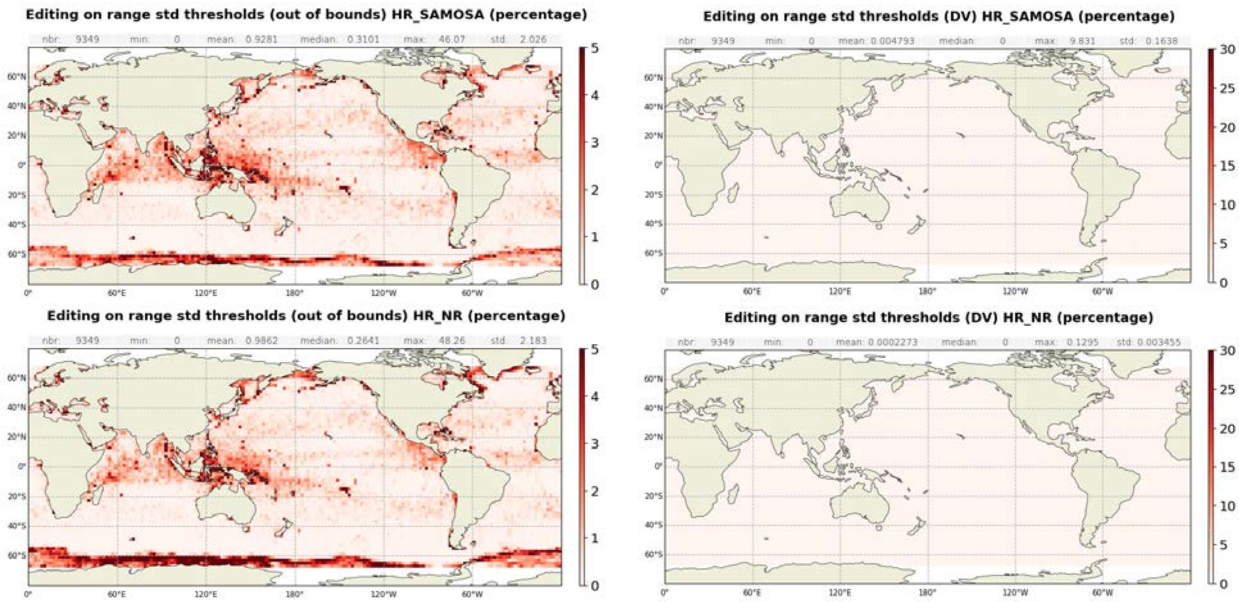

Figure 19: Maps of average percentage of data edited on range std threshold for both HR SAMOSA (top) and HR NR (bottom), for out of bounds (left) and default value (right), computed over 2025.

Figure 20 presents the percentage of data edited based on sigma0 standard deviation criterion. It is about 3.92 % for LR MLE4, 2.57 % for LR NR, 0.77 % for HR SAMOSA and 0.99 % for HR NR. Most of the out of bound sigma0 standard deviation are located in regions with heavy rain, primarily around Indonesia (figure 21).

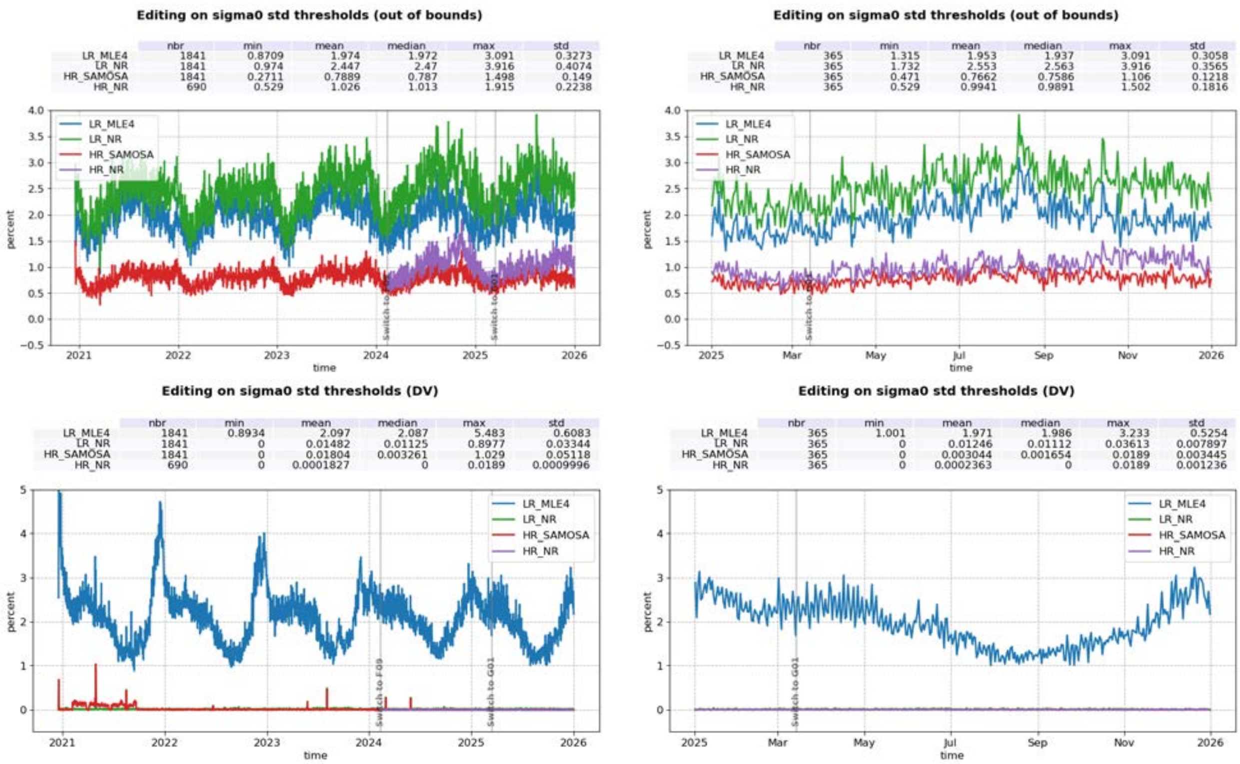

Figure 20: Percentage of data edited on sigma0 std threshold for LR MLE4 (blue), LR NR (green), HR SAMOSA (red) and HR NR (purple) per day, for out of bounds (top) and default value (bottom) over the entire mission lifetime (left) and 2025 only (right).

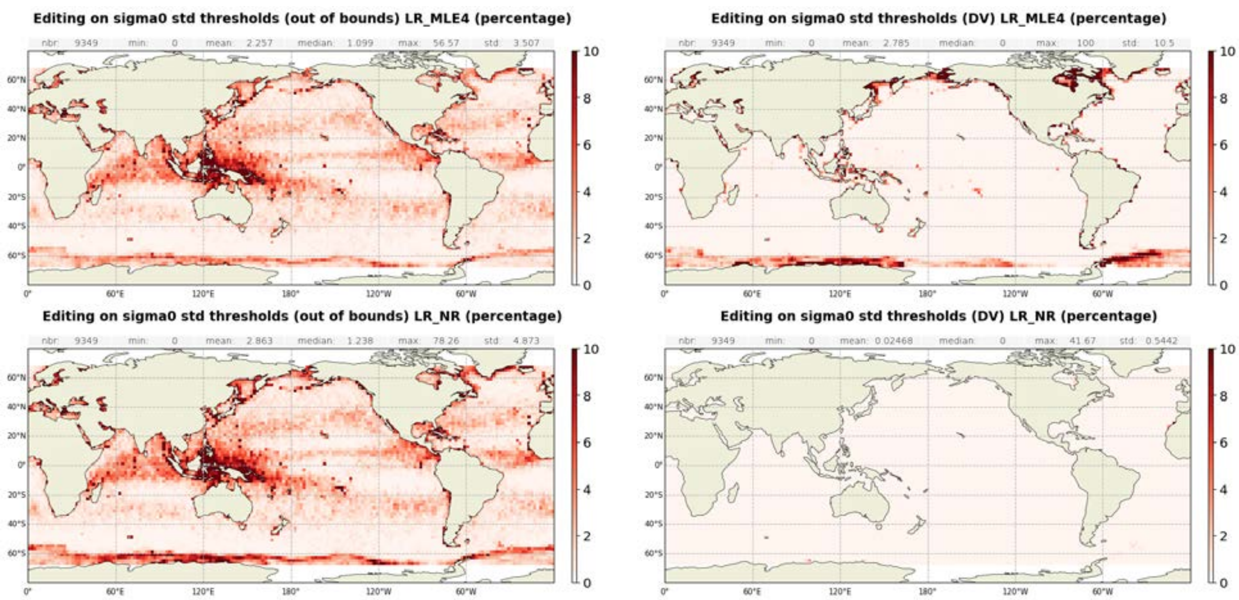

Figure 21: Maps of average percentage of data edited on sigma0 std threshold for both LR MLE4 (top) and LR NR (bottom), for out of bounds (left) and default value (right), computed over 2025.

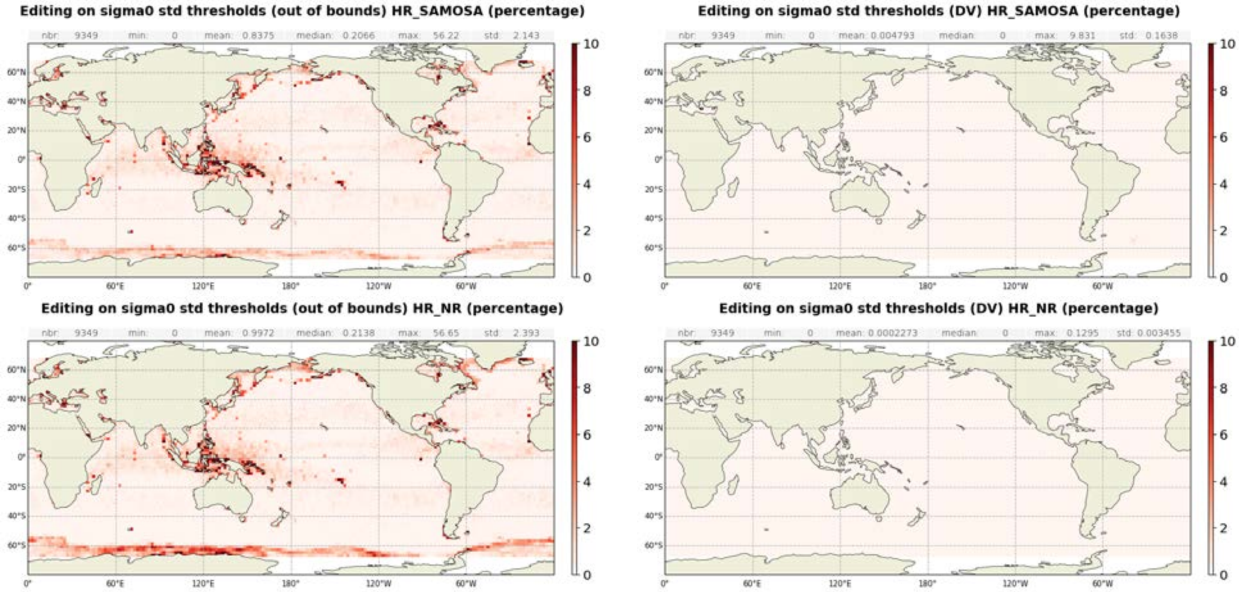

Figure 22: Maps of average percentage of data edited on sigma0 std threshold for both HR SAMOSA (top) and HR NR (bottom), for out of bounds (left) and default value (right), computed over 2025.

Backscatter coefficient

The percentage of edited measurements due to backscatter coefficient criterion is represented on top of figure 23. It is about 2.05 % for LR MLE4, 0.16 % for LR NR, 0.11 % for HR SAMOSA and 0.18 % for HR NR. For LR MLE4, most of these edited measurements are at DV and located in coastal areas, ice margins and wet zones (see figures 24 and 25).

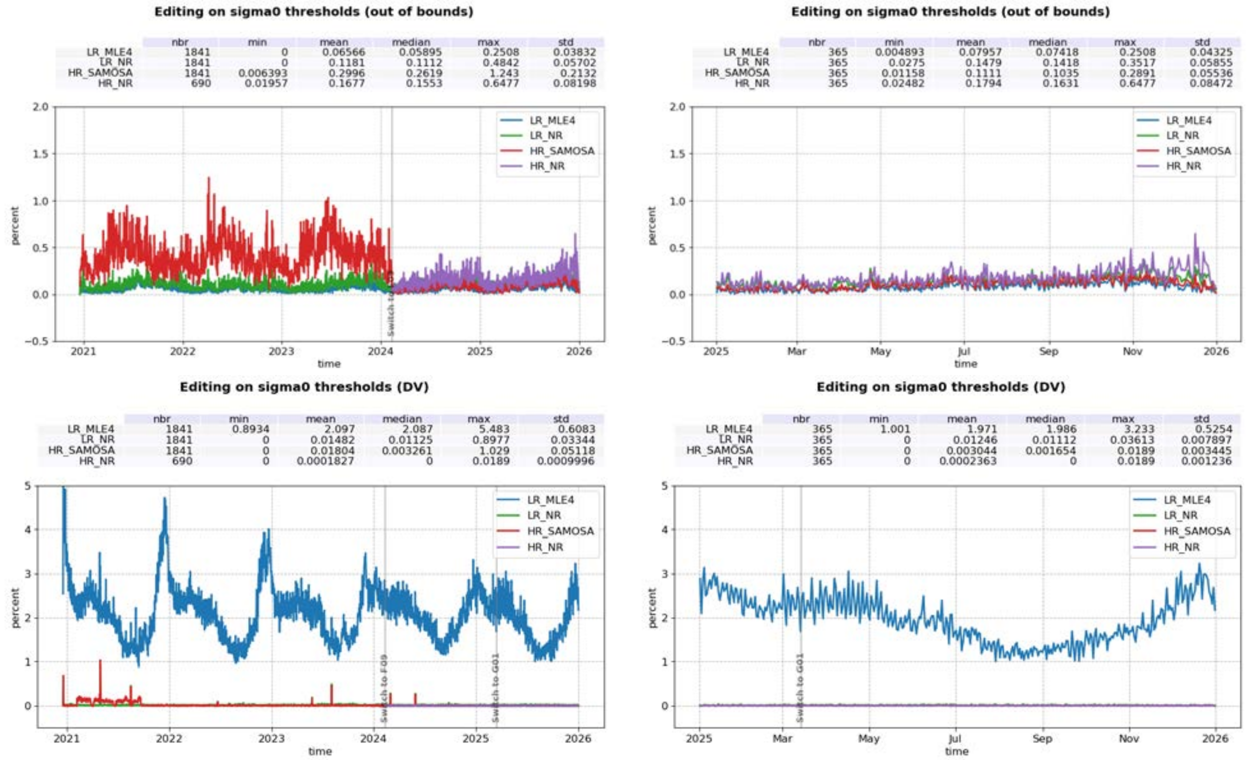

Figure 23: Percentage of data edited on sigma0 threshold for LR MLE4 (blue), LR NR (green), HR SAMOSA (red) and HR NR (purple) per day, for out of bounds (top) and default value (bottom) over the entire mission lifetime (left) and 2025 only (right).

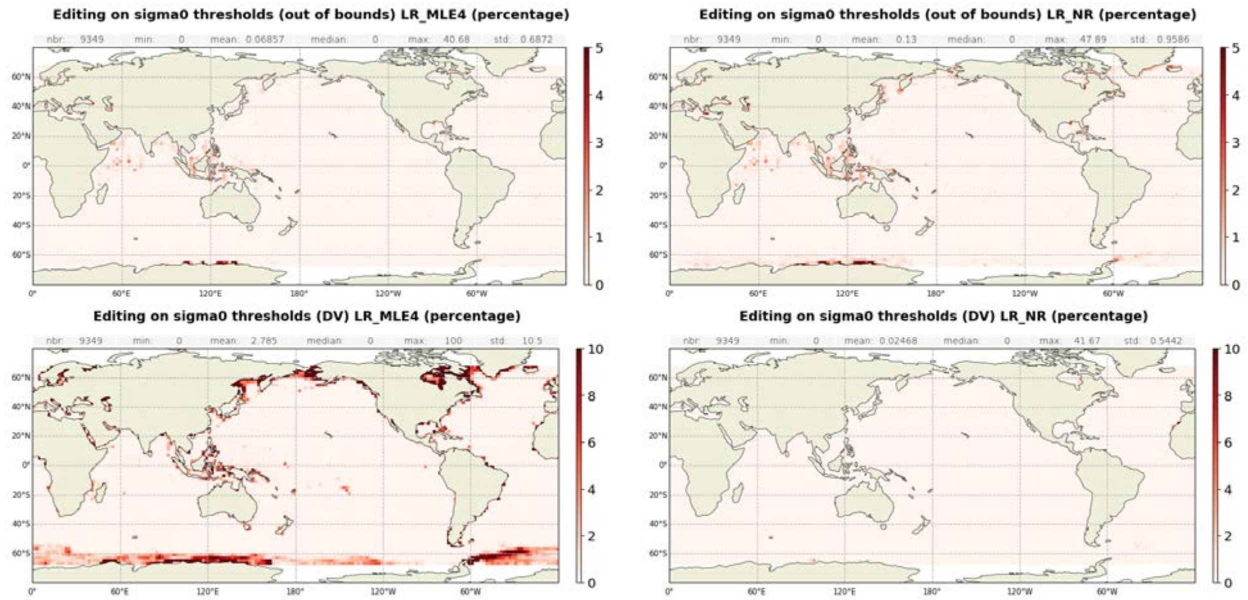

Figure 24: Maps of average percentage of data edited on sigma0 threshold for both LR MLE4 (left) and LR NR (right), for out of bounds (top) and default value (bottom), computed over 2025.

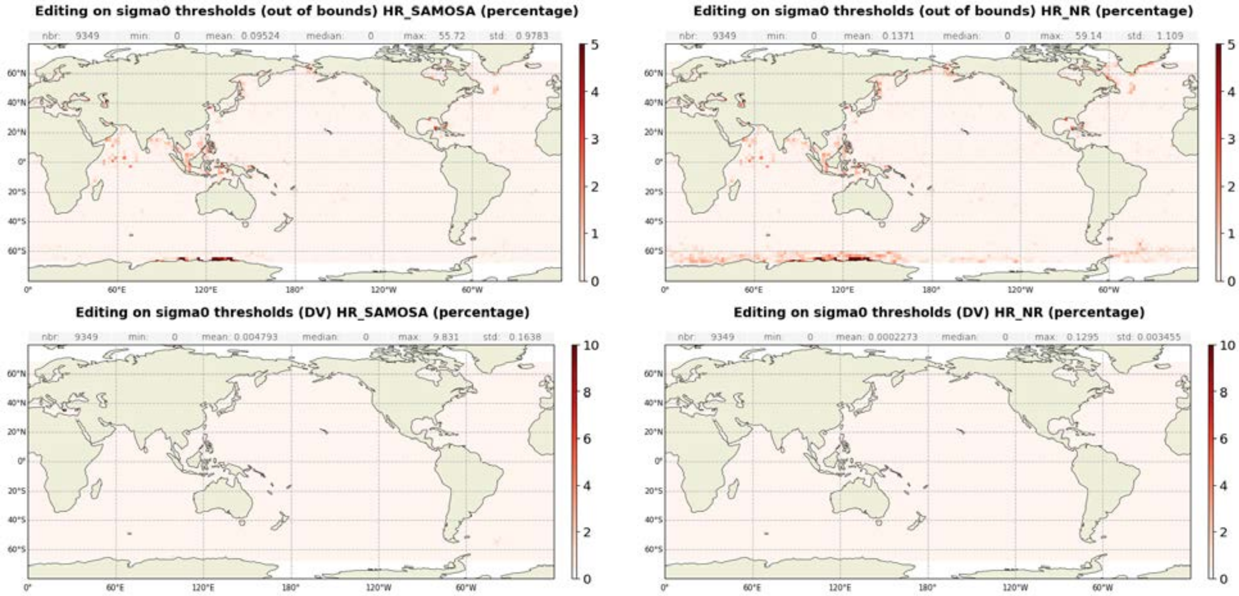

Figure 25: Maps of average percentage of data edited on sigma0 threshold for both HR SAMOSA (left) and HR NR (right), for out of bounds (top) and default value (bottom), computed over 2025.

Significant wave height

The percentage of edited measurements due to significant wave heights criterion is represented on figure 26, and is about 2.39 % for LR MLE4, 0.27 % for LR NR, 0.09 % for HR SAMOSA and 0.43 % for HR NR. In LR MLE4, they are mostly due to default value data, and are located in circumpolar areas, while out of bounds values are located in coast regions, in the Mediterranean Sea and around Indonesia (figure 27). In HR NR, a higher percentage of measurements is edited in low SWH areas (figure 28) than in SAMOSA. This is due to the fact that in NR, SWH values can be negative, unlike in SAMOSA retracking, and negative SWH are edited in our process (see table 4).

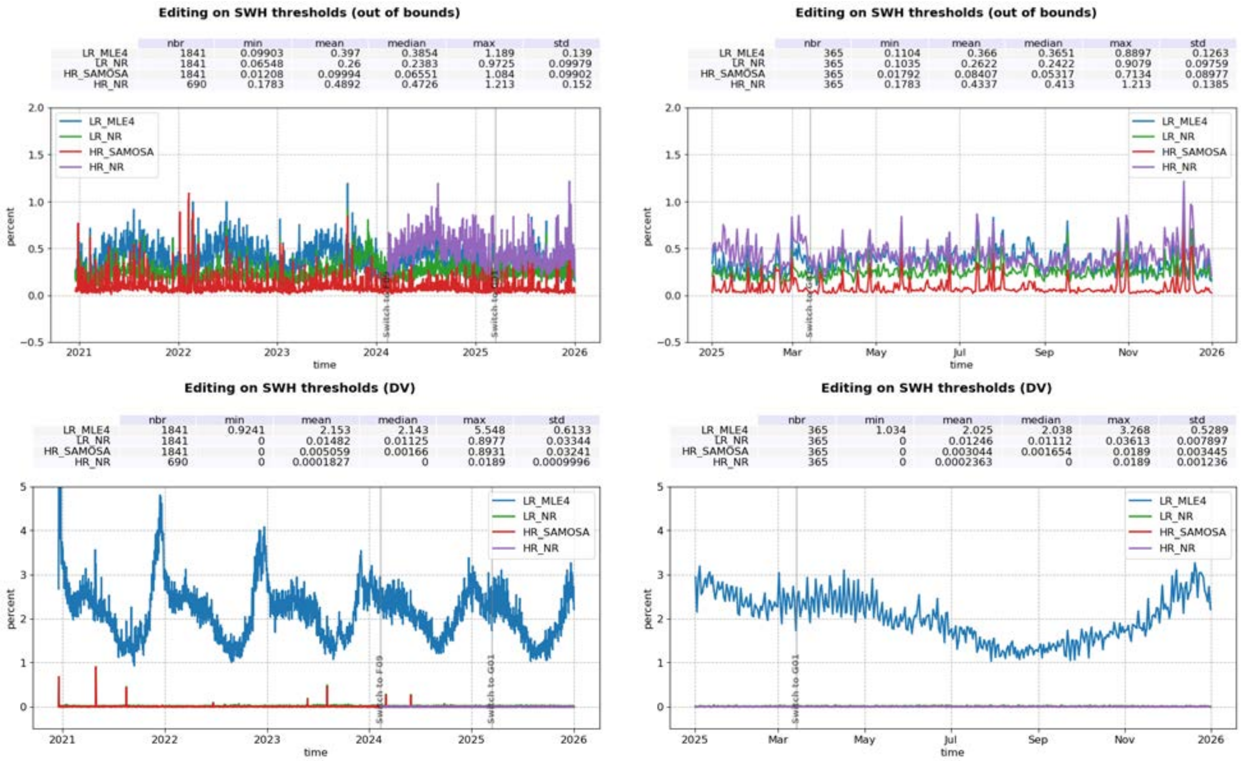

Figure 26: Percentage of data edited on SWH threshold for LR MLE4 (blue), LR NR (green), HR SAMOSA (red) and HR NR (purple) per day, for out of bounds (top) and default value (bottom) over the entire mission lifetime (left) and 2025 only (right).

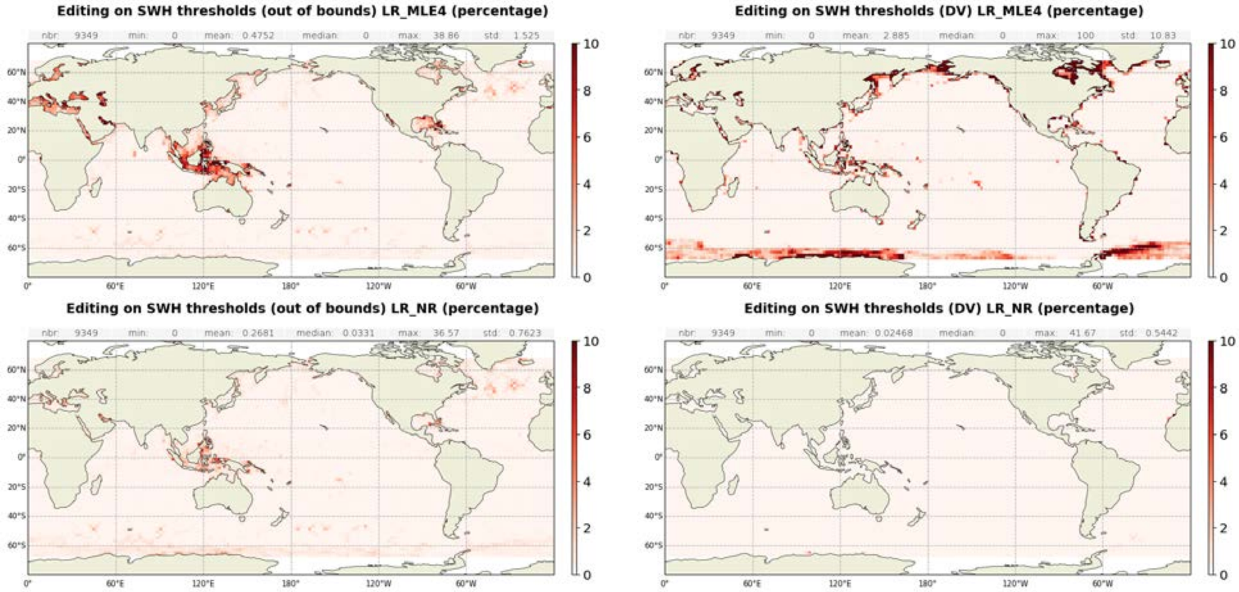

Figure 27: Maps of average percentage of data edited on SWH threshold for both LR MLE4 (top) and LR NR (bottom), for out of bounds (left) and default value (right), computed over 2025.

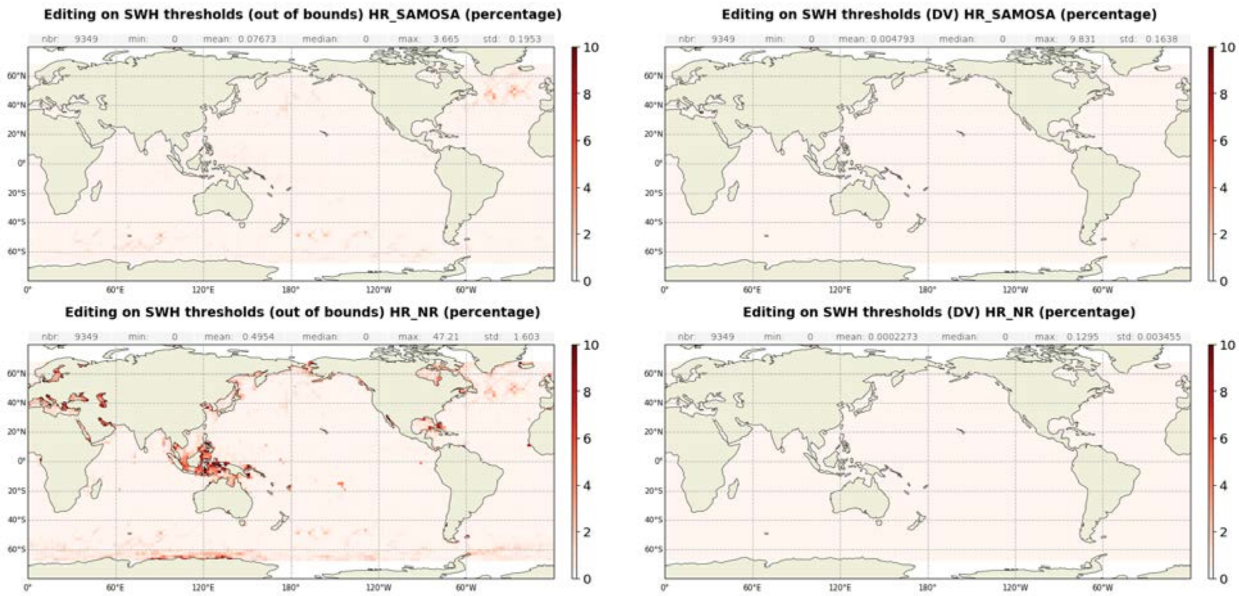

Figure 28: Maps of average percentage of data edited on SWH threshold for both HR SAMOSA (top) and HR NR (bottom), for out of bounds (left) and default value (right), computed over 2025.

Wind speed

The percentage of edited measurements due to altimeter wind speed criterion is represented on figure 29. It is about 2.18 % for LR MLE4, 0.86 % for LR NR, 1.20 % for HR SAMOSA and 0.95 % for HR NR. Measurements are exclusively edited because of default values.

Wind speed is also edited when it includes negative values. Nevertheless, sea state bias is available even for negative wind speed values. Therefore, the percentage of edited altimeter wind speed data is higher than the percentage of edited sea state bias data (Table 4).

Maps on figure 30 showing percentage of measurements edited by altimeter wind speed criterion is correlated with maps 27, 28 (SWH), and 24, 25 (sigma0).

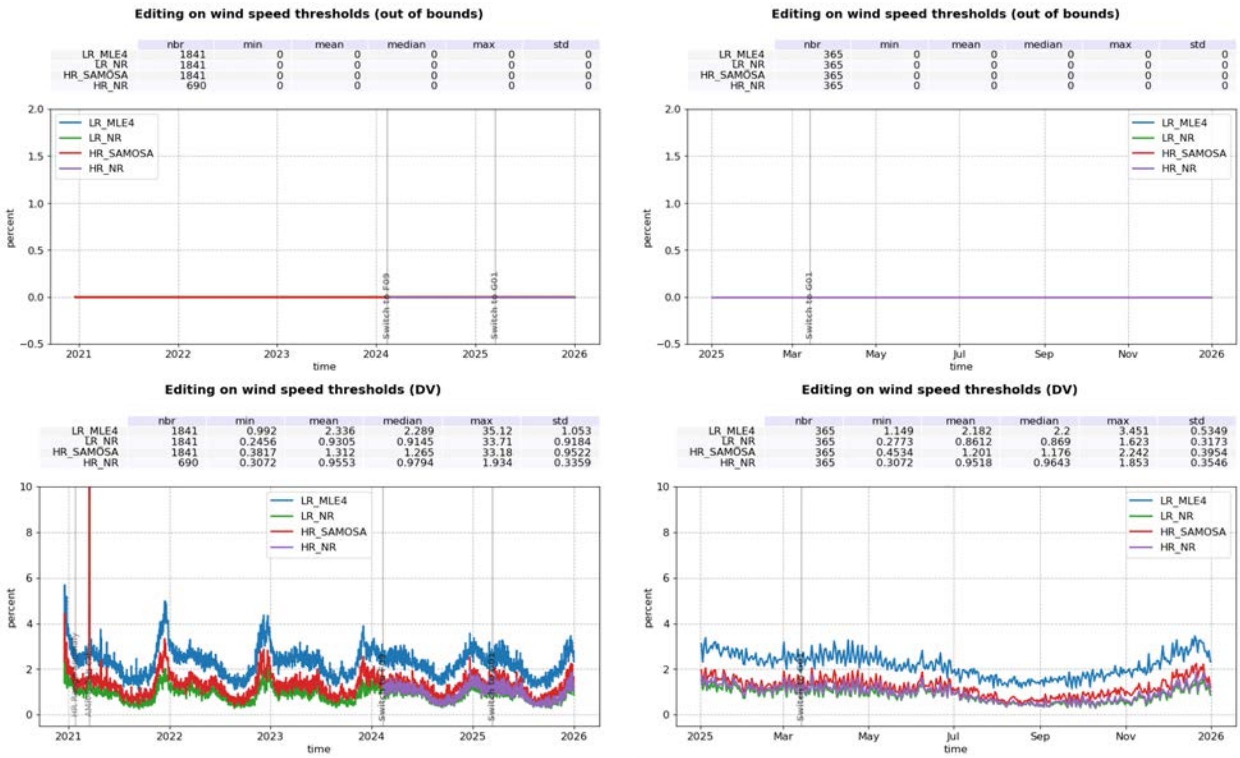

Figure 29: Percentage of data edited on wind speed threshold for LR MLE4 (blue), LR NR (green), HR SAMOSA (red) and HR NR (purple) per day, for out of bounds (top) and default value (bottom) over the entire mission lifetime (left) and 2025 only (right).

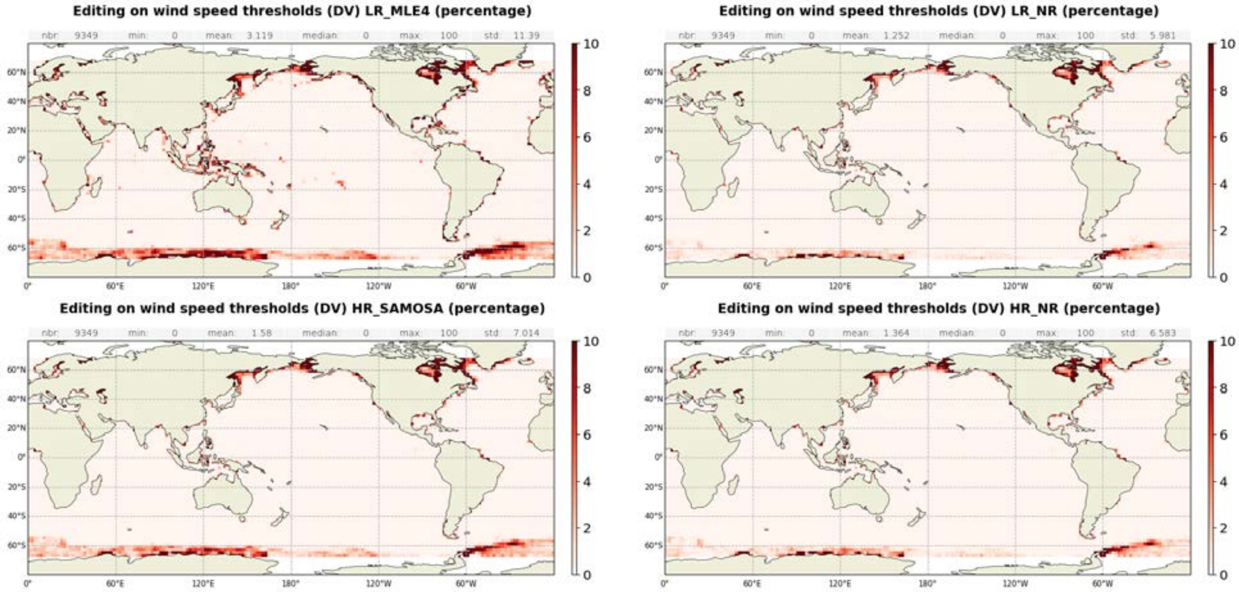

Figure 30: Maps of average percentage of data edited on wind speed threshold for LR MLE4 (top left), LR NR (right top), HR SAMOSA (bottom left) and HR NR (bottom right), for default value, computed over 2025.

Sea state bias

Regarding the sea state bias criterion, the percentage of edited measurements is about 2.02 % in LR MLE4, 0.01 % in LR NR and less than 0.01 % for HR retrackings. These are exclusively due to default value data (figure 31). The difference can also be observed on wind-speed and significant wave height threshold criteria (which are both used for SSB computation).

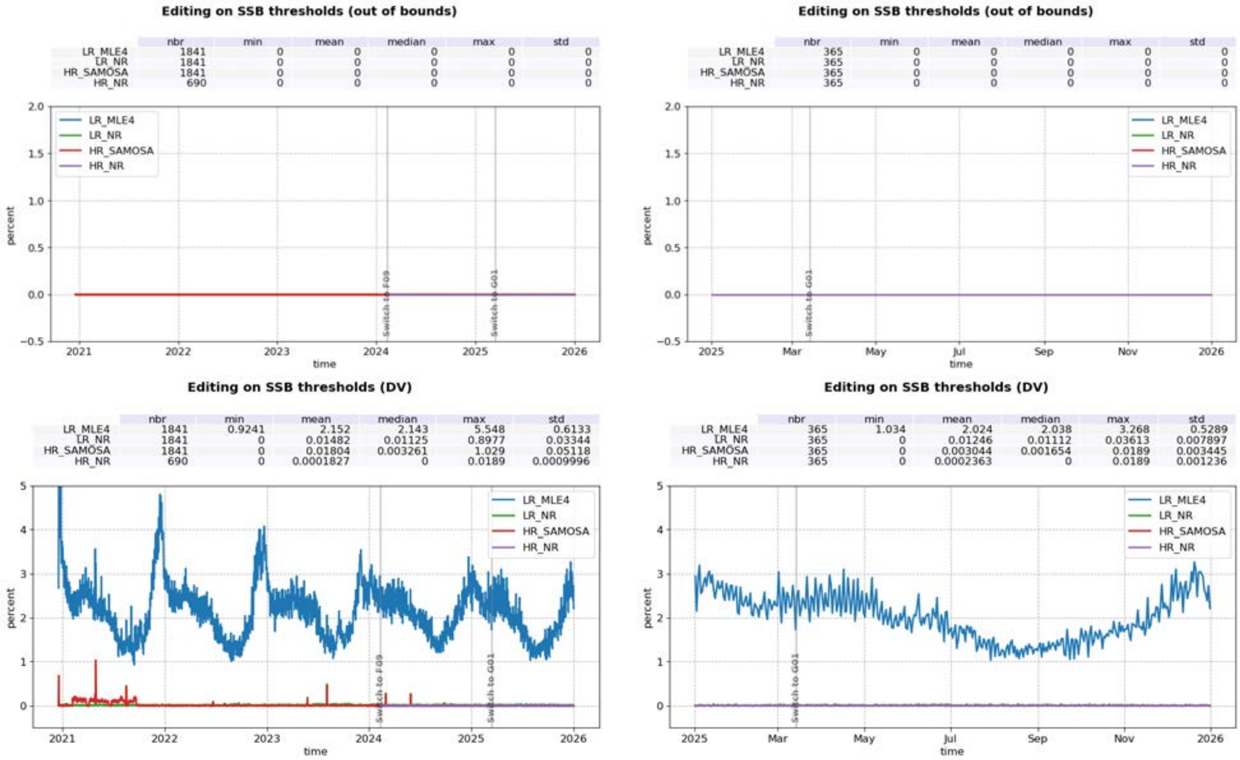

Figure 31: Percentage of data edited on SSB threshold for LR MLE4 (blue), LR NR (green), HR SAMOSA (red) and HR NR (purple) per day, for out of bounds (top) and default value (bottom) over the entire mission lifetime (left) and 2025 only (right).

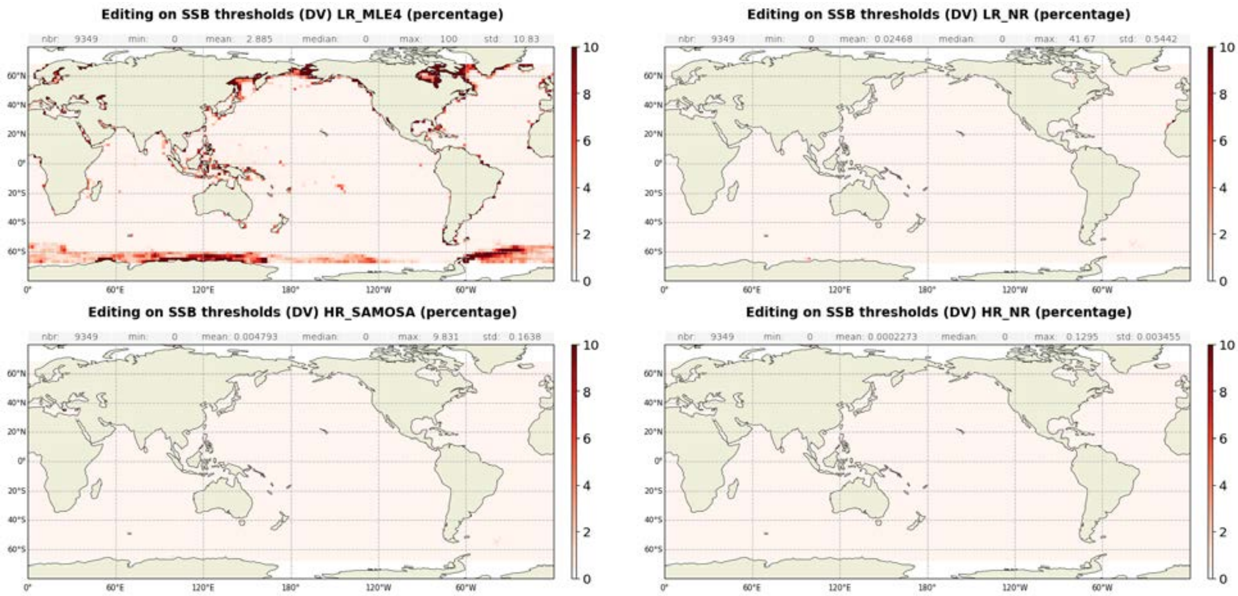

Figure 32: Maps of average percentage of data edited on SSB threshold for both LR MLE4 (top left), LR NR (top right), HR SAMOSA (bottom left) and HR NR (bottom right), for default value, computed over 2025.

Filtered ionospheric correction

The mean percentage of edited data by threshold criterion on filtered ionospheric correction is 2.74 % for LR MLE4, 2.51 % for LR NR, 2.75 % for HR SAMOSA and 2.50 % for HR NR.
Note that the ionospheric correction is only computed in LR (C-band being only available in LR) and LR MLE4 and NR ionospheric corrections are used in HR products for SAMOSA and NR respectively. The small differences visible between LR and HR monitoring in figure 33 are due to the difference in data availability between the modes.
The maps on figure 34 show that measurements edited by filtered dual frequency ionosphere correction are mostly found near coasts and at ice frontiers.

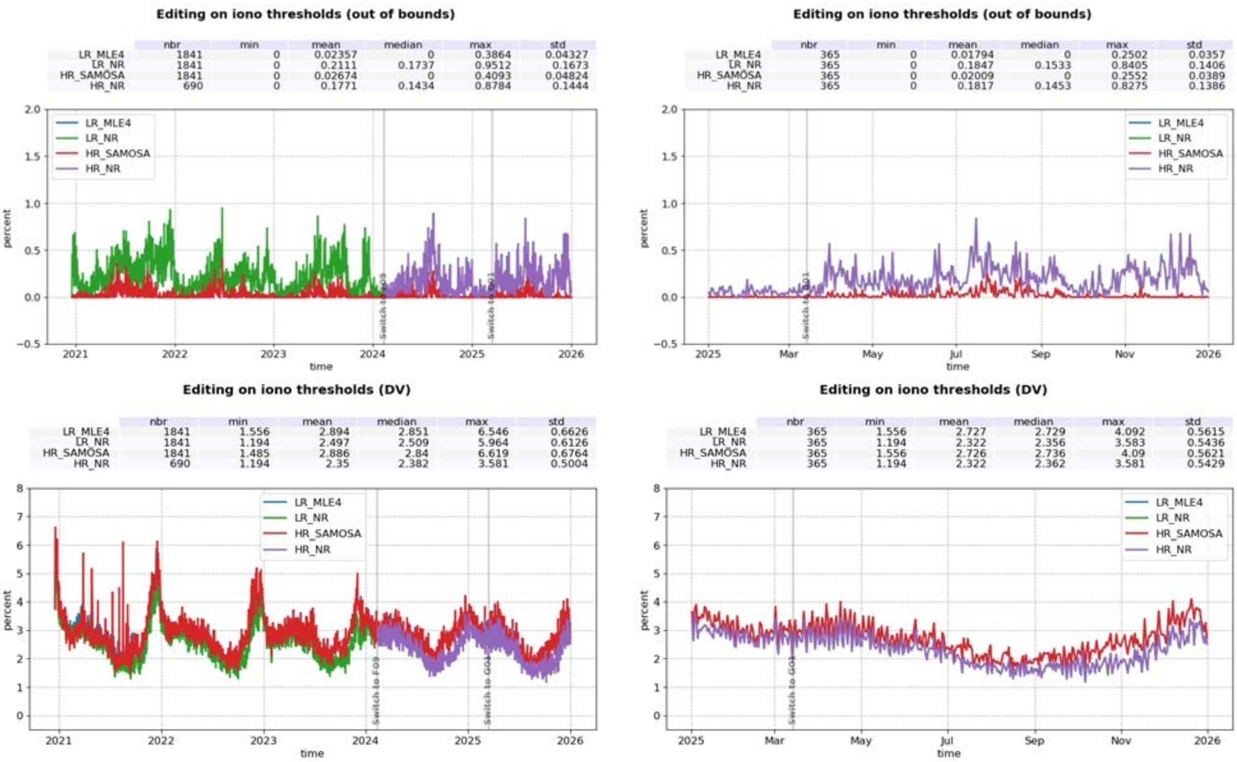

Figure 33: Percentage of data edited on filtered ionospheric correction threshold for LR MLE4 (blue), LR NR (green), HR SAMOSA (red) and HR NR (purple) per day, for out of bounds (top) and default value (bottom) over the entire mission lifetime (left) and 2025 only (right).

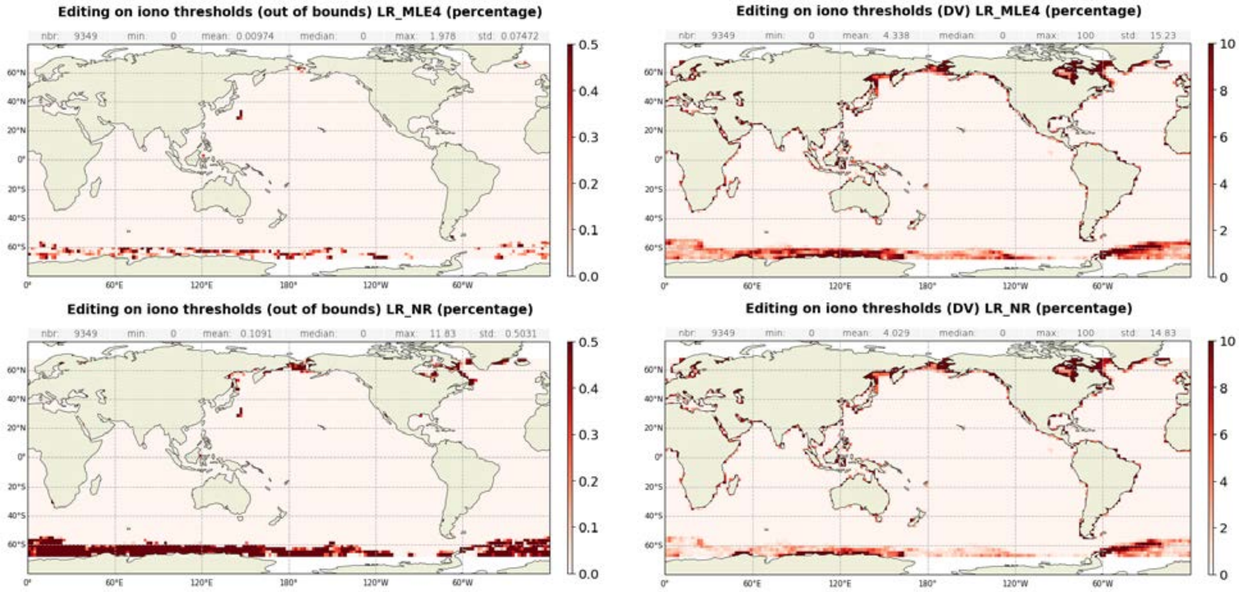

Figure 34: Maps of average percentage of data edited on LR filtered ionospheric correction threshold for both LR MLE4 (top) and LR NR (bottom), for out of bounds (left) and default value (right), computed over 2025.

Square off nadir angle

The percentage of edited data on the square off nadir angle criterion (in LR data) is 0.85 % in MLE4 and 1.46 % in NR, as shown in figure 35. Maps on figure 36 show that edited measurements are mostly found in coastal regions and regions with disturbed waveforms.

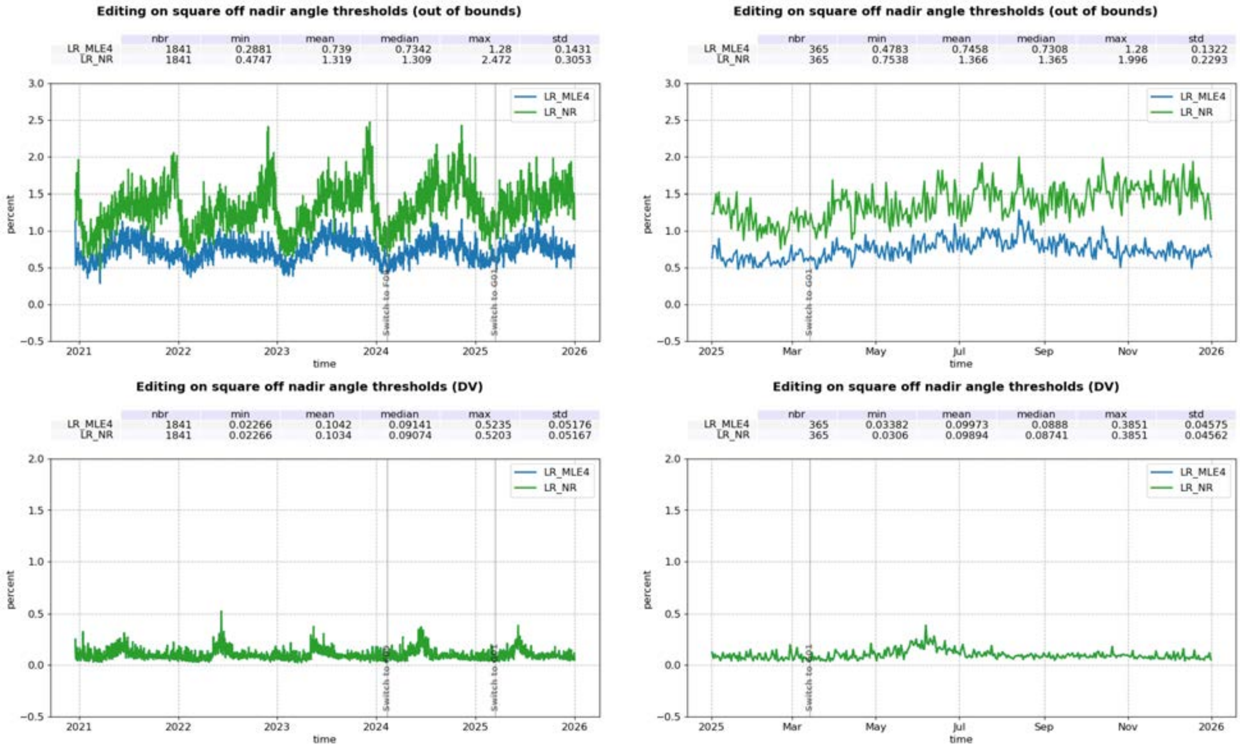

Figure 35: Percentage of data edited on square off nadir angle threshold for both LR MLE4 (blue) and LR NR (green) per day, for out of bounds (top) and default value (bottom) over the entire mission lifetime (left) and 2025 only (right).

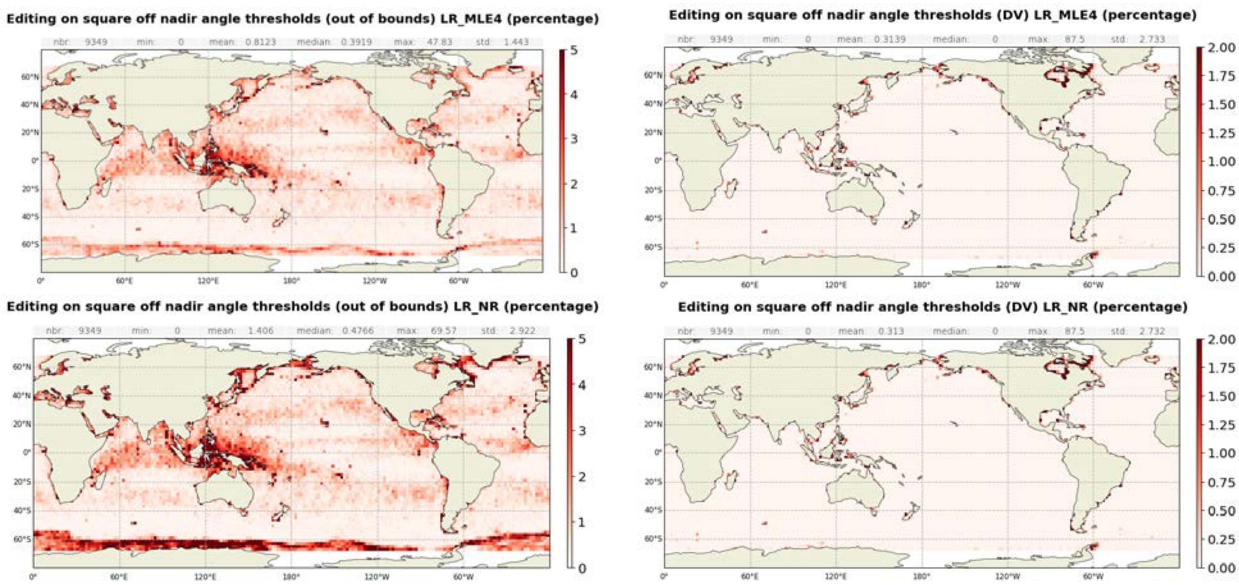

Figure 36: Maps of average percentage of data edited on square off nadir angle threshold for both LR MLE4 (top) and LR NR (bottom), for out of bounds (left) and default value (right), computed over 2025.

Ocean tide equilibrium

A very small fraction of measurements, both in LR and HR, are edited based on the equilibrium ocean tide model being at default value. This impacts about 0.06 % of data in all modes (figure 37).

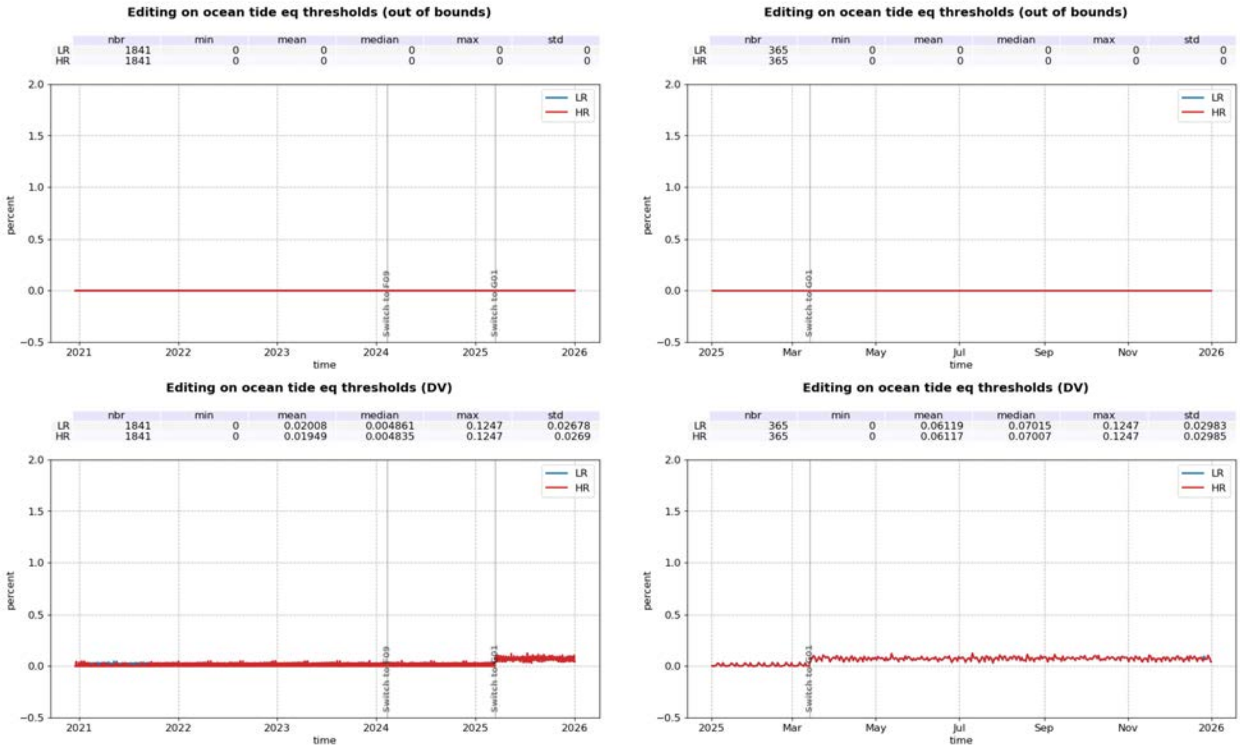

Figure 37: Percentage of data edited on equilibrium tide threshold for LR (blue) and HR (red) per day, for out of bounds (top) and default value (bottom) over the entire mission lifetime (left) and 2025 only (right).

Ocean tide

The percentage of edited measurements due to ocean tide is about 0.09 % for all processing (figure 38). The ocean tide correction is a model output, there should therefore be no edited measurement. Indeed, there are no measurements edited in open ocean areas (figure 39). These measurements are exclusively at default values.

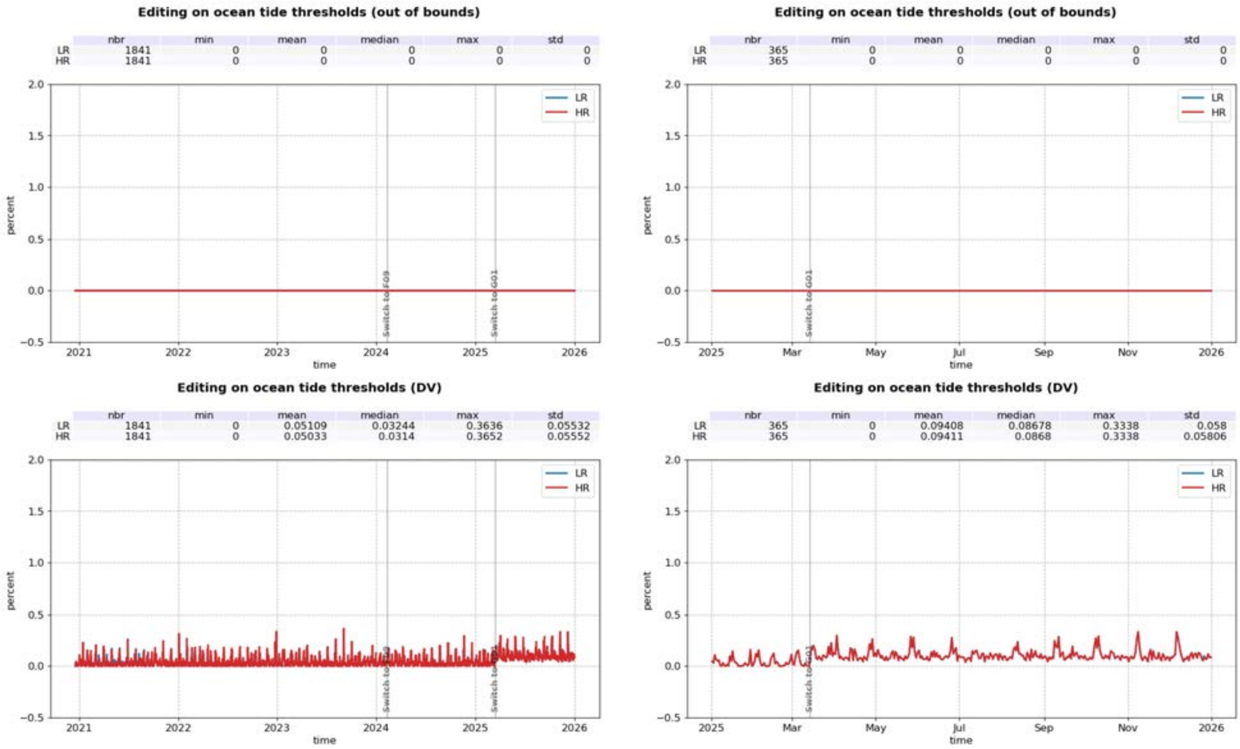

Figure 38: Percentage of data edited on ocean tide threshold for LR (blue) and HR (red) per day, for out of bounds (top) and default value (bottom) over the entire mission lifetime (left) and 2025 only (right).

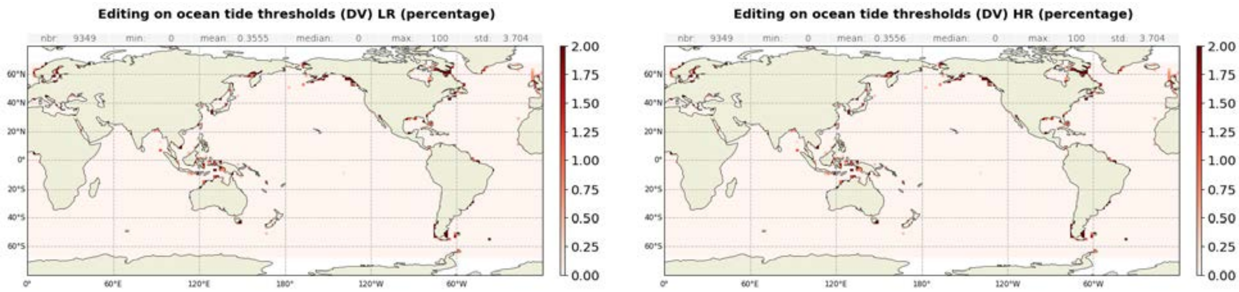

Figure 39: Maps of average percentage of data edited on ocean tide threshold for LR (left) and HR (right), for default value, computed over 2025.

Wet tropospheric correction

The percentage of edited measurements due to radiometer wet troposphere correction criterion is represented in figure 40. It is 0.09 % in both LR and HR modes. As expected, edited data are located in the ITCZ (see figure 41).
A peak of edited wet troposphere correction is observed in the LR dataset on 06/09/2025 (cycle 177, track 218), due to the nominal field being set to DV. This anomaly is linked to a ground segment anomaly (UNS 12534). This peak does not appear in the HR monitoring as the corresponding track is totally missing in this mode.

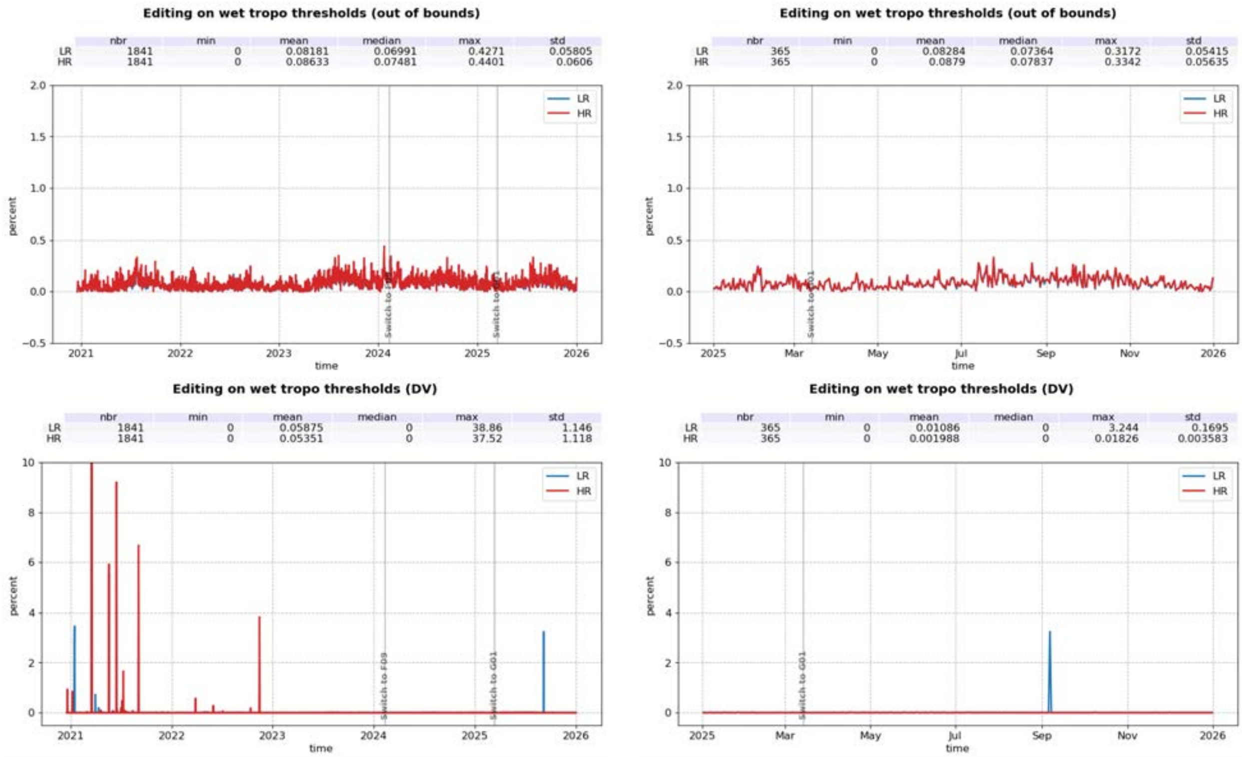

Figure 40: Percentage of data edited on wet tropospheric correction threshold for LR (blue) and HR (red) per day, for out of bounds (top) and default value (bottom) over the entire mission lifetime (left) and 2025 only (right).

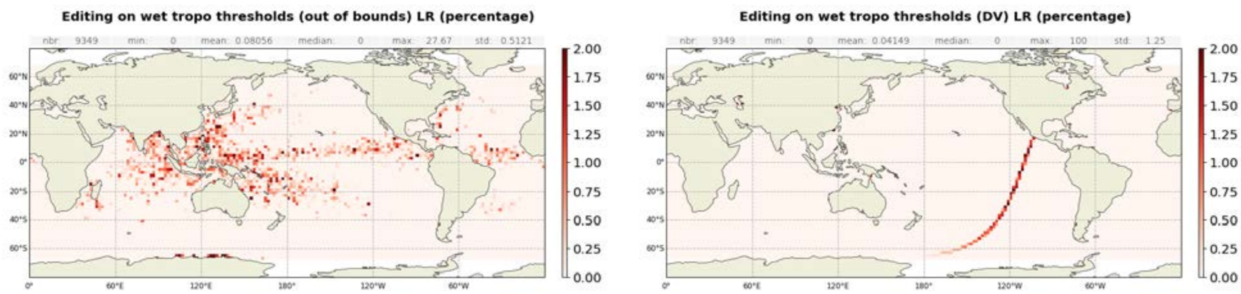

Figure 41: Maps of average percentage of data edited on radiometer wet tropospheric correction threshold, for out of bounds (left) and default value (right), computed over 2025.

Sea surface height

Uncorrected sea surface height represents the difference between the orbit and the altimeter range in Ku-band. Figure 42 summarizes the editing resulting from the sea surface height threshold criterion. It removes in average 2.32 % of data for LR MLE4, 1.73 % for LR NR and less than 0.01 % of data for HR. In LR, the editing is exclusively due to range measurements at default values near coasts, in wet zones, as well as regions with low significant wave heights or over sea ice (figure 43).

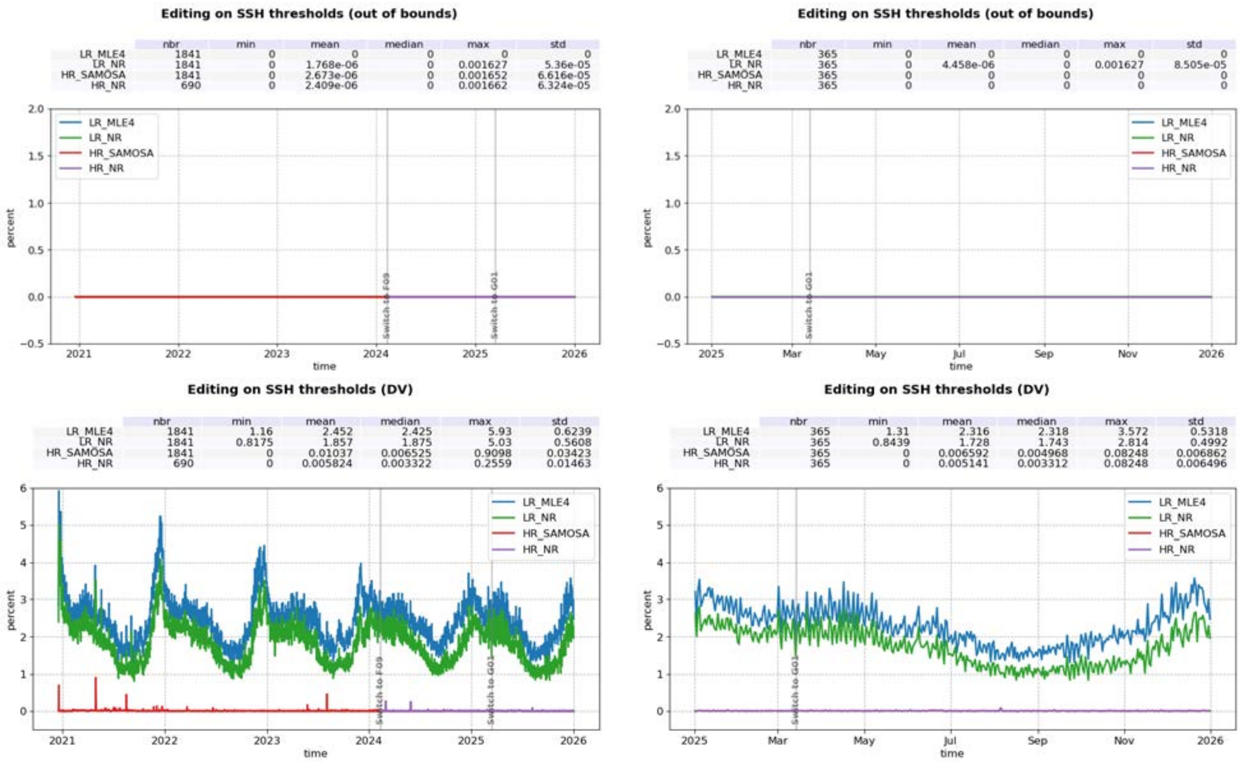

Figure 42: Percentage of data edited on SSH threshold for LR MLE4 (blue), LR NR (green), HR SAMOSA (red) and HR NR (purple) per day, for out of bounds (top) and default value (bottom) over the entire mission lifetime (left) and 2025 only (right).

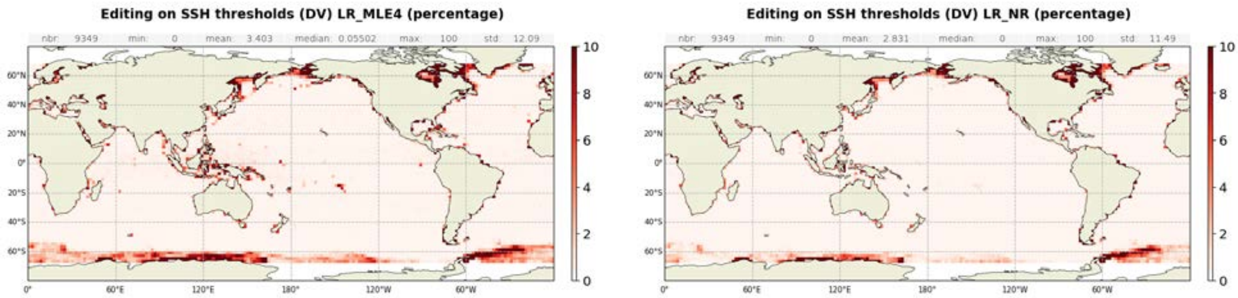

Figure 43: Maps of average percentage of data edited on SSH threshold for LR MLE4 (left), LR NR (right), for default value, computed over 2025.

Sea level anomaly

The percentages of edited data by threshold criterion on SSHA are 3.32 % in LR MLE4, 2.68 % in LR NR, 2.93 % in HR SAMOSA and 2.52 % in HR NR (figure 44) over 2025. Edited measurements are almost entirely due to the SSHA being at default value, mostly due to ionospheric correction and, for LR MLE4, SSB. Due to its decreasing level, the Caspian sea is now almost entirely edited on the SLA criterion.

A peak in edited SSHA values is observed in the LR dataset on the 06/09/2025 (cycle 177, track 218). This results from a ground segment anomaly (UNS 12534), which caused the SSHA nominal field to be flagged as DV. This peak does not appears in the HR monitoring as the corresponding track is totally missing in this mode.

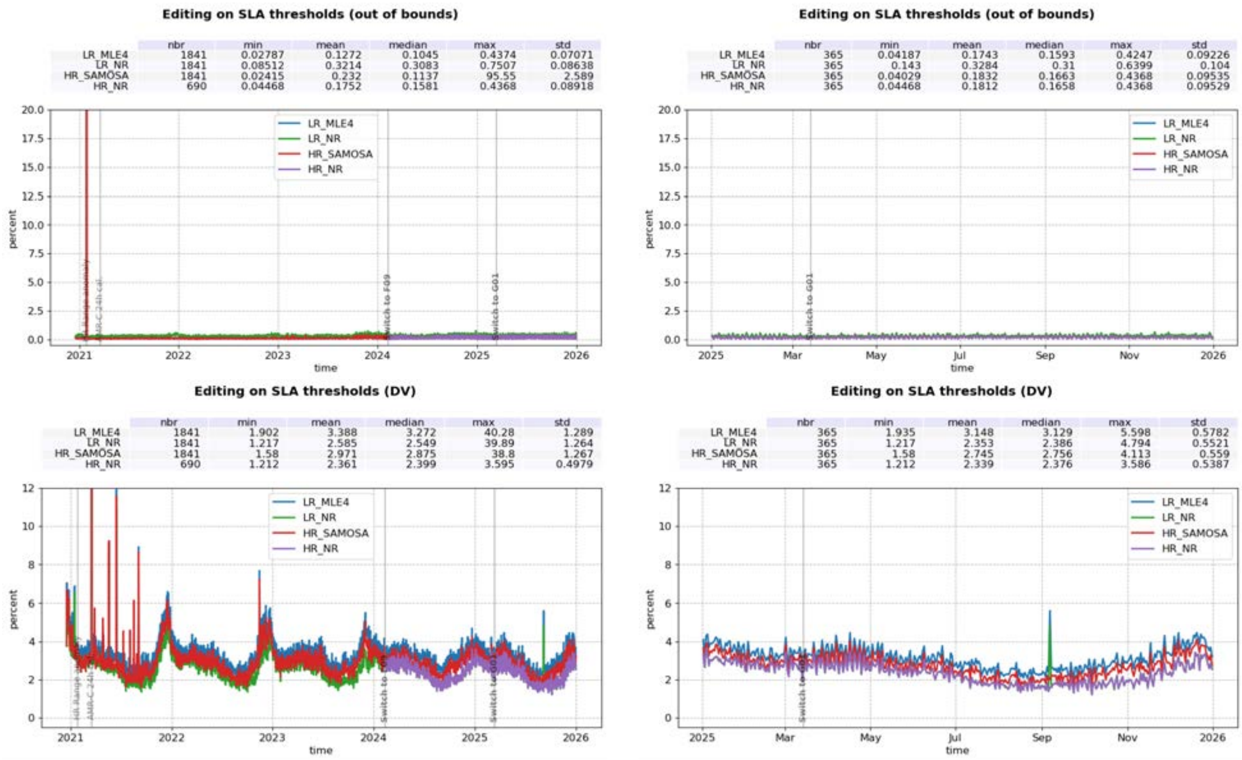

Figure 44: Percentage of data edited on SLA threshold for LR MLE4 (blue), LR NR (green), HR SAMOSA (red) and HR NR (purple) per day, for out of bounds (top) and default value (bottom) over the entire mission lifetime (left) and 2025 only (right).

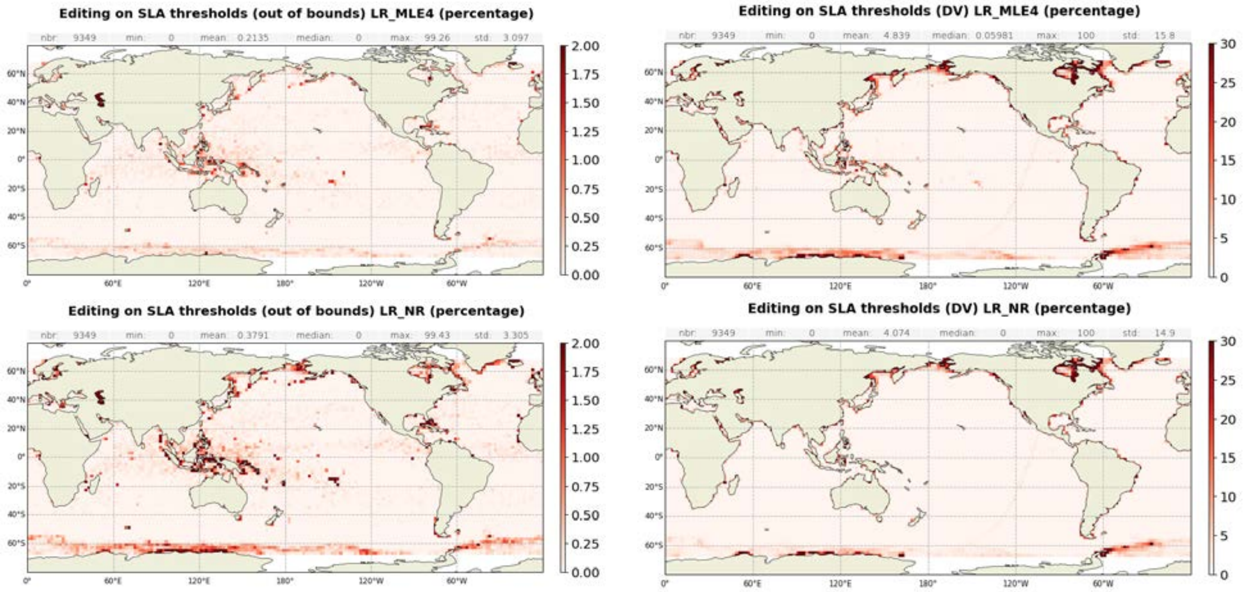

Figure 45: Maps of average percentage of data edited on SLA threshold for both LR MLE4 (top) and LR NR (bottom), for out of bounds (left) and default value (right), computed over 2025.

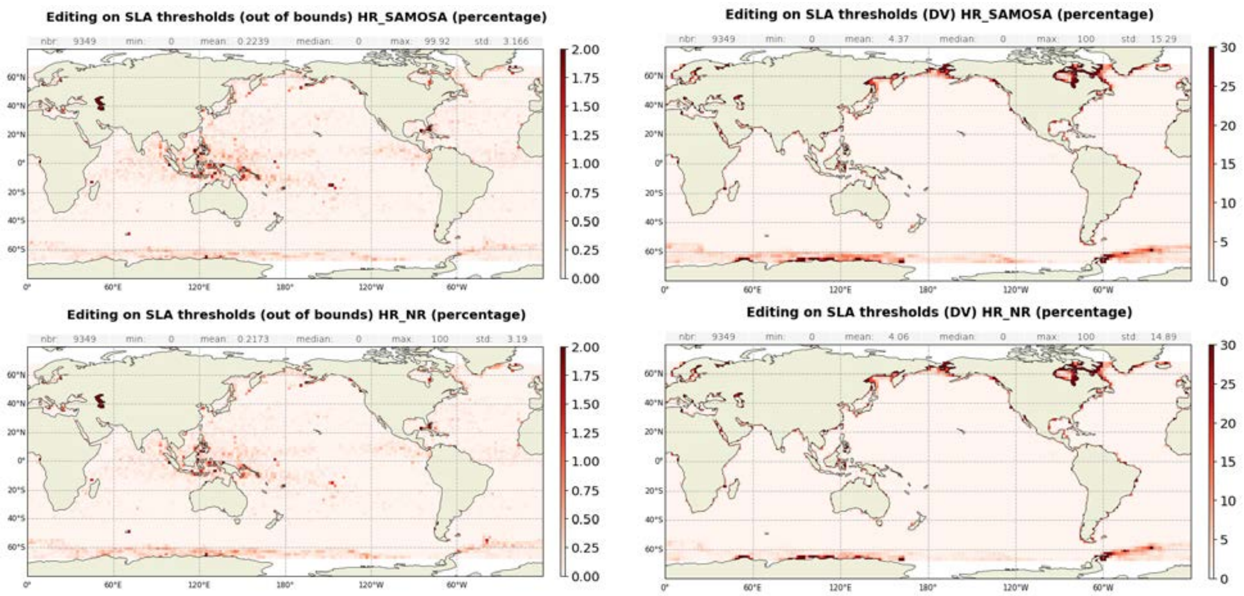

Figure 46: Maps of average percentage of data edited on SLA threshold for both HR SAMOSA (top) and HR NR (bottom), for out of bounds (left) and default value (right), computed over 2025.

4.2.4. Along-track SSHA consistency

Once the thresholds editing is applied, the consistency of the along-track sea surface height anomaly is checked. The SSHA statistics are computed on a pass-by-pass basis, using data selected over open ocean and in areas of low oceanic variability. A pair of thresholds on mean and standard deviation are set as editing criteria. The details are listed in table 5.
No pass has been edited on this criterion over the full mission lifetime.

Parameters	Set 1	Set 2
Selection		
Bathymetry	$<$-1000m	$<$-1000m
Coastal distance	$>$100km	$>$100km
Oceanic variability	$<$0.3m	$<$0.1m
Min number of measurements	3	200
Thresholds		
Mean (absolute value)	0.3m	0.15m
STD	0.4m	0.2m

Table 5: Table of parameters used for the editing on the SSHA pass statistics. These parameters are identical in HR and LR.

4.2.5. Coastal data quality

Coastal areas present a challenge due to the lower quality of altimetric measurements because of land contamination.

Figure 47 shows the percentage of edited data per day within 20 km of the coastline for both LR and HR datasets. As expected, mean values are significantly higher than over the open ocean with 60.6 % of data edited in LR MLE4, 59.9 % in LR NR, 48.6 % in HR SAMOSA and 48.9 % in LR NR.

The annual signal due to sea ice coverage is still visible, but with a larger amplitude and inverted phase compared to the global signal. This likely reflects a stronger influence of Northern Hemisphere sea ice when restricting the analysis to coastal areas, whereas the global signal is primarily driven by Southern Hemisphere sea ice coverage.

The number of edited data peaks around March, reaching approximately 70 % for LR and 60 % for HR measurements. It then gradually decreases until October, when it reaches minimum values of about 50 % for LR and 40 % for HR, before rising at a faster rate during the polar winter.

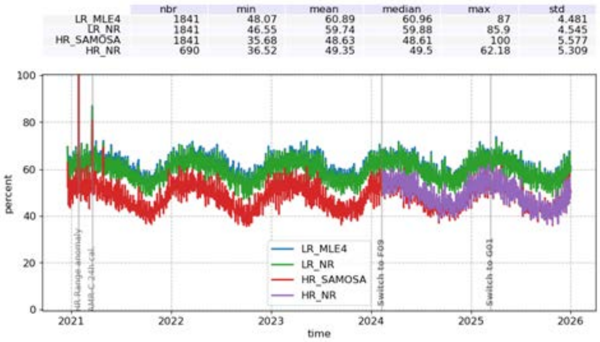

	nbr	min	mean	median	max	std
LR_MLE4	1841	48.07	60.89	60.96	87	4.481
LR_NR	1841	46.55	59.74	59.88	85.9	4.545
HR_SAMOSA	1841	35.68	48.63	48.61	100	5.577
HR_NR	690	36.52	49.35	49.5	62.18	5.309

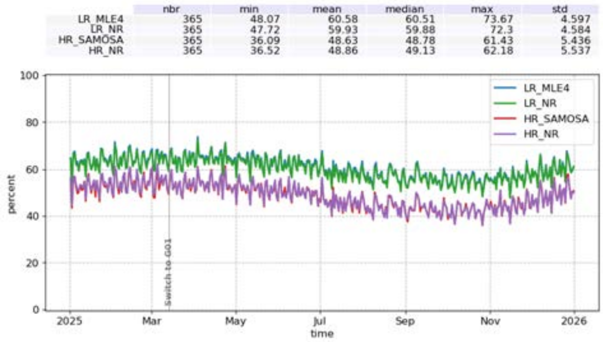

	nbr	min	mean	median	max	std
LR_MLE4	365	48.07	60.58	60.51	73.67	4.597
LR_NR	365	47.72	59.93	59.88	72.3	4.584
HR_SAMOSA	365	36.09	48.63	48.78	61.43	5.436
HR_NR	365	36.52	48.86	49.13	62.18	5.537

Figure 47: Percentage of edited data over ocean within 20 km of the coast for LR MLE4 (blue), LR NR (green), HR SAMOSA (red) and HR NR (purple) per day over the entire mission lifetime (left) and 2025 only (right).

The maps of figure 48 represent the percentage of edited coastal data for LR MLE4, LR NR, HR SAMOSA and HR NR, over the year 2025.

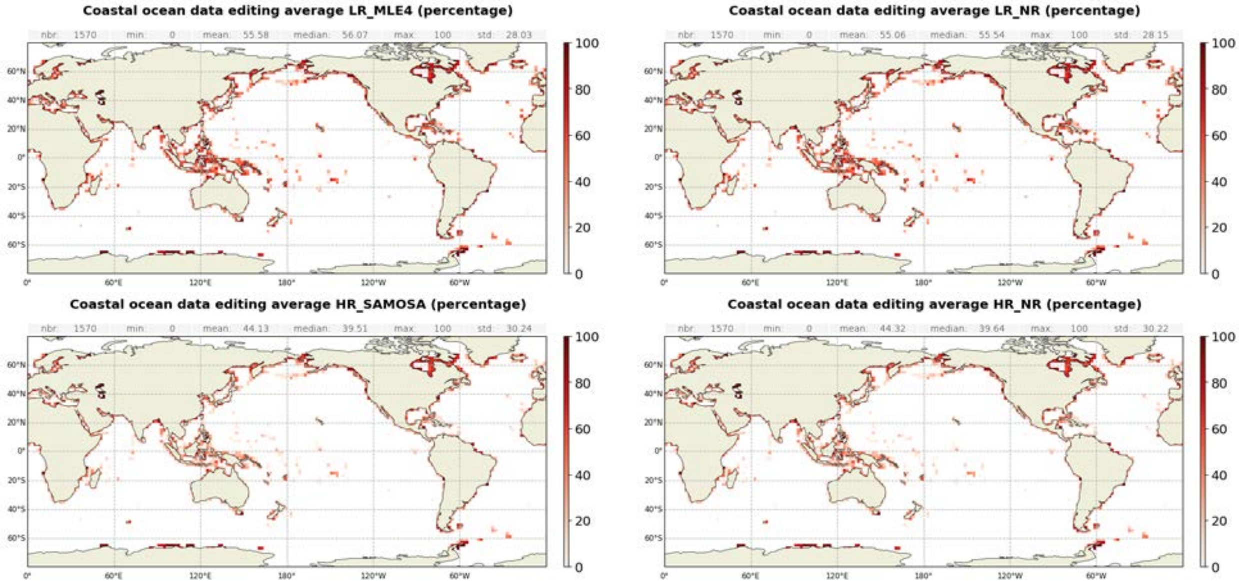

Figure 48: Maps of average percentage of edited ocean data within 20 km of the coast for LR MLE4 (top left), LR NR (top right), HR SAMOSA (bottom left) and HR NR (bottom right), computed over 2025.

4.2.6. Validated data summary

The total number of valid data over ocean is plotted for all retrackers in figure 49. In 2025, the average number of valid points per day is slightly higher for HR SAMOSA and HR NR (about 54,800 points per day) than for LR MLE4 and LR NR (about 54,000 points per day). This difference is mainly due to the better data quality provided by HR retrackers in wet-zone and coastal areas.

The impact of the wildfires near Fairbanks station is clearly visible on the 10/07/2025, with a significant reduction in the number of valid measurements due to a large amount of missing data (11 tracks affected).

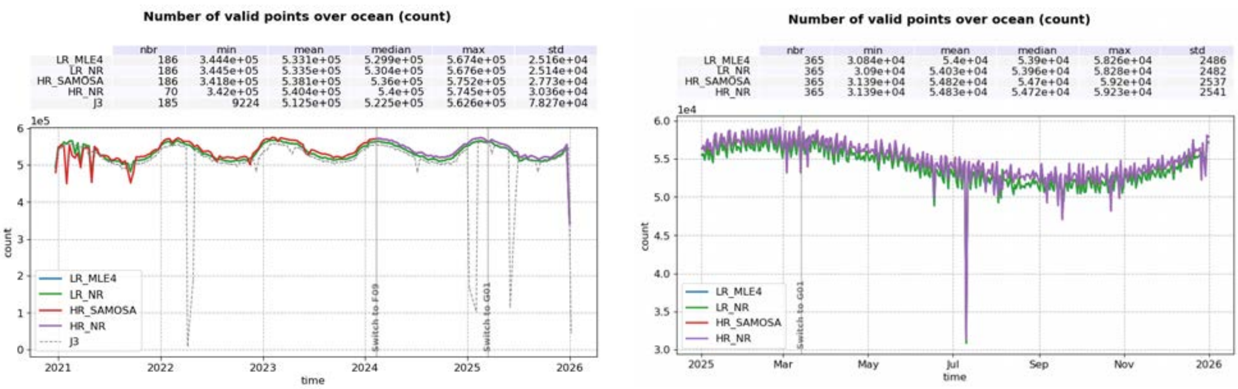

Figure 49: Total number of valid ocean measurements for LR MLE4 (blue), LR NR (green), HR SAMOSA (red) and HR NR (purple) per cycle over the entire mission lifetime (left) and per day over 2025 only (right).

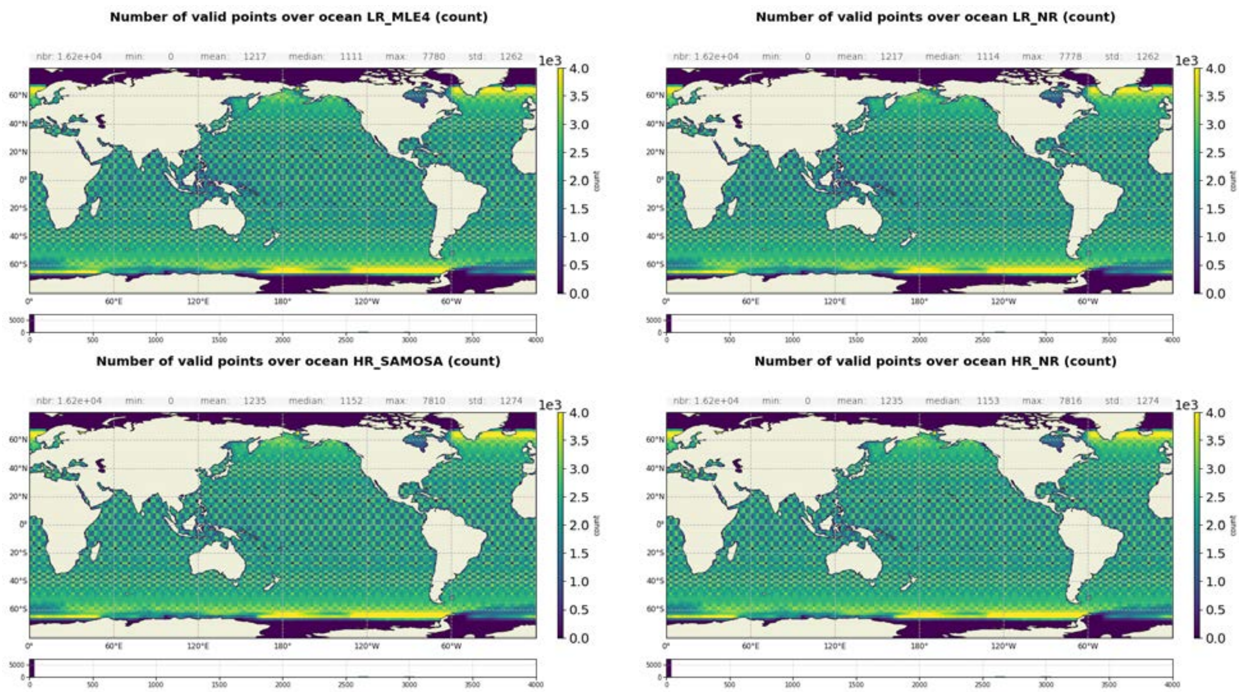

Figure 50: Total number of valid ocean measurements for LR MLE4 (top left), LR NR (top right), HR SAMOSA (bottom left) and HR NR (bottom right), computed over 2025.

5 Monitoring of altimeter and radiometer parameters

Means and standard deviations of Sentinel-6 MF main parameters have been monitored over 2025. The goal of this chapter is to summarize these monitoring, along with Jason-3 daily monitoring for comparison. Only the main results are included in this chapter.

Note that the diagnostics presented in this section include data processed with both the F09 and G01 processing baselines, resulting in non-homogeneous products such as maps and histograms. Analyses based on homogeneous metrics are provided in the G01 reprocessing report ([8]).

5.1. 20 Hz range measurements

The monitoring of the number and standard deviation of 20 Hz elementary range measurements used to derive 1 Hz data is presented here. These two parameters are computed during the altimeter ground processing. Before performing a regression to derive the 1 Hz range from 20 Hz data, a MQE (mean quadratic error) criterion is used to select valid 20 Hz measurements. This first step of selection consists in verifying that the 20 Hz waveforms can be approximated by a Brown echo model (Brown, 1977 [11], Thibaut et al. 2002 [12]).
Then, through an iterative regression process, elementary ranges too far from the regression line are discarded until convergence is reached. Details on this process are available in the Sentinel-6 MF L2 Product Generation Specification [3]. Thus, monitoring the number of 20 Hz range measurements and the standard deviation computed among them is likely to reveal changes at instrumental level.

5.1.1. 20 Hz range measurements number

Figure 51 presents the average number of 20 Hz elementary range measurements used to derive 1 Hz range estimates in Ku and C-band. In Ku-band, a higher average number of elementary measurements is used in LR mode (19.6 for both MLE4 and NR) than in HR (18.5 for both SAMOSA and NR), while LR C-band lies in between (19.1).
These values are stable over time and are in line with Jason-3 for LR data. Note that variations in Jason-3 can be observed from April to May, corresponding to orbit changes during the tandem phase with Sentinel-6 MF.

A slight latitude dependency can be seen in Ku-band for Sentinel-6 MF (figure 52), with lower values at high latitude. This is expected because the Sentinel-6 MF PRF varies with altitude, the number of averaged 20Hz measurements is slightly lower at high latitudes. The behavior is different on Jason-3 (bottom panel), more dependent on sea state conditions. For the C band (figure 53), values are lower near the coast and at high latitudes. This is expected as C band has a larger footprint than Ku band, and is more sensitive to coastline and ice presence.

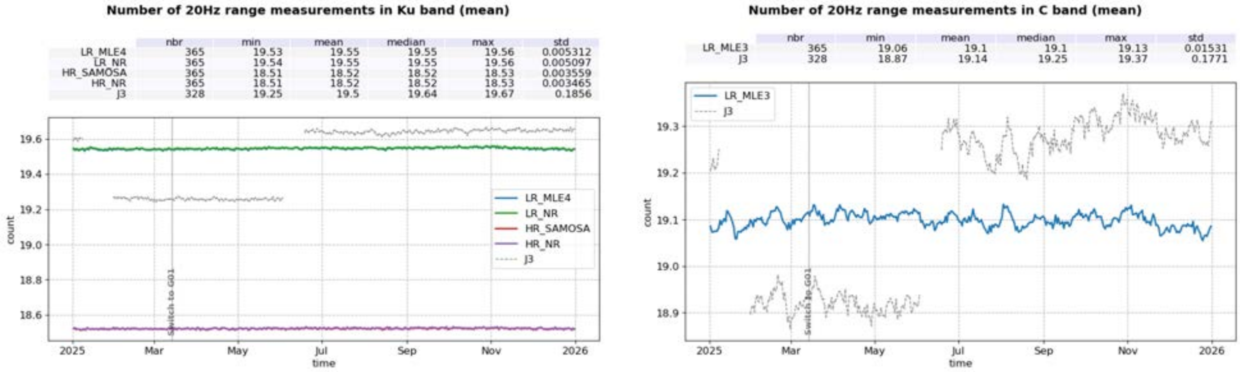

Figure 51: Mean number of 20Hz range measurements for LR MLE4 (blue), LR NR (green), HR SAMOSA (red) and HR NR (purple) per day, in Ku-band (left) and C-band (right, LR MLE3 only).

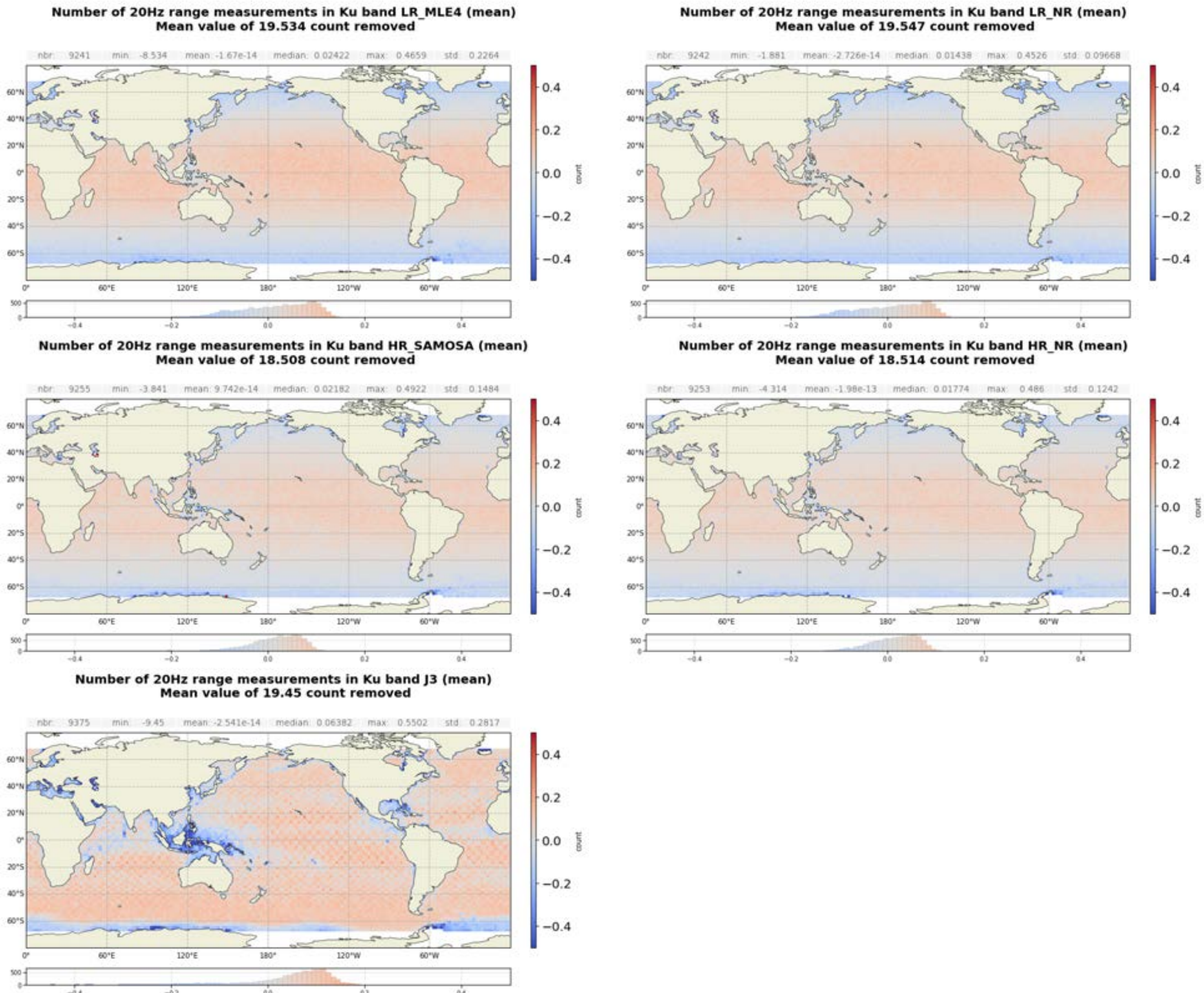

Figure 52: Centred maps of mean number of 20Hz range measurements. Top: maps for Sentinel-6 MF LR Ku band (left : MLE4, right : NR), middle: maps for Sentinel-6 MF HR (left : SAMOSA , right : NR), bottom : map for Jason-3 Ku band. Computed over 2025.

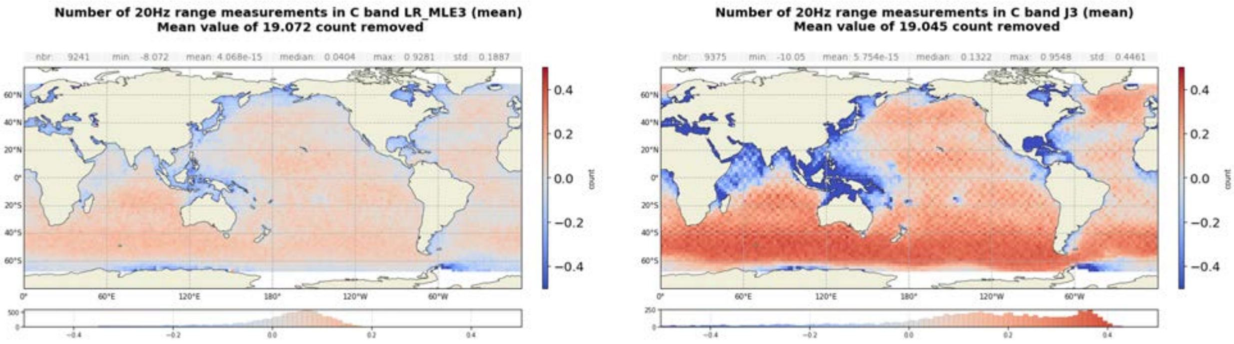

Figure 53: Centred maps of mean number of 20Hz range measurements in C band for Sentinel-6 MF (left) and Jason-3 (right).

5.1.2. 20 Hz range measurements standard deviation

Figure 54 presents the standard deviation of the 20 Hz elementary range measurements used to derive 1Hz ranges in Ku and C band (left and right panels respectively) per day. In Ku-band, Sentinel-6 MF LR range standard deviation is similar between MLE4 and NR, and lower than Jason-3 by 1.0 cm on average. It shows the improvement brought by Sentinel-6 MF in terms of noise.
Sentinel-6 MF HR range noise is even lower than LR, by 2.8 cm for both SAMOSA and NR, thanks to the HR processing.

Due to the reduced number of pulses, Sentinel-6 MF C-band range standard deviation (26.2 cm) is higher than Jason-3 (17.5 cm).

Standard deviation of measurements is correlated to significant wave height (figure 55).

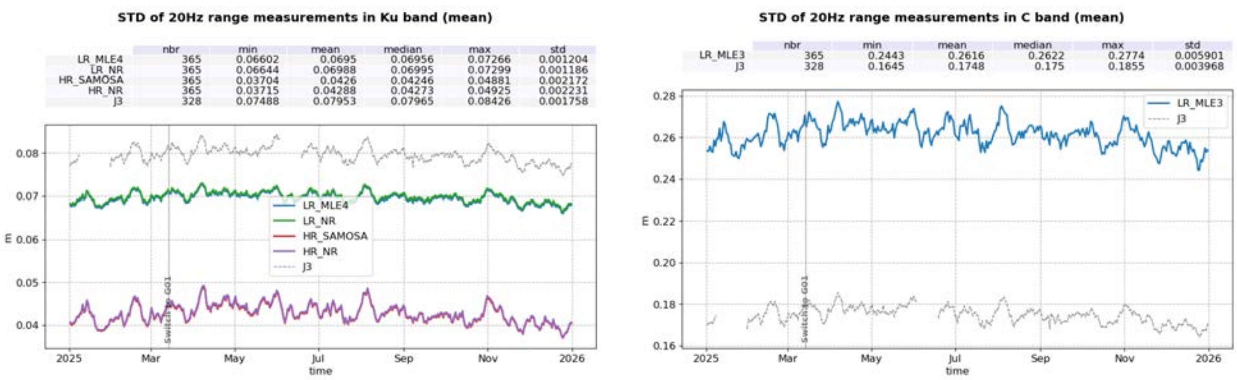

Figure 54: Mean STD of 20Hz range measurements for LR MLE4 (blue), LR NR (green), HR SAMOSA (red) and HR NR (purple) per day, in Ku-band (left) and C-band (right, LR MLE3 only, in blue).

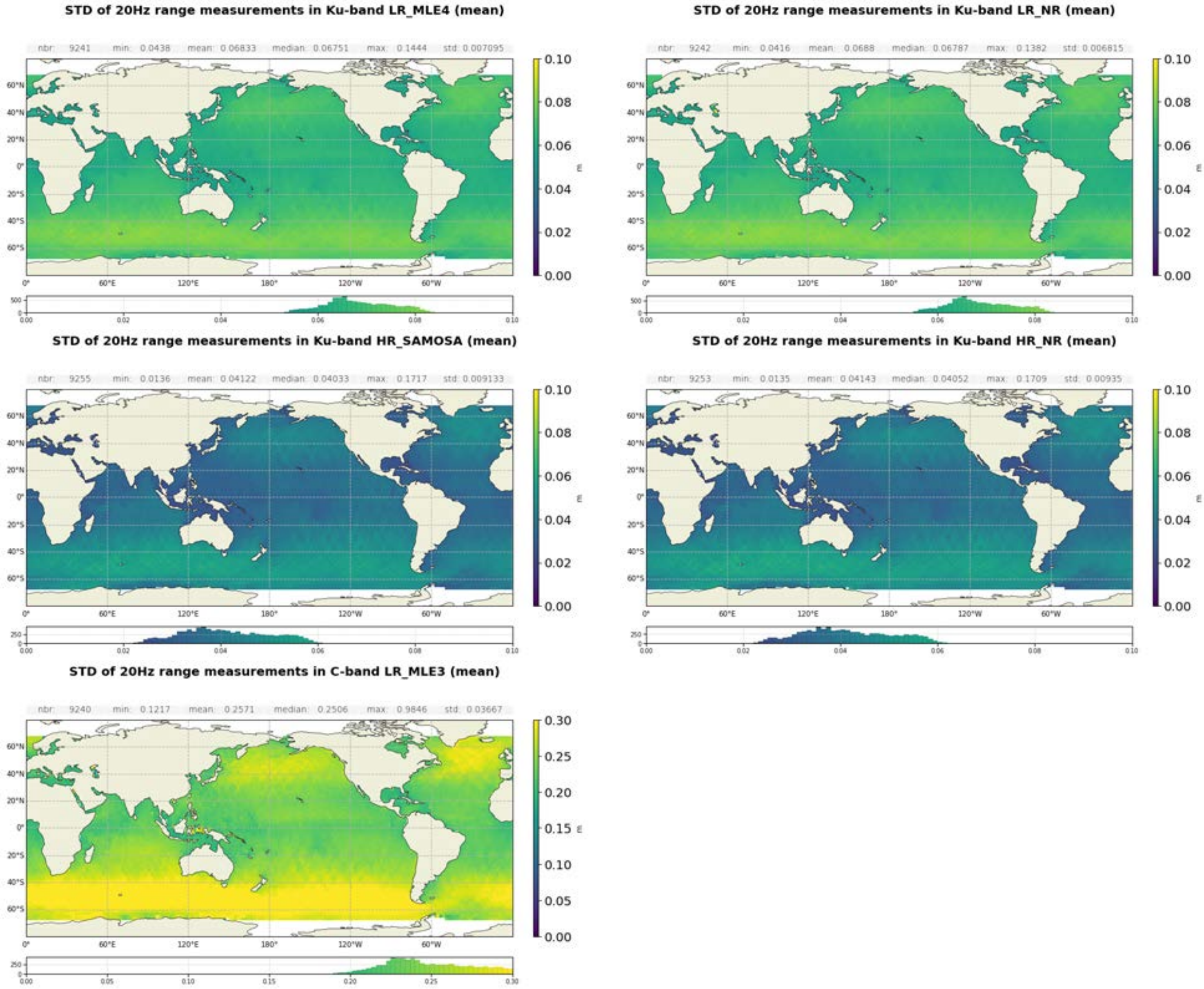

Figure 55: Maps of mean STD of 20Hz range measurements for Ku-band LR MLE4 (top left), LR NR (top right), HR SAMOSA (middle left), HR NR (middle right) and C band (bottom). Computed over 2025.

5.2. Off nadir angle from waveform

This section analyses the square of the off-nadir angle derived from MLE4 and NR waveform retrackers from LR dataset. The off-nadir angle is derived from the slope of the trailing edge of the waveform during the altimeter processing: it can either be caused by real platform mispointing or by backscattering properties of the surface.

The square of the off-nadir angle, averaged on a daily basis (taking into account valid measurements only), has been plotted for Sentinel-6 MF and Jason-3 on figure 56. PB G01 allowed to align MLE4 mispointing with NR thanks to the update of MLE4 instrumental Look-Up Tables, with a mean value of 0.003 deg^2. Prior to this update, MLE4 mispointing was 0.005 deg^2 higher than NR one. Apart from this improvement, all three time series are stable in time.

The corresponding maps for 2025, presented on figure 57, shows higher square off nadir angle in coastal areas and around Indonesia. Figure 58 shows the dependency between the waveform mispointing and the SWH. Mispointing is higher at low SWH (above 0.03 deg^2 at 0 m for both NR and MLE4), however there is no correlation above 2m SWH for either MLE4 and NR.
The standard deviation of the square off nadir angle (right panel) is also much higher at low SWH.

The mispointing distributions are presented in Figure 59 for Sentinel-6 MF and Jason-3. Sentinal-6 MF distribution is centered around 0.004 and 0.003 deg^2 for MLE4 and NR respectively, while Jason-3's is centered on 0.

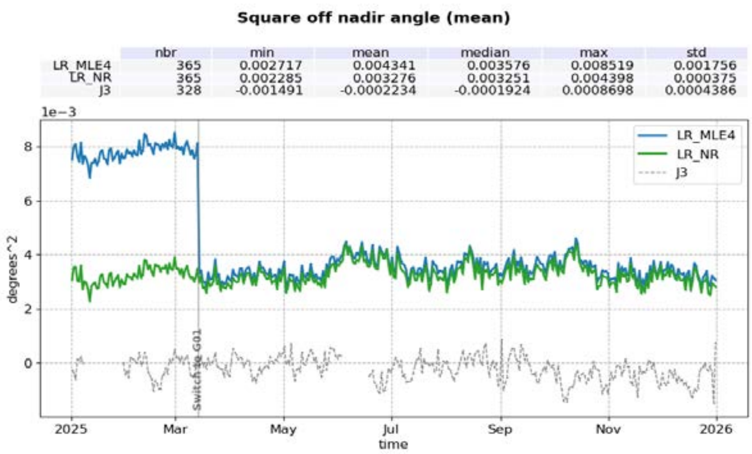

Figure 56: Mean square off nadir angle per day for LR MLE4 (blue) and LR NR (green).

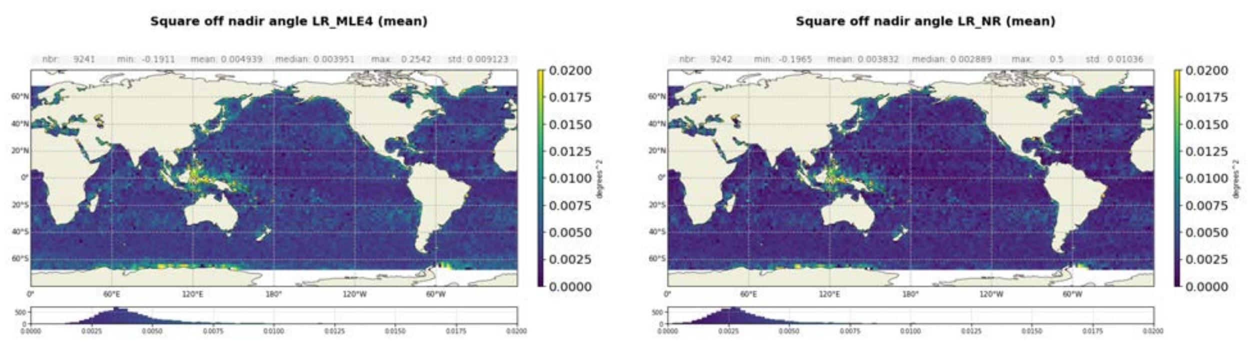

Figure 57: Map of mean square off nadir angle for LR MLE4 (left) and LR NR (right). Computed over 2025.

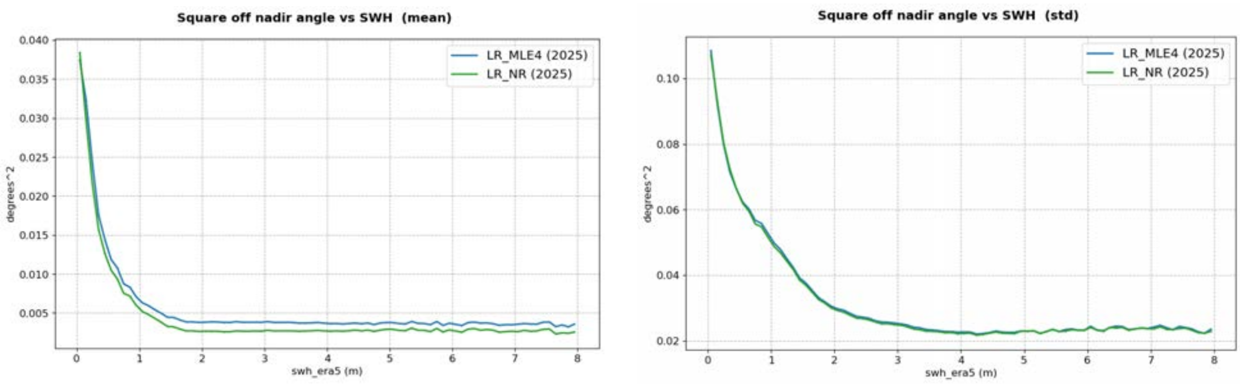

Figure 58: Square off nadir angle wrt SWH for MLE4 (blue) and NR (green).

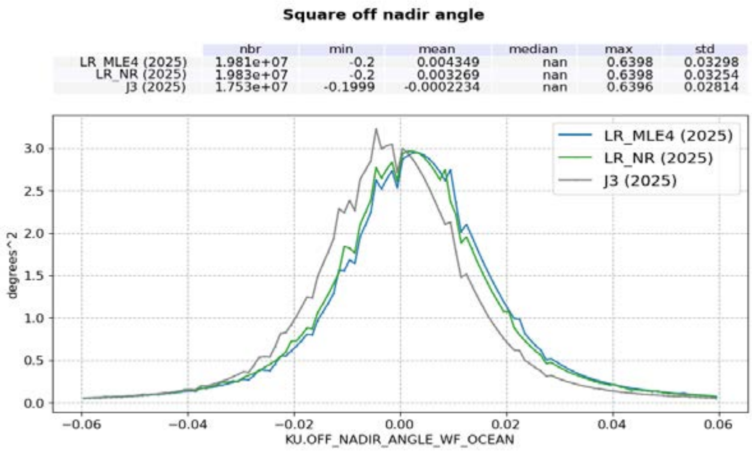

Figure 59: Histogram of square off nadir angle for Sentinel-6 MF MLE4 (blue), NR (green) and Jason-3 (black).

5.3. Range

The mean differences between Sentinel-6 MF HR and LR ranges are centered around 1.6 cm for HR SAMOSA - LR MLE4 (figure 60 in black) and less than 1 mm for HR NR - LR NR (in grey). At the PB G01 update, a jump of about -5 mm is visible for HR SAMOSA - LR MLE4. It is due to the external path delay update as well as an erroneous LUT update which has been corrected on April 14, resulting in a second jump of about + 2mm.

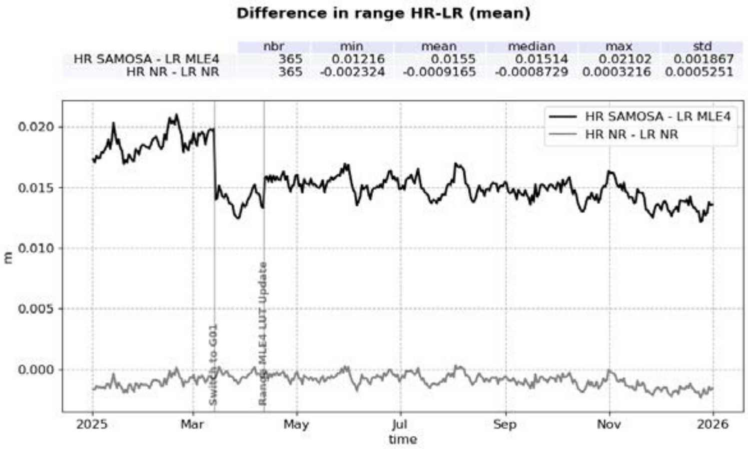

Figure 60: HR SAMOSA - LR MLE4 (black) and HR NR - LR NR (grey) differences in range per day.

The biases between HR and LR ranges are strongly correlated to SWH, as shown in figure 61. Between HR SAMOSA and LR MLE4, the range bias increases by 3.8 cm between 1 and 7 m waves. This correlation is mostly explained by the impact of the different values of wave skewness coefficient used in the LR retrackings (skewness 0.1) and in the HR SAMOSA retracking side (no skewness). This is why the correlation is reduced to about +2.0 cm between 1 and 7 m SWH in the bias between HR NR, which has a skewness set to 0.1 as well, and LR NR. The residual dependency between LR NR and HR NR is under investigation and probably partly due to the pulse-to-pulse correlation effect on LR data. An update of the alpha-p LUT function for HR SAMOSA to account for the skewness would improve consistency with other retrackers.

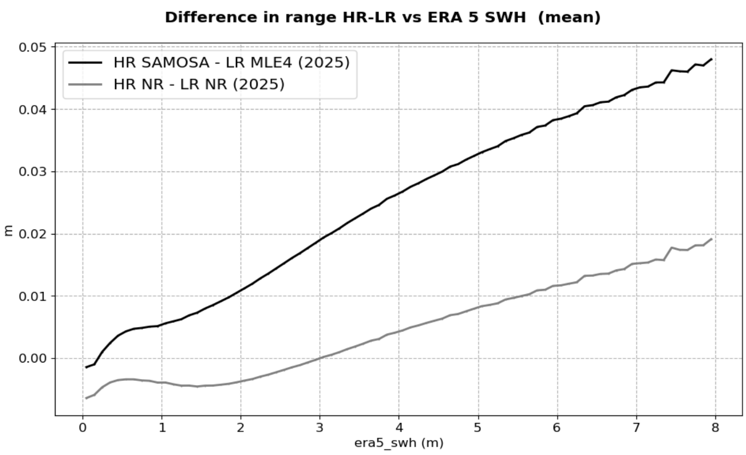

Figure 61: HR SAMOSA - LR MLE4 (black) and HR NR - LR NR (grey) range differences as a function of ERA5 model SWH.

Along track wind has a known effect on HR data and more particularly on HR range [13]. To highlight this impact, two gridded maps of HR (SAMOSA and NR respectively) versus LR (MLE4 and NR respectively) range differences are drawn on figures 62 and 63 respectively, one for ascending tracks and the other one for descending tracks. Next, the difference between these two maps is computed (ascending minus descending). Such a process allows to remove all systematic errors on the bias (such as waves) and to only highlight HR variations with respect to LR that depend on track direction. In both cases, bottom left panels clearly show an anti-correlation to meridional wind patterns (bottom right), ranging between -1 and 1 cm.

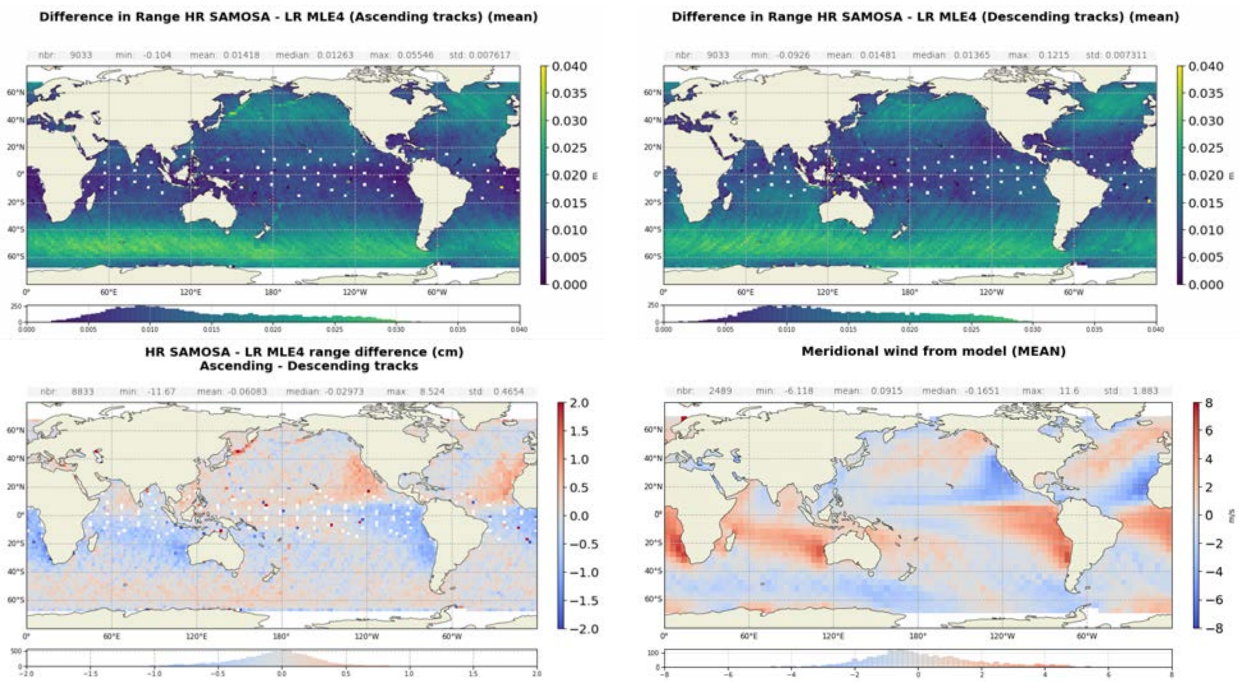

Figure 62: Maps of HR SAMOSA - LR MLE4 difference in range, for ascending tracks (top left) and descending tracks (top right). Bottom left: difference of the two maps above. Bottom right : along-track wind from model. Computed over 2025.

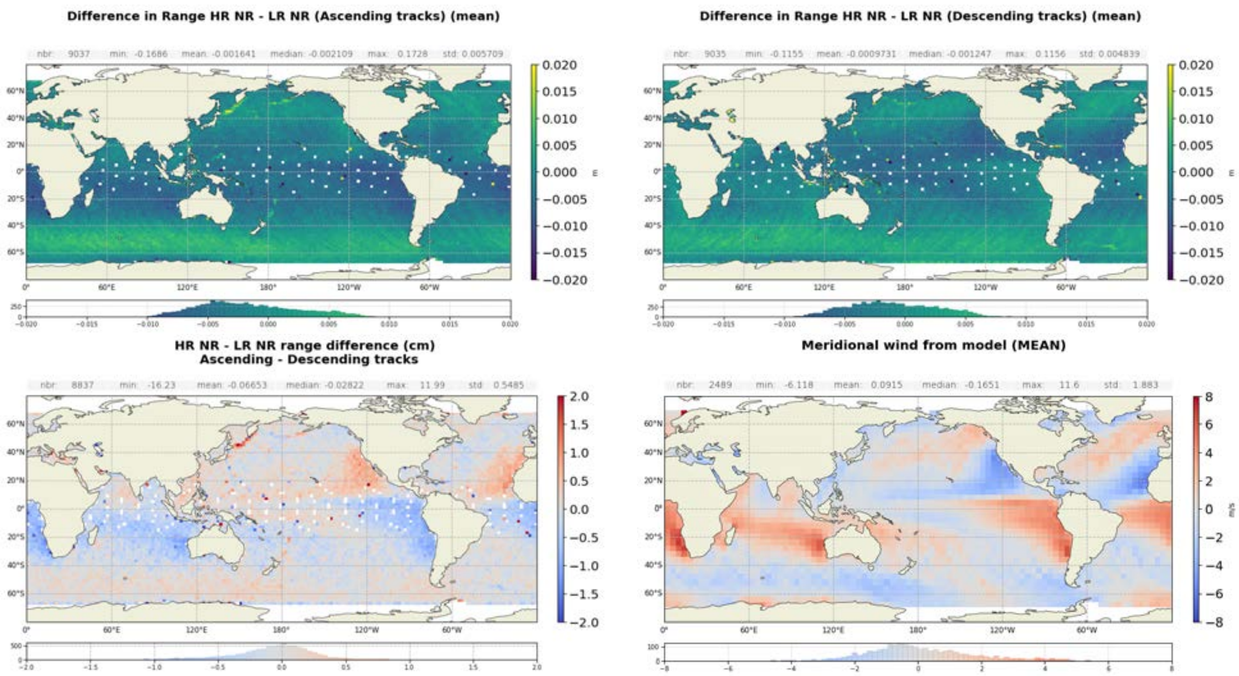

Figure 63: Maps of HR NR - LR NR difference in range, for ascending tracks (top left) and descending tracks (top right). Bottom left: difference of the two maps above. Bottom right : along-track wind from model. Computed over 2025.

The daily monitoring of LR NR - LR MLE4 range difference is presented on figure 65. A -5 mm jump is observed at the time of the PB G01 deployment, followed by a +2 mm jump associated with the LUT correction applied exclusively to the MLE4 range, ultimately bringing LR MLE4 and LR NR ranges into full consistency. The jump of -2 mm visible at the date of the PB F09 deployment is related with a constant bias introduced to correct the LR NR retracker. Note that the time series is still too short to quantify the impact of the NR on long-term stability with respect to MLE4. The standard deviation monitoring (right panel) presents a yearly variation with higher values from June to September and lower values from December to May, and can be linked with seasonal SWH variations (cf below).
The distributions of range biases are presented in figure 64. LR bias is 0.4 mm while HR bias is less stable due to skewness difference and centered around 16.1 mm.

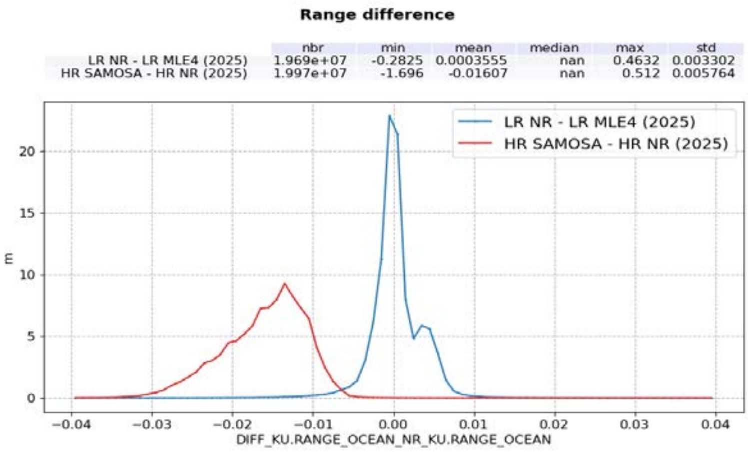

Figure 64: Histogram of HR SAMOSA - LR MLE4 (blue) and HR NR - LR NR (red) differences in range.

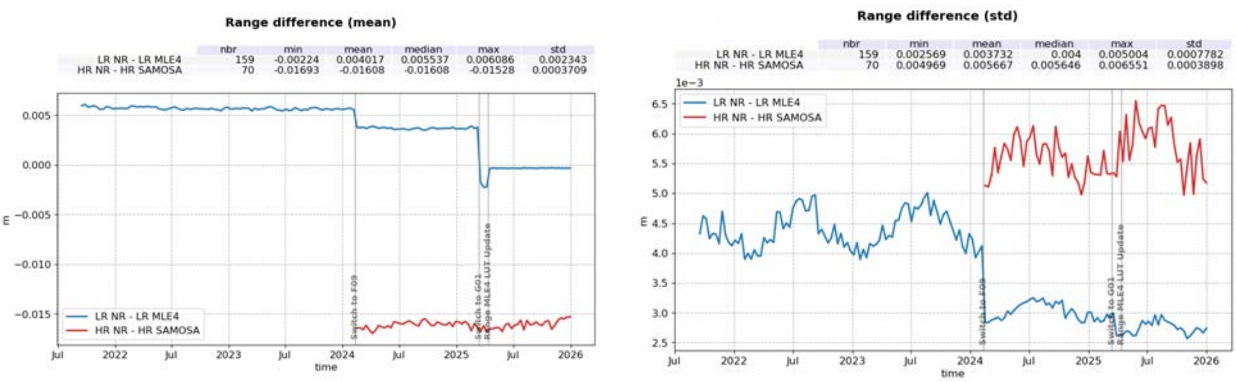

Figure 65: Time monitoring of Sentinel-6 MF LR NR - LR MLE4 (blue) and HR NR - HR SAMOSA (red) range difference per cycle, for the mean (left) and the standard deviation (right).

On figure 66 are presented the maps of the LR NR - LR MLE4 and HR NR - HR SAMOSA range differences (top panels) and their dependencies to ERA5 model SWH (bottom panel). In LR, the differences present no significant correlation with SWH. In HR, there is a bias of -2.1 cm between 1 and 7 m SWH, and caused by the skewness difference between SAMOSA and NR, as explained before.

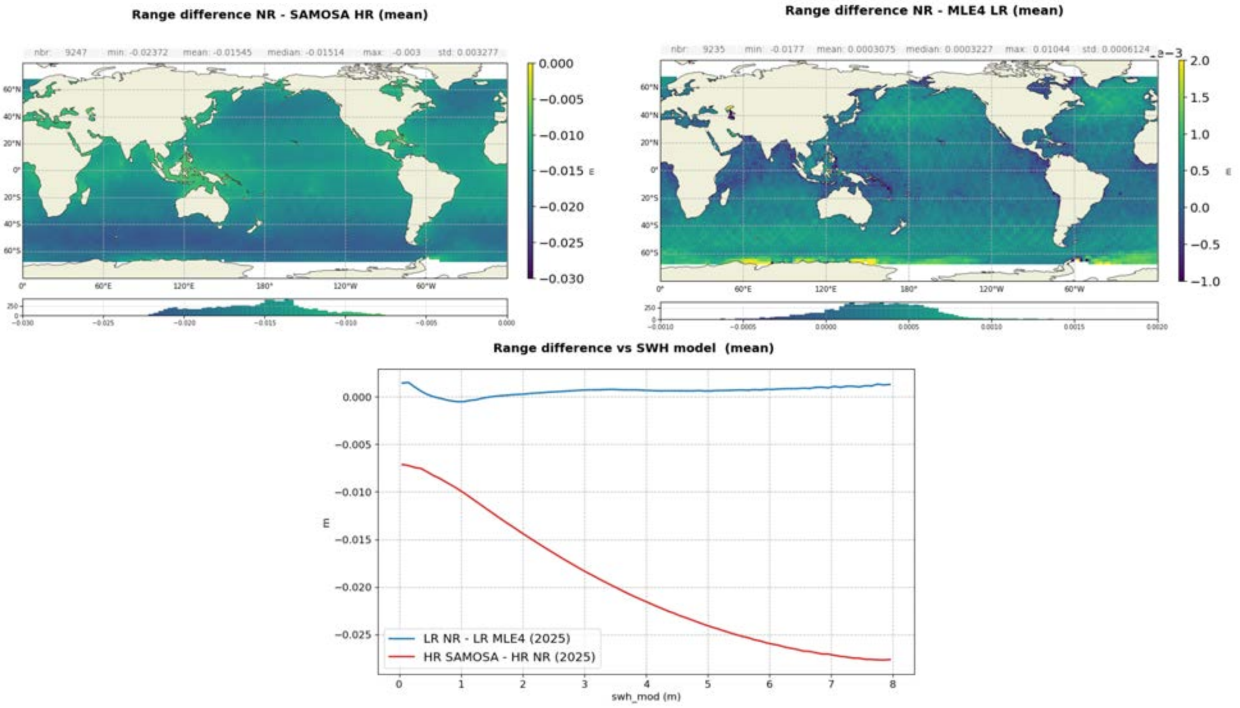

Figure 66: HR-LR differences for Ku-band range for HR NR - HR SAMOSA (top left) and LR NR - LR MLE4 (top right). Bottom: difference with respect to ERA5 SWH.

5.4. Significant wave height

The mean geographical distribution of SWH over 2025 for each retracking solution (either LR or HR) is depicted in figure 67 for Ku- and C-band . All solutions show a similar geographical pattern.

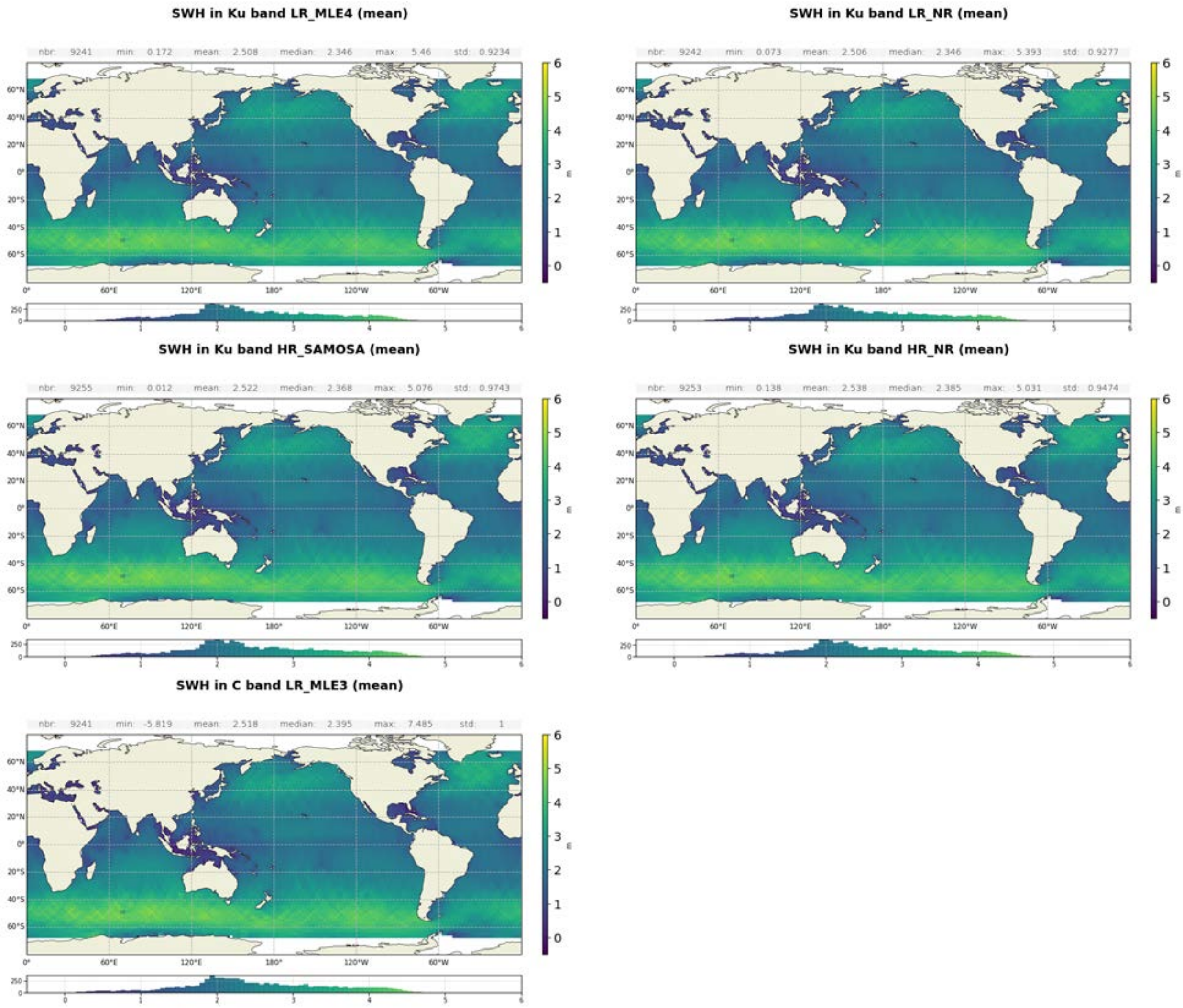

Figure 67: Maps of mean SWH for Ku band LR MLE4 (top left), LR NR (top right), HR SAMOSA (middle left), HR NR (middle right) and C band (bottom). Computed over 2025.

The mean Ku band SWH value is centered around 2.69 m for LR MLE4, 2.69 m for LR NR, 2.70 m for HR SAMOSA and 2.72 m for HR NR. Sentinel-6 MF LR Ku band SWH are in line with Jason-3, centered around 2.69 m, except at very low wave heights, where Sentinel-6 MF performs better, due to its improved handling of low wave heights in the Level 2 processing. This is now also true for Sentinel-6 MF HR Ku Band SWH since PB G01 update was applied. For the C-band, the average SWH is 2.71 m for both Sentinel-6 MF and Jason-3, which are now in line following the LUT update applied at PB G01. These values are stable over time, as shown in figure 68.

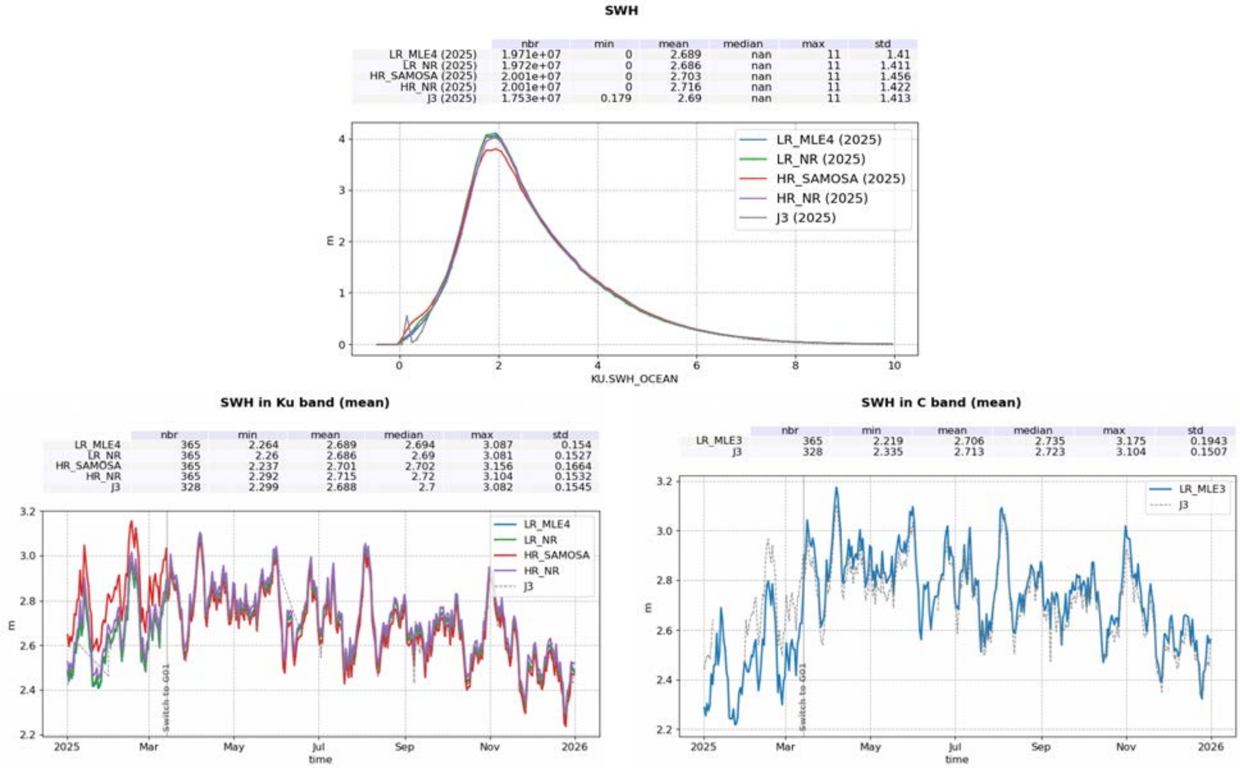

	nbr	min	mean	median	max	std
LR_MLE4 (2025)	1.971e+07	0	2.689	nan	11	1.41
LR_NR (2025)	1.972e+07	0	2.686	nan	11	1.411
HR_SAMOSA (2025)	2.001e+07	0	2.703	nan	11	1.456
HR_NR (2025)	2.001e+07	0	2.716	nan	11	1.422
J3 (2025)	1.753e+07	0.179	2.69	nan	11	1.413

	nbr	min	mean	median	max	std
LR_MLE4	365	2.264	2.689	2.694	3.087	0.154
LR_NR	365	2.26	2.686	2.69	3.081	0.1527
HR_SAMOSA	365	2.237	2.701	2.702	3.156	0.1664
HR_NR	365	2.292	2.715	2.72	3.104	0.1532
J3	328	2.299	2.688	2.7	3.082	0.1545

	nbr	min	mean	median	max	std
LR_MLE3	365	2.219	2.706	2.735	3.175	0.1943
J3	328	2.335	2.713	2.723	3.104	0.1507

Figure 68: Top : Histogram of Ku-band SWH for Sentinel-6 MF LR MLE4 (blue), LR NR (green), HR SAMOSA (red), HR NR (purple) and Jason-3 (black). Bottom: daily monitoring of SWH mean in Ku-band (left) and C-band (right).

The difference between Sentinel-6 MF HR SAMOSA and LR MLE4 SWH is reduced by 20 cm thanks to the vertical wave motion correction applied for HR SAMOSA in PB G01. As a result, both retrackers are now fully consistent, with a residual bias of about -4 mm (figure 69 right panel). The difference ranges from about -5 to 12 cm between 1 and 7 m SWH (figure 69 bottom panel). The difference between Sentinel-6 MF HR NR and LR NR SWH is stable in time, with an average value of 4.8 cm, and an essentially flat correlation with sea state between 1 and 7 m SWH. The residual bias is still under investigation.

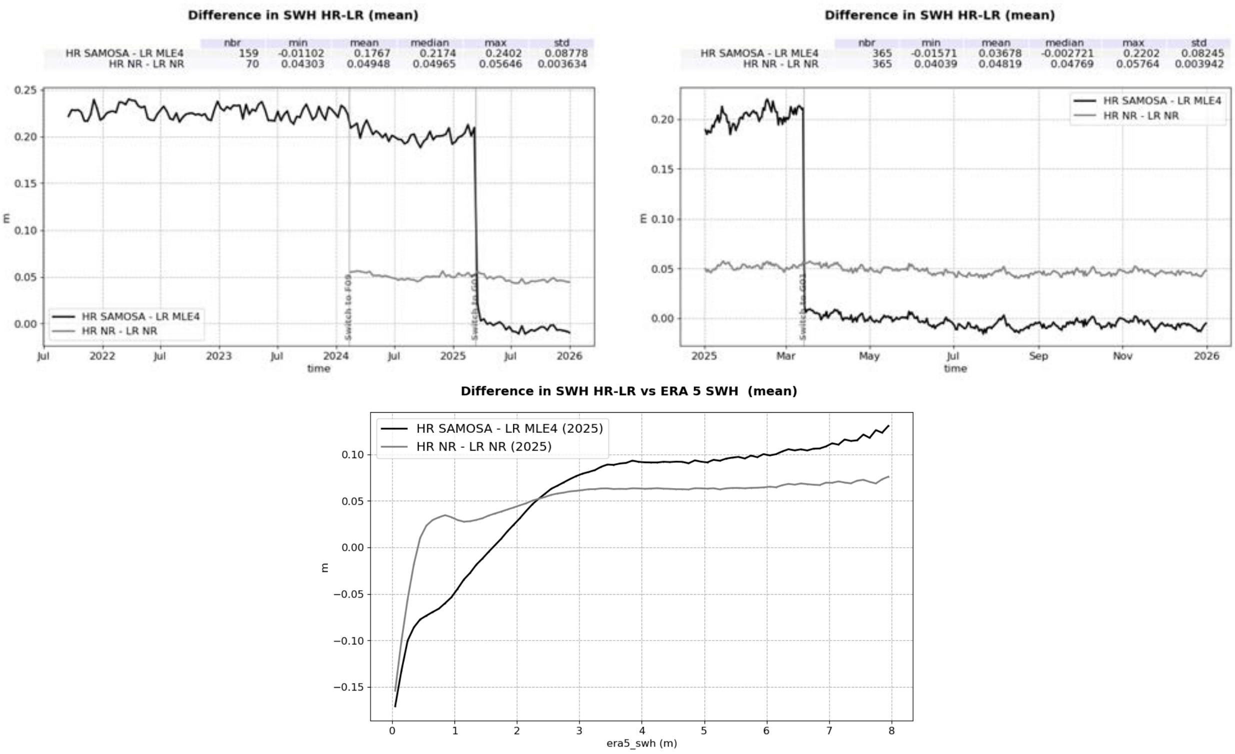

Figure 69: HR-LR differences for Ku-band SWH for SAMOSA - MLE4 (black) and NR (grey). Top left: mean per cycle over side B, top right: mean per day over 2025. Bottom: difference with respect to ERA5 SWH.

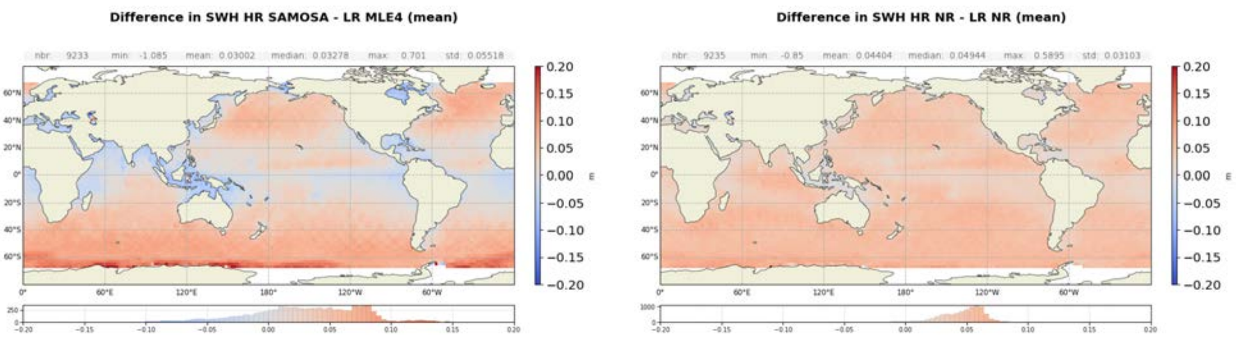

Figure 70: HR-LR differences for Ku-band SWH for SAMOSA - MLE4 (left) and NR (right). Computed over 2025.

LR NR - LR MLE4 differences do not show significant correlation to SWH, only a global bias that is strongly reduced by -1.4 cm with the MLE4 LUT update in PB G01, allowing a better consistency between both retrackers with a -1.6 mm average residual bias. Looking at the corresponding long-term monitoring (blue curve on figure 71 top left panel), a small jump of about 1 cm is visible on the 2023-10-05. It is linked to the deployment of the PB F08 patch version, correcting an anomaly on LR NR SWH (see section 3.4. for more details). The impact of the VWM correction applied on HR SAMOSA is also visible in the HR NR - HR SAMOSA difference (red curve on figure 71), with a +19 cm jump at PB G01 update, leading to a residual bias of about 5 cm. As for the correlation to sea state, the dependence is strongly reduced in the PB G01, with differences ranging from +10 cm to +1 cm between 1 and 7 m, while ranging from +2 cm to -33 cm for PB F09.

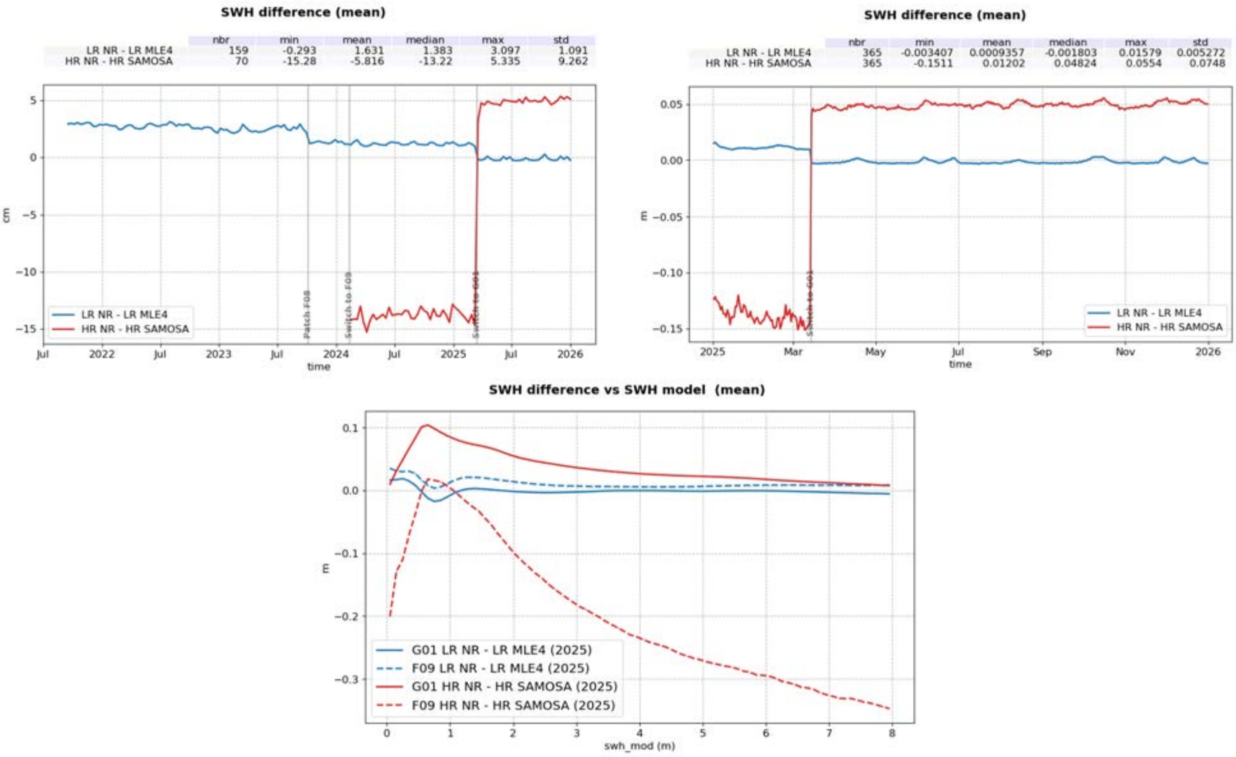

Figure 71: Ku-band SWH differences for LR NR - LR MLE4 (blue) and HR SAMOSA - HR NR (red). Top left: mean per cycle over side B, top right: mean per day over 2025. Bottom: difference with respect to ERA5, using G01 data (solid lines) and F09 data (dashed lines).

Figure 72 shows the difference between the altimeter and ERA5 SWH over side B for all retrackers.

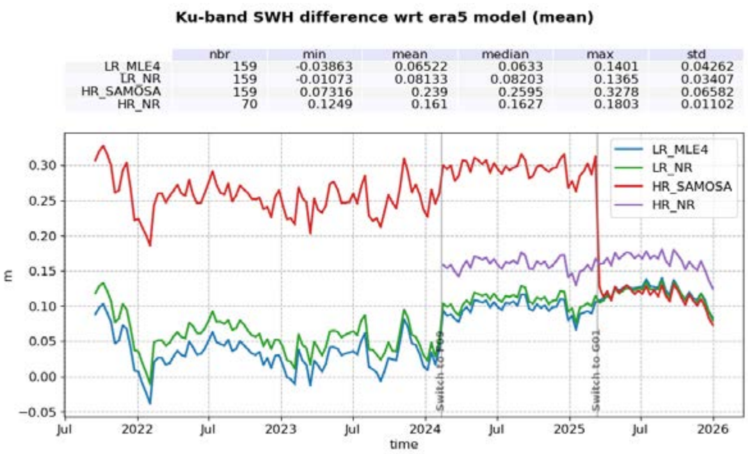

	nbr	min	mean	median	max	std
LR_MLE4	159	-0.03863	0.06522	0.0633	0.1401	0.04262
LR_NR	159	-0.01073	0.08133	0.08203	0.1365	0.03407
HR_SAMOSA	159	0.07316	0.239	0.2595	0.3278	0.06582
HR_NR	70	0.1249	0.161	0.1627	0.1803	0.01102

Figure 72: Cyclic mean of the altimeter minus ERA5 model SWH difference for LR MLE4 (blue), LR NR (green), HR SAMOSA (red) and HR NR (purple). Computed over side B.

5.5. Backscatter coefficient

The monitoring of the backscatter coefficient (sigma0) per day is presented on figure 73. LR backscatter coefficients are aligned and centered around 13.2 dB. In HR, the two sigma0 are also very similar (centered around 11.9 dB for SAMOSA and 11.8 dB for NR). These values are close to the Jason-3 value of 13.6 dB. This is true as well for the C band, with a sigma0 centered around 14.6 dB for Sentinel-6 MF and 15.3 dB for Jason-3. Note that the PB G01 update involved a +0.02 dB shift in the averaged LR MLE4 values, and a +0.04 dB shift for all other retrackers. These shifts resulted from the combination of -0.02 dB due to the LUT update (applied to MLE4 only) and +0.04 dB due to the g-scaling update ([8]).

The geographical distributions of the Ku-band HR (SAMOSA and NR), Ku band LR (MLE4 and NR) and C-band sigma0 are presented in figure 74. No significant difference observed at first order between the different sigma0 geographical distributions.

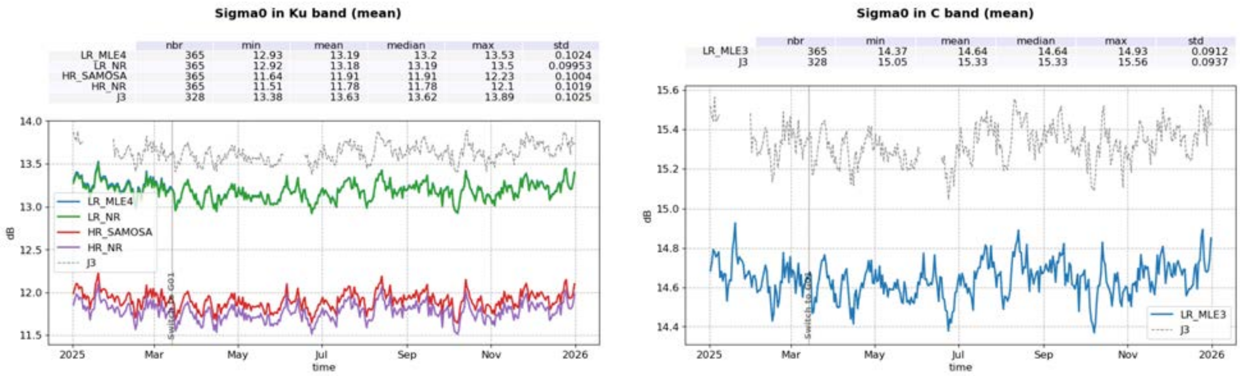

Figure 73: Daily monitoring of Sigma0 mean in Ku-band (left) for Sentinel-6 MF LR MLE4 (blue), LR NR (green), Sentinel-6 MF HR (red) and Jason-3 (black) and C-band (right).

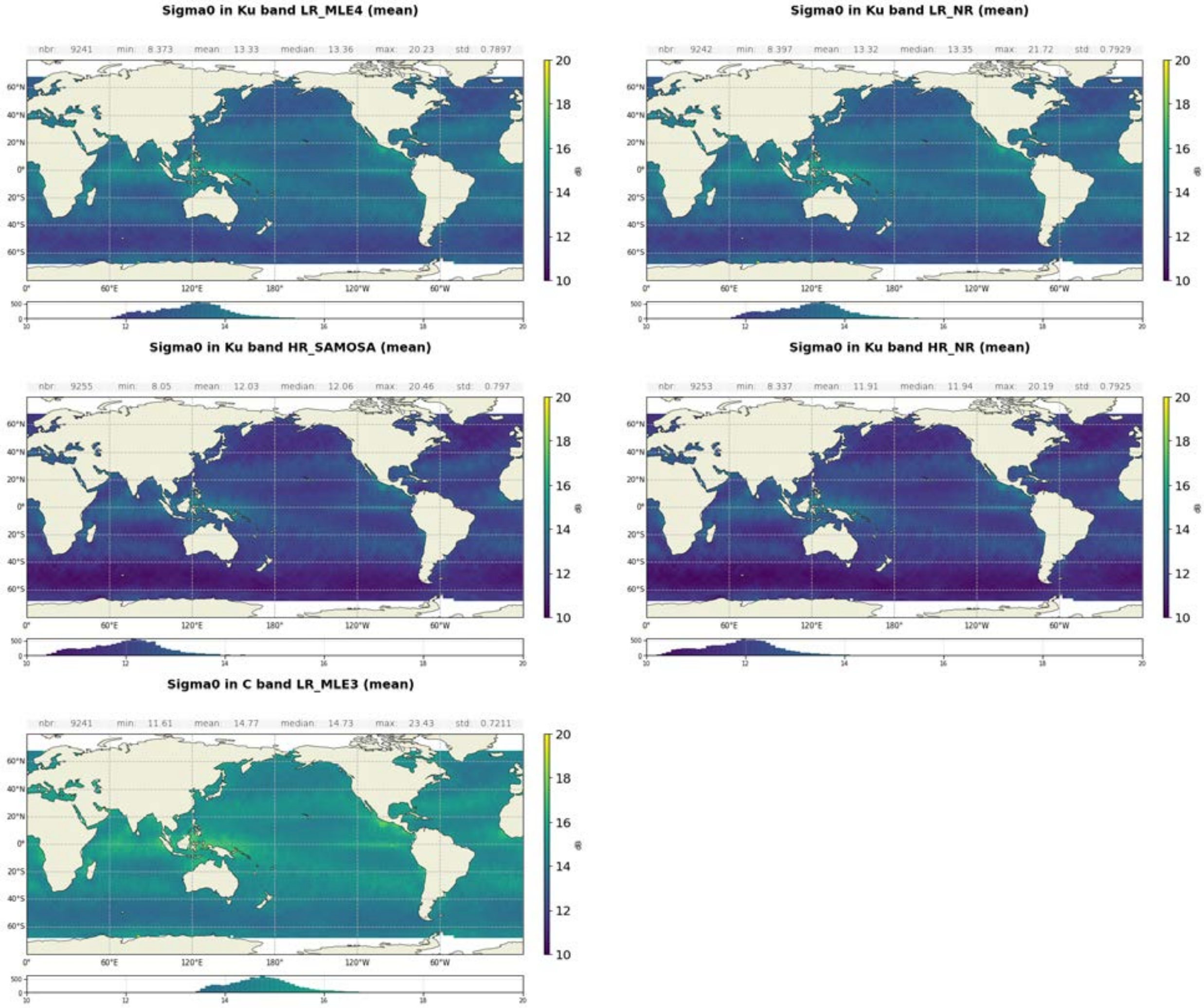

Figure 74: Maps of mean sigma0 for Ku-band LR MLE4 (top left), LR NR (top right), HR SAMOSA (middle left), HR NR (middle right) and C band (bottom). Computed over 2025.

Figure 75 presents the sigma0 differences between NR and MLE4 in LR mode as well as NR and SAMOSA in HR mode. The MLE4 LUT update signs as a jump in the monitoring of LR retracker differences, leading to improved alignment between them. For HR retrackers, the difference remains stable over time, with a -0.13 dB average bias.

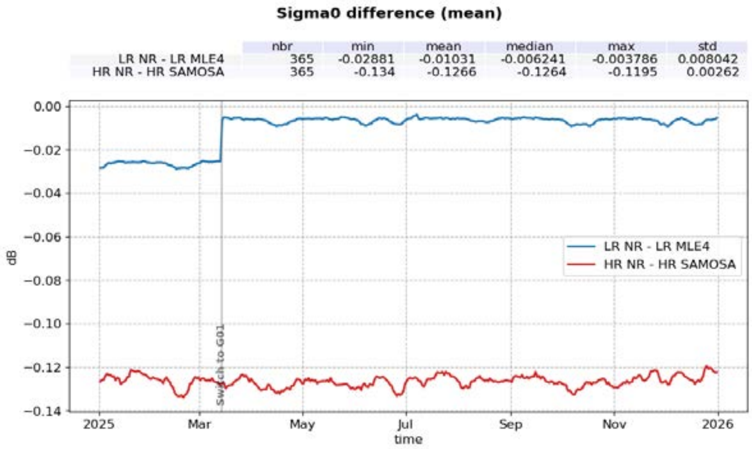

Figure 75: Monitoring of the LR NR - MLE4 (blue) and HR NR - SAMOSA (red) sigma0 differences per day, over 2025.

Figure 76 presents the HR SAMOSA - LR MLE4 (black) and HR NR - LR NR (grey) sigma0 differences. LR MLE4 LUT update still signs, reducing LR MLE4 difference with HR SAMOSA to -1.34 dB. The difference between NR retrackers is stable and centred around -1.46 dB.

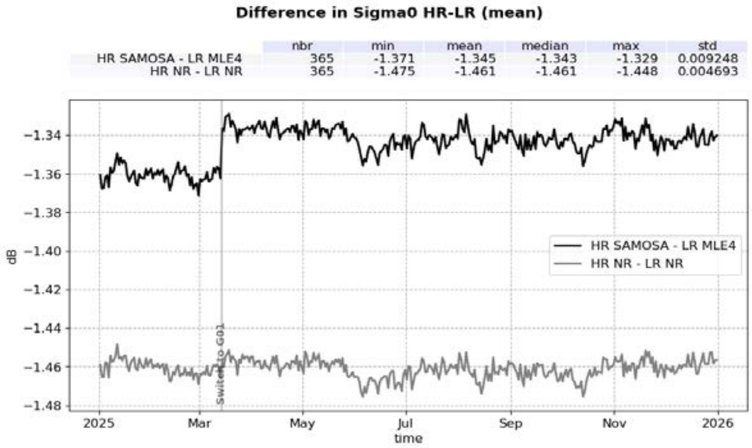

Figure 76: Daily monitoring of the HR SAMOSA - LR MLE4 (black) and HR NR - LR NR (grey) sigma0 difference, over 2025.

5.6. Wind speed

For Sentinel-6 MF wind speed computation, the same algorithm as for Jason-3 GDR-F is applied (Collard, 2005 [18]). Its computation takes in input Sentinel-6 MF sigma0 and SWH derived from each mode and retracker. The geographical distribution of altimeter wind speed over 2025 is presented in figure 67 for Sentinel-6 MF LR and HR, and Jason-3. All wind speeds averaged over 2025 share similar geographical patterns.

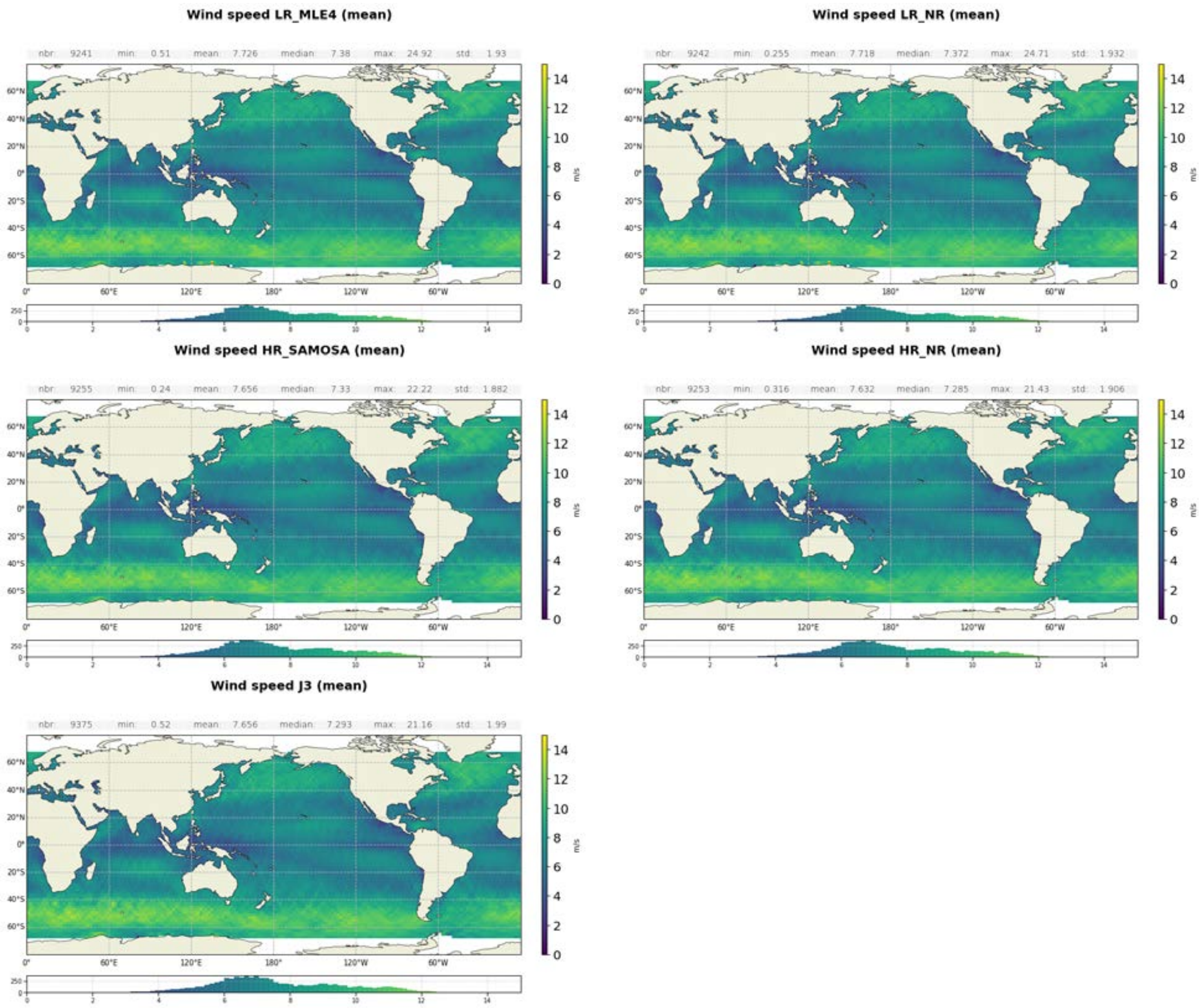

Figure 77: Maps of mean wind speed for LR MLE4 (top left), LR NR (top right), HR SAMOSA (middle left), HR NR (middle right) and Jason-3 (bottom). Computed over 2025.

The monitoring of the wind speed per day is presented on figure 78 and the corresponding distribution on figure 79. Wind speed is of the same order between all datasets, centered around 8.0 m/s for Sentinel-6 MF LR retrackers as well as Jason-3, and 7.9 m/s for HR, with similar variations, no drift or jump. After PB G01 update, the averaged wind speed values shifted by +23 cm/s for LR MLE4, +27 cm/s for LR NR and +16 cm/s for both HR retrackers. This is due to the g-scaling update in sigma0 and, for MLE4 only, the LUT update ([8]). In terms of consistency with Jason-3 wind speed, PB G01 improved alignment for LR retrackers, while slightly reducing it for HR retrackers.

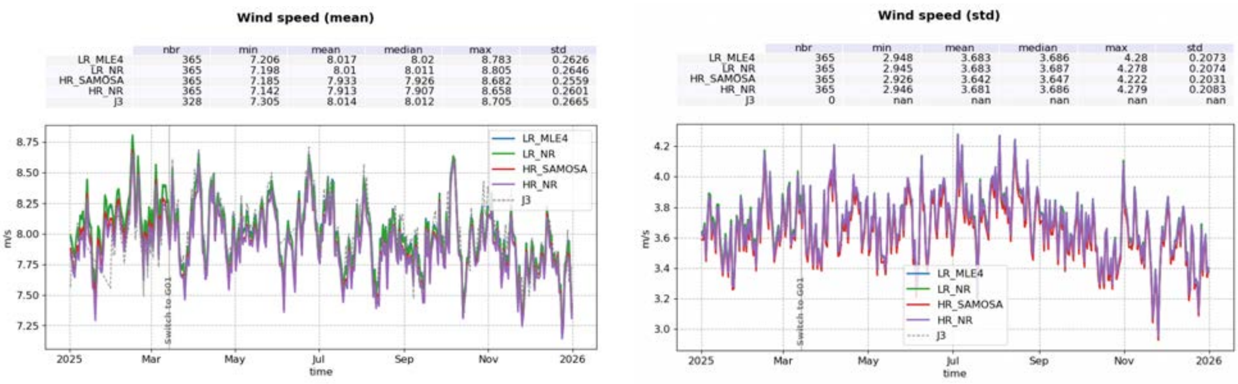

Figure 78: Mean (left) and standard deviation (right) wind speed per day for LR MLE4 (blue), LR NR (green), HR SAMOSA (red), HR NR (purple) and Jason-3 (black).

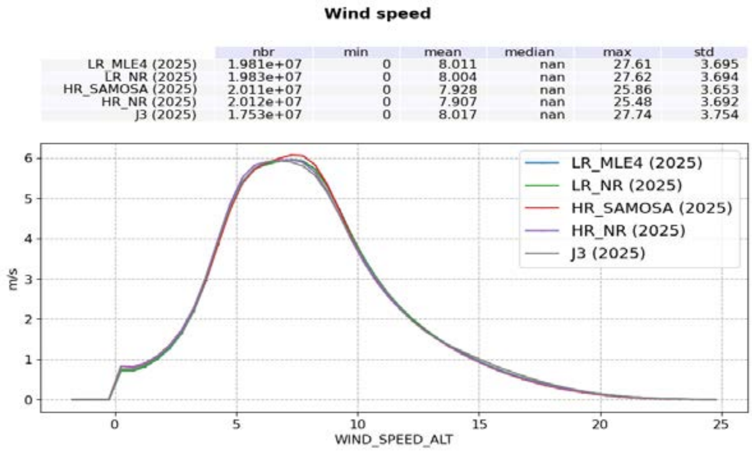

Figure 79: Histogram of wind speed for Sentinel-6 MF LR MLE4 (blue), LR NR (green), HR SAMOSA (red), HR NR (purple) and Jason-3 (black). Computed over 2025.

Figure 80 presents the wind speed differences between retrackers in LR and HR modes in blue and red respectively. Thanks to PB G01 update, the absolute differences were reduced by 1.4 cm/s and 2.5 cm/s for LR and HR retrackers respectively. In PB G01, the LR NR - LR MLE4 difference is stable, whereas the HR NR - HR SAMOSA differences seem to show a drift of very small amplitude, of the order of -2 cm/s since the baseline update, and stronger temporal variations. This drift is under investigation.

The corresponding maps (bottom panels) present a correlation with high Mean Sea Surface (MSS) gradients and a different bias on the Caspian Sea in LR mode. Such a behavior originates from sigma0, as map of LR MLE4 versus LR NR sigma0 present the same features (as reported in [17]). The origin of this MSS gradient sensitivity difference between the two LR retrackers is yet to be understood.
HR NR versus HR SAMOSA difference is strongly correlated to SWH. The bias increases by +28 cm/s between 1 and 7 m SWH, while LR NR and LR MLE4 wind-speeds do not present significant correlation to sea state.

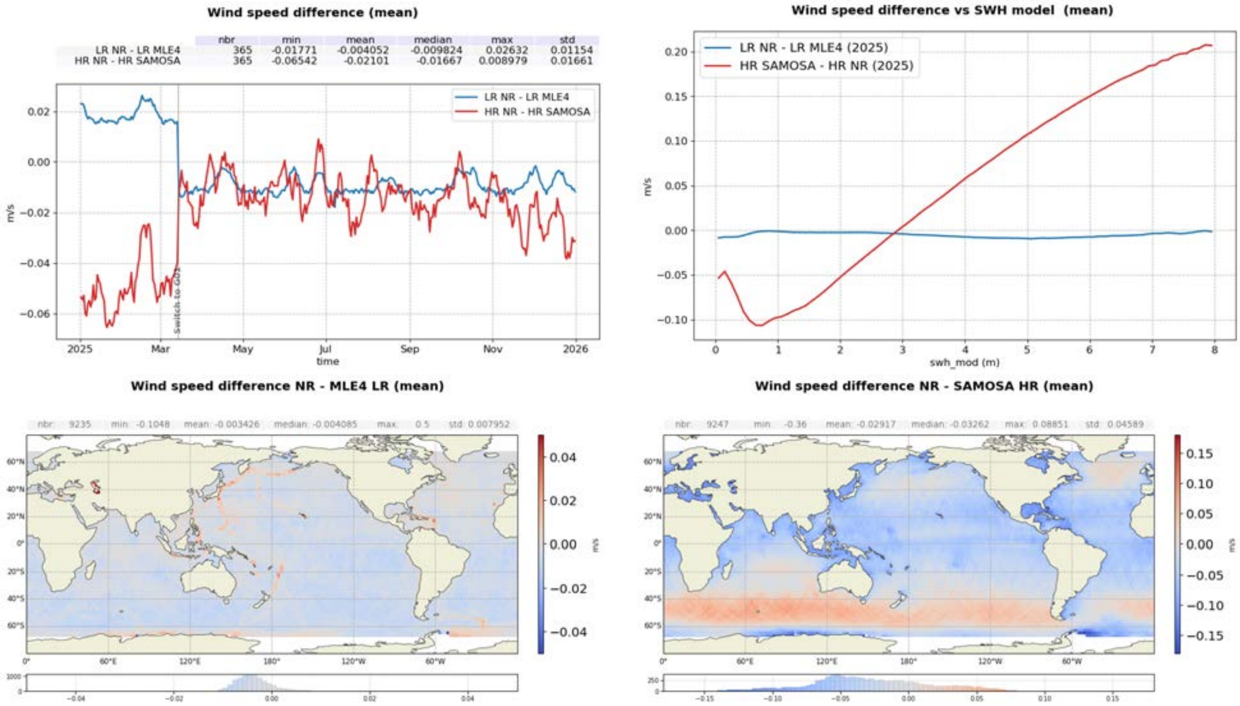

Figure 80: Monitoring per day (top left), correlation to model SWH (top right) and maps (bottom panels) of the LR NR - MLE4 and HR NR - SAMOSA wind speed differences.

The monitoring of the HR SAMOSA - LR MLE4 (black) and HR NR - LR NR (grey) wind speed differences is presented in figure 81. As expected, differences are reduced at PB G01 update, by about 2 cm/s for HR SAMOSA - LR MLE4, and 9 cm/s for HR NR - LR NR. Seasonal variability is also visible.

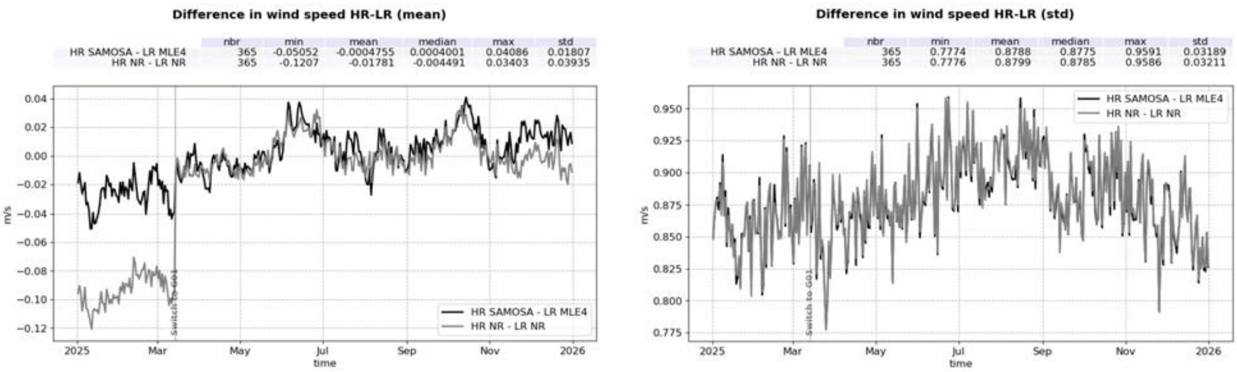

Figure 81: Mean (left) and standard deviation (right) HR SAMOSA - LR MLE4 (black) and HR NR - LR NR (grey) wind speed difference per day.

The monitoring of the difference between the altimeter-derived wind speed and the wind speed model is plotted on figure 82. After PB G01 update, the daily mean differences were reduced for all retrackers, reaching approximately 6.8 cm/s for LR MLE4, 6.5 cm/s for LR NR, 6.5 cm/s for HR SAMOSA and 6.0 cm/s for HR NR. Sentinel-6 MF wind speed measurements now show better agreement with the wind speed model than Jason-3, which exhibits mean differences relative to the model of about 9.9 cm/s. Apart from these improvements, the time series remain stable.

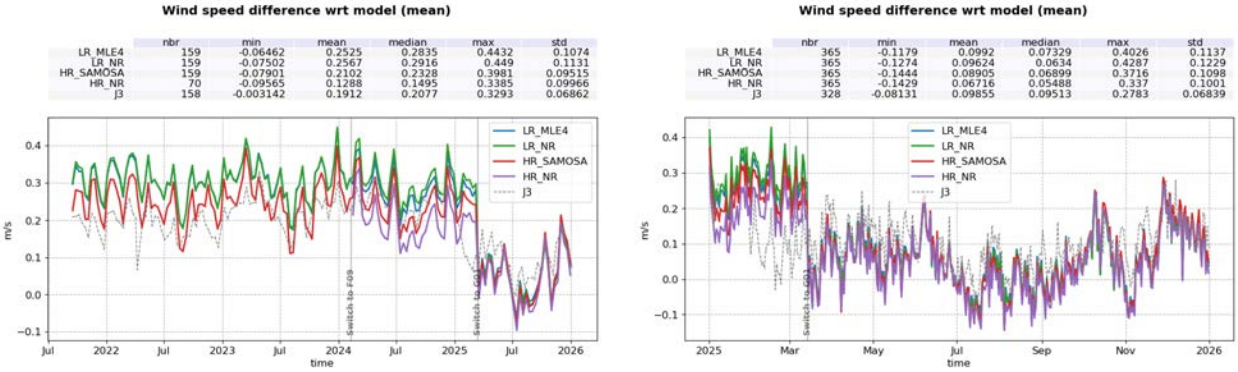

Figure 82: Mean per cycle over side B (left) and per day over 2025 only (right) wind speed difference w.r.t. model for LR MLE4 (blue), LR NR (green), HR SAMOSA (red), HR NR (purple) and Jason-3 (grey).

5.7. Sea state bias

Sentinel-6 MF sea state biases (SSB) are computed using Jason-3 GDR-F SSB parametrization. Its computation takes in input Sentinel-6MF wind-speed and SWH derived from each mode and retracker. More details are available in the L2 PGS [3].

Maps of Ku-band SSB averaged over the year 2025 show the same geographical patterns between Jason-3 and Sentinel-6 MF retrackers (figure 83).

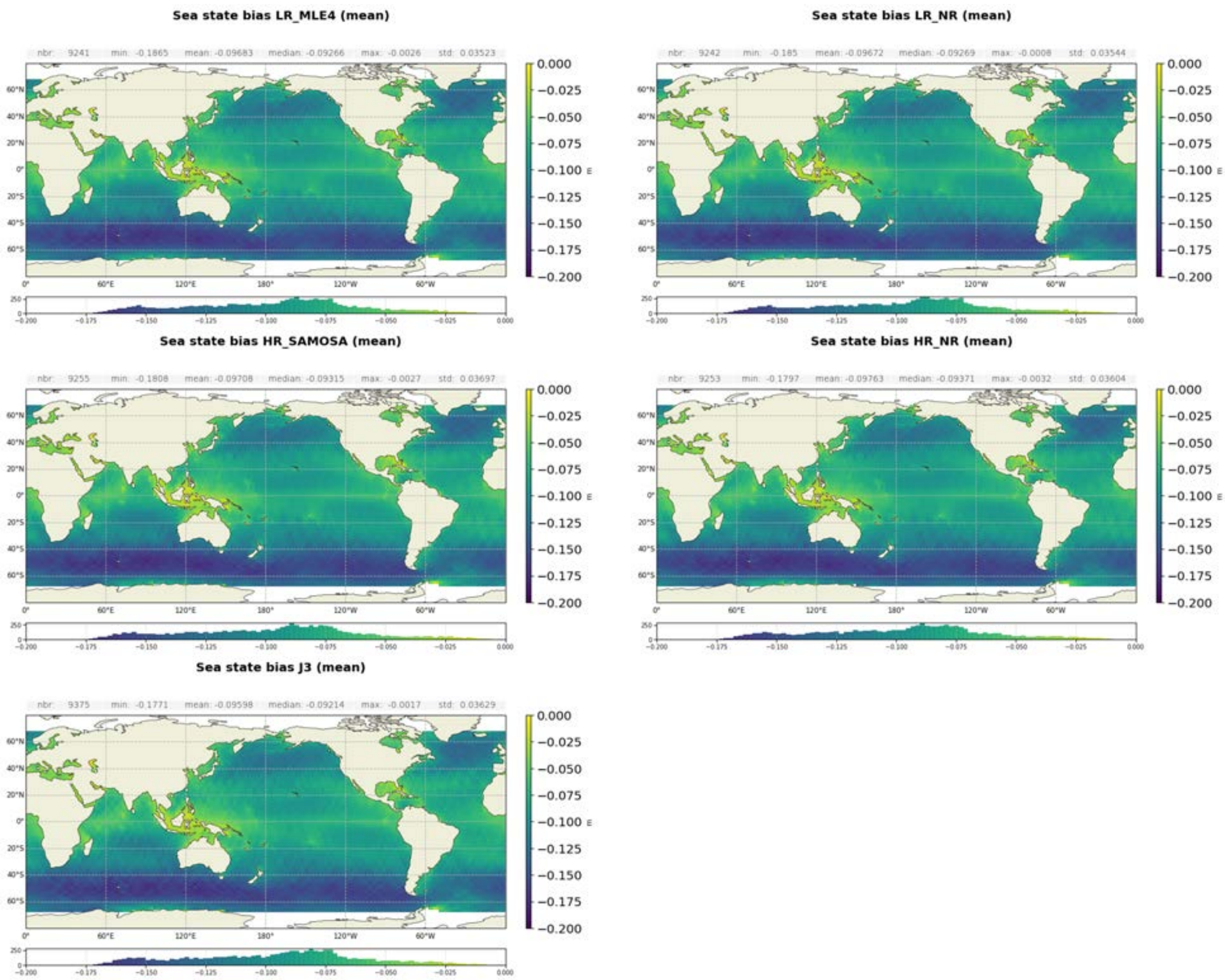

Figure 83: Maps of mean SSB for LR MLE4 (top left), LR NR (top right), HR SAMOSA (middle left), HR NR (middle right) and Jason-3 (bottom). Computed over 2025.

Ku-band SSB are centered around -10.4 cm for all Sentinel-6 MF retrackers, as well as for Jason-3. The PB G01 update enabled HR SAMOSA SSB to become more consistent with the other retrackers.
In C-band, the average SSB is approximately -9.4 cm for both Sentinel-6 MF and Jason-3. These values are stable over time, as shown in figure 84.

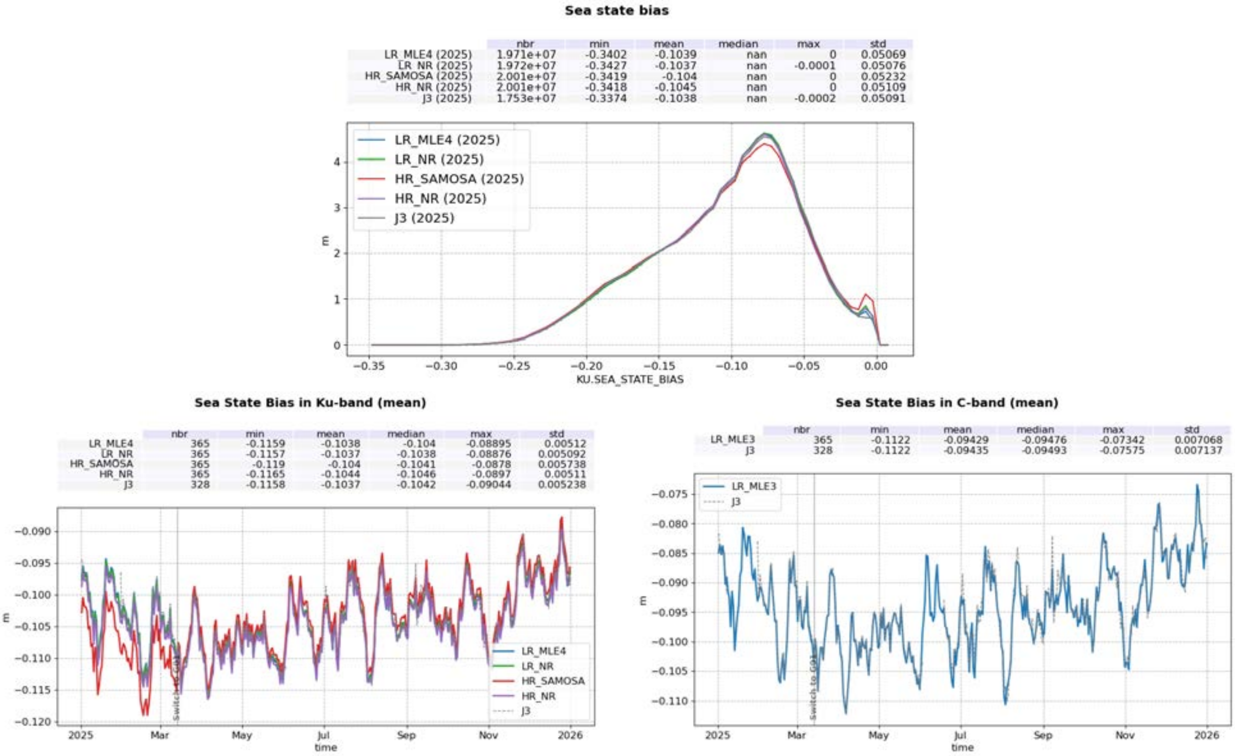

Figure 84: Top : Histogram of Ku-band SSB for Sentinel-6 MF LR MLE4 (blue), LR NR (green), HR SAMOSA (red), HR NR (purple) and Jason-3 (black), over 2025. Bottom: daily monitoring of SSB means in Ku-band (left) and C-band (right).

Figure 85 shows the SSB differences between LR NR and LR MLE4, and between HR NR and HR SAMOSA. A jump is observed at the PB G01 update in both monitoring, reducing the absolute mean values by 0.45 mm for LR NR - LR MLE4 and 2.7 mm for HR NR - HR SAMOSA, with a reversal of sign. After the PB G01 update, LR MLE4 becomes fully consistent with LR NR. For HR retrackers, a residual mean difference of -1.7 mm remains, with a dependence on sea state, varying from approximately -3 mm to +1 mm for SWH between 1 and 7 m.

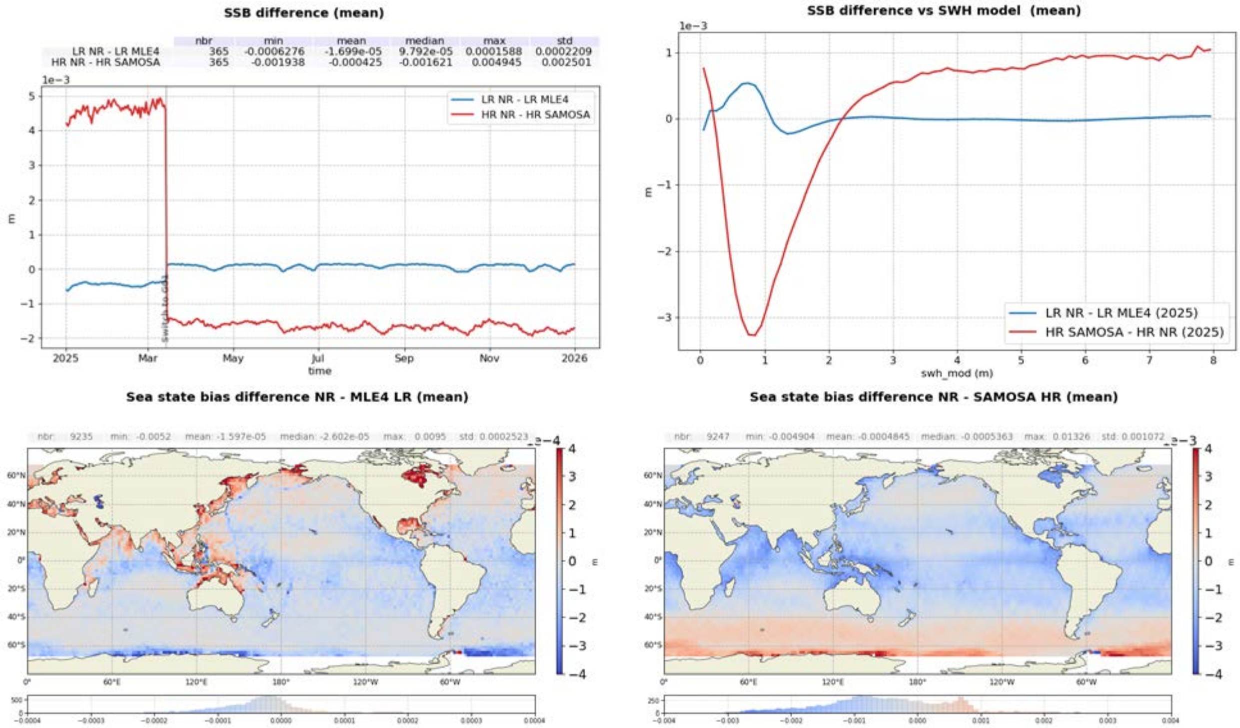

Figure 85: Monitoring per day (top left), correlation to model SWH (top right) and maps (bottom panels) of the LR NR minus MLE4 and HR NR minus SAMOSA SSB differences.

The monitoring of the HR - LR SSB differences is presented on figure 86. The improvement of the HR SAMOSA SSB in PB G01 (mostly related with VWM correction now applied to SAMOSA SWH estimates) leads to a jump in the HR SAMOSA - LR MLE4 difference, bringing the two retrackers into full consistency. A small jump of about -0.1 mm is also visible for HR NR - LR NR at the PB G01 update, which is linked to vertical wave motion being now applied at 20Hz for HR NR and HR SAMOSA, causing a change for small waves and therefore slightly biasing the SSB.

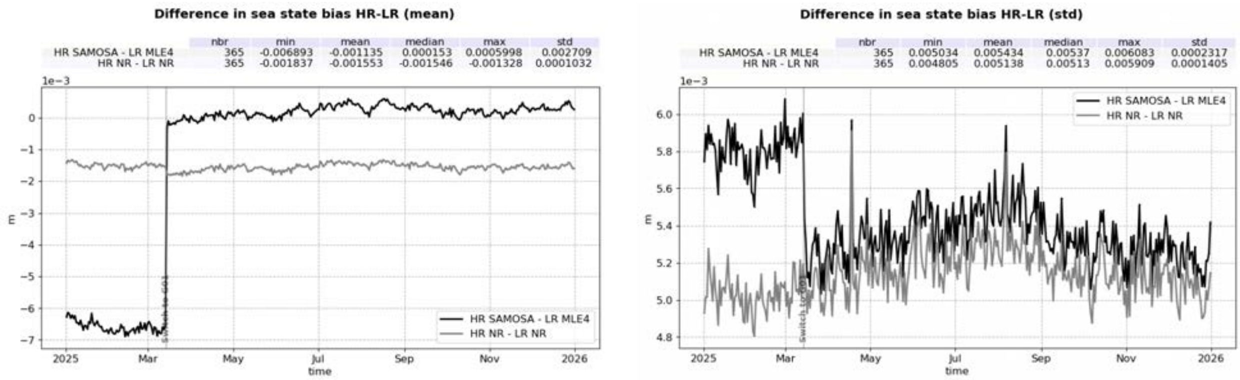

Figure 86: Mean (left) and standard deviation (right) HR-LR MLE4 SSB difference per day.

Small differences in SSB can be linked to the fact that all retrackers share the same SSB parametrization, that has been computed for Jason-3. Dedicated parametrization could improve the consistency between retrackers, especially for SAMOSA that seems to be the most impacted in terms of biases, distribution shape and correlation to SWH.

5.8. Ionospheric correction

Sentinel-6 MF altimeter ionosphere correction is derived from LR data, in Ku and C-band. The ionosphere correction in HR products is copied from LR products and thus identical.

The filtering process of dual-frequencies ionospheric correction is described in [19].

The monitoring of the filtered dual-band ionospheric correction is presented in figure 87, along with the corresponding distributions. There is a very good agreement between Sentinel-6 MF LR MLE4, LR NR and Jason-3 ionospheric corrections, that follow the same variations. Lower values are observed before April due to an intensification of the solar cycle. Averages in 2025 are 5.5 cm for both Sentinel-6 MF retrackers and 5.3 cm for Jason-3, the bias being stable over time.
The geographical distribution of Sentinel-6 MF filtered ionospheric correction is presented on figure 88.

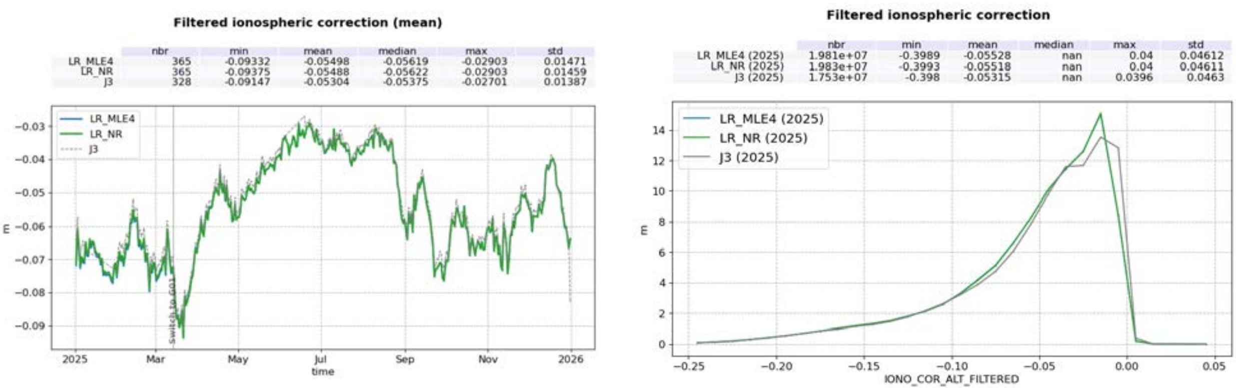

Figure 87: Monitoring of filtered ionospheric correction for Sentinel-6 MF LR MLE4 (blue), LR NR (green) and Jason-3 (black). Left: Mean per day. Right : Histogram. Computed over 2025.

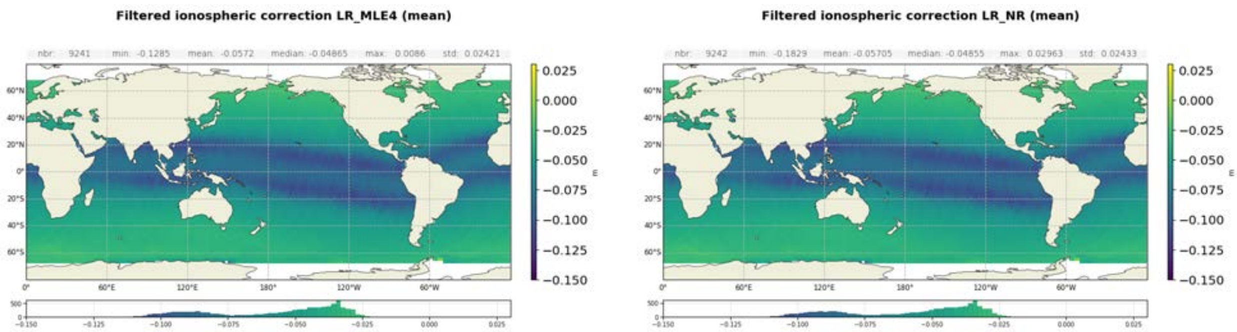

Figure 88: Maps of mean filtered ionospheric correction for Sentinel-6 MF LR MLE4 (left) and LR NR (right). Computed over 2025.

Figure 89 presents the daily monitoring of the NR - MLE4 filtered ionospheric correction difference. Two small discontinuities are visible along the series: -1.2 mm at the PB G01 update and +0.4 mm at the MLE4 LUT update.

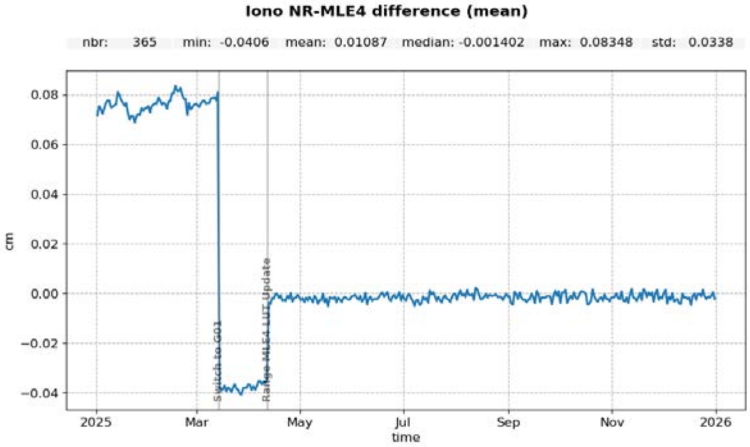

Figure 89: Time monitoring of the NR - MLE4 filtered ionospheric correction difference per day in cm.

The monitoring of the filtered minus GIM model ionospheric corrections differences is presented on figure 90. As expected, both Sentinel-6 MF MLE4 and NR curves, as well as Jason-3, follow identical variations. Sentinel-6 MF altimeter ionosphere corrections show on average a better consistency to GIM model than Jason-3. The biases with respect to GIM are centered around 1.2 cm for both Sentinel-6 MF retrackers, while it is 1.4 cm for Jason-3.
A significant spike is observed in the Sentinel-6 MF time series, associated with abnormal values in the GIM ionospheric correction between 2025/07/08 and 2025/07/10 (cycle 171, passes 198–248). More specifically, during this period the GIM ionospheric correction is largely missing from the Sentinel-6 MF L2 data and the few available measurements occur primarily on descending tracks, where they exhibit anomalous values.

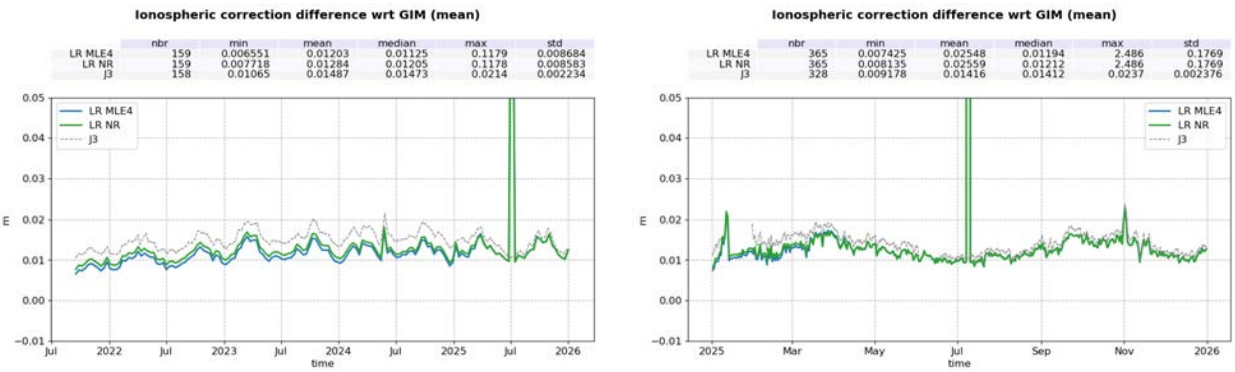

Figure 90: Mean per cycle over side B (left) and per day over 2025 only (right) filtered iono - GIM iono for Sentinel-6 MF LR MLE4 (blue), LR NR (green) and Jason-3 (black).

The maps of altimeter versus GIM difference are presented in figure 91. Sentinel-6 MF and Jason-3 present similar biases along the geomagnetic equator and their overall distribution is similar.

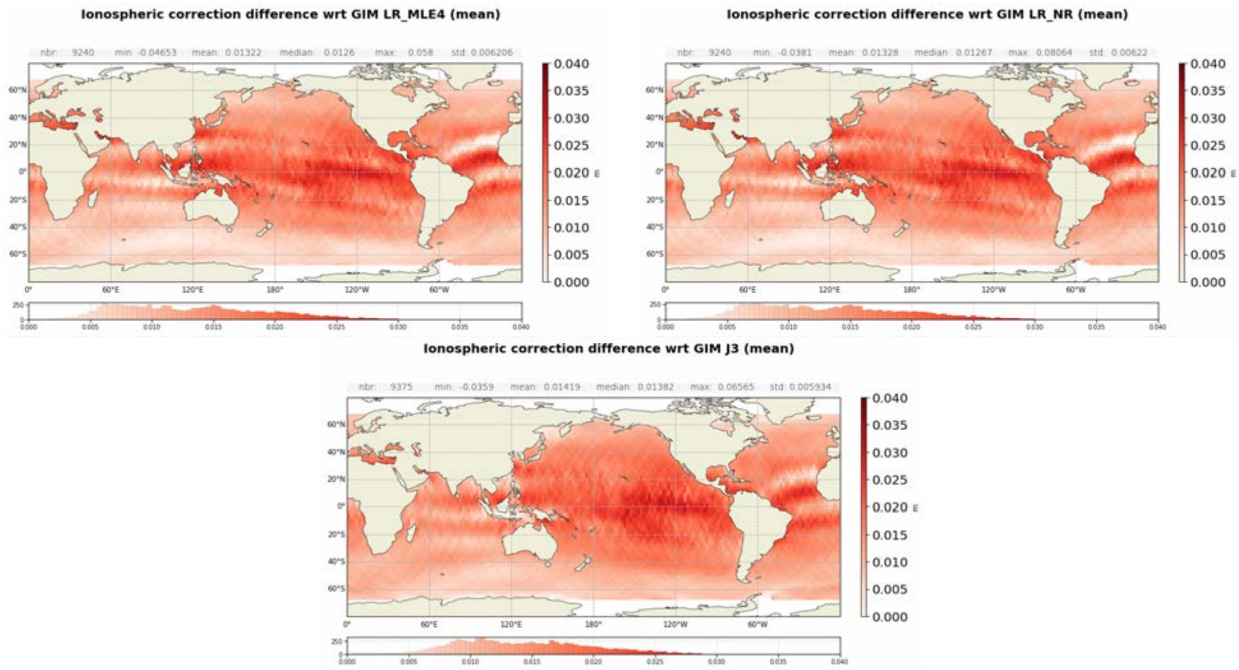

Figure 91: Maps of mean filtered ionospheric correction - GIM iono for Sentinel-6 MF LR MLE4 (left), LR NR (right) and Jason-3 (bottom). For Sentinel-6 MF retrackers, tracks of cycle 171 with abnormal GIM ionospheric corrections were omitted when computing the maps. Computed over 2025.

5.9. Radiometer wet troposphere correction

5.9.1. Overview

In order to evaluate radiometer wet troposphere correction, liquid water content, water vapour content and atmospheric attenuation, Sentinel-6 uses a three-frequencies AMR (Advanced Microwave Radiometer) (18.7, 23.8 and 34.0 GHz), similar to the one used on Jason-3, in combination to HRMR (High Resolution Microwave Radiometer) data for more reliable measurements in coastal areas.

Note that the 23.8 GHz channel is the primary water vapour sensing channel, meaning a higher water vapour concentration leads to larger 23.8 GHz brightness temperature values. As a consequence, top right and bottom right parts of figure 92 are anti-correlated. Moreover, the 34 GHz channel and the 18.7 GHz channel, which have less sensitivity to water vapour, facilitate the removal of the contributions from cloud liquid water and excess surface emissivity of the ocean surface due to wind, which also act to increase the 23.8 GHz brightness temperature.

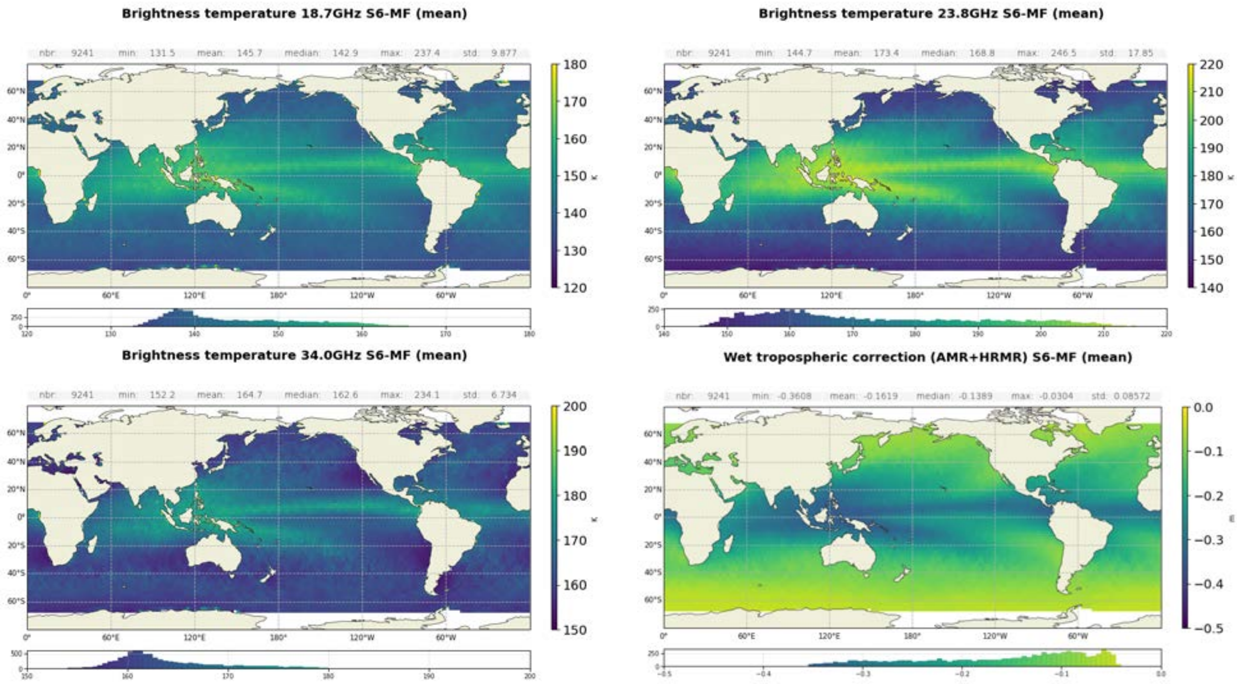

Figure 92: Maps of mean brightness temperature for channels 18.7 GHz (top left), 23.8GHz (top right), 34.0GHz(bottom left) in K and mean wet tropospheric correction (bottom right) in m. Computed over 2025.

The distributions of the wet tropospheric corrections for Sentinel-6 MF and Jason-3 are presented on figure 93. Both distributions are similar, with Sentinel-6 MF centered around 15.3 cm and Jason-3 around 15.4 cm.

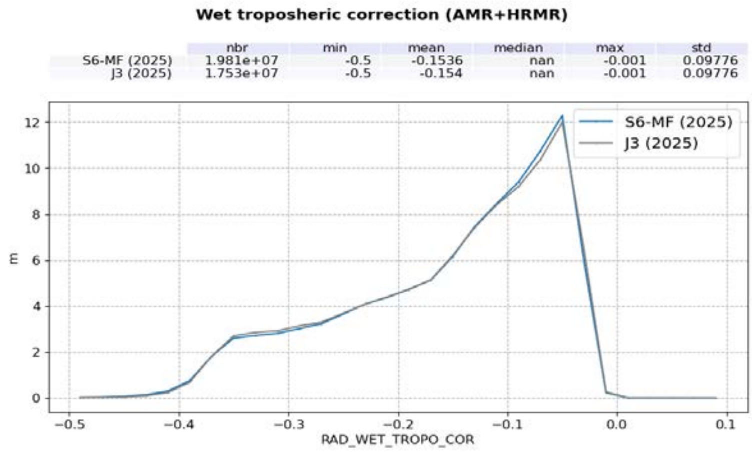

Figure 93: Histogram of wet tropospheric correction in m for Sentinel-6 MF (blue) and Jason-3 (black) computed over 2025.

5.9.2. Comparison with model

The wet troposphere correction computed from ECMWF model data has been used to check the Sentinel-6 MF and Jason-3 radiometer corrections. The cross-comparison between all radiometers and models available is necessary to analyse the stability of each wet troposphere correction. An overview of the wet troposphere correction importance for mean sea level is given in Obligis et al. [20].

The difference between measured and model data is computed on a daily basis and is plotted on figure 94 for Sentinel-6 MF and Jason-3 for comparisons. Over 2025, the wet tropospheric correction for Sentinel-6 MF is closer to the model than Jason-3 (0.9 mm and 1.1 mm respectively).

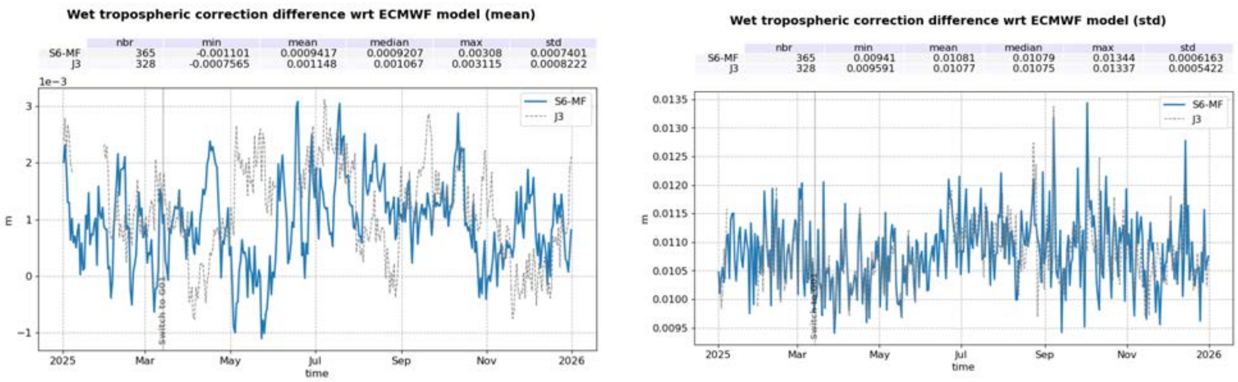

Figure 94: Mean (left) and standard deviation (right) HRMR+AMR wet troposphere correction - ECMWF model per day for Sentinel-6 MF (blue) and Jason-3 (black).

The maps of the differences between measured and model data are presented in figure 95. They show that Sentinel-6 MF and Jason-3 present a similar overall distribution.

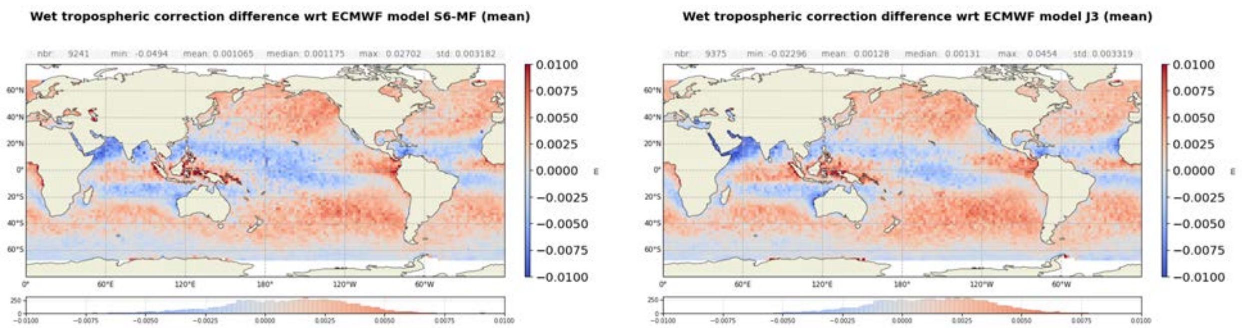

Figure 95: Maps of mean HRMR+AMR wet troposphere correction - ECMWF model for Sentinel-6 MF (left) and Jason-3 (right).

5.9.3. Comparison with AMR computed correction

HRMR radiometer is designed to support AMR radiometer with the purpose of extending microwave retrievals near the coast under cloud-free conditions. In order to estimate HRMR contribution, the wet troposphere correction computed with AMR measurement only is subtracted from the one computed with the combined HRMR+AMR measurement. The resulting daily monitoring (figure 96, left) shows that the HRMR reduces the mean wet troposphere correction by 0.1 mm. As expected, the differences are mainly located on coastal areas (figure 97), with values close to zero over open ocean, and increasing values near the coast (figure 96, right). There are also sub-millimeter variations over time.

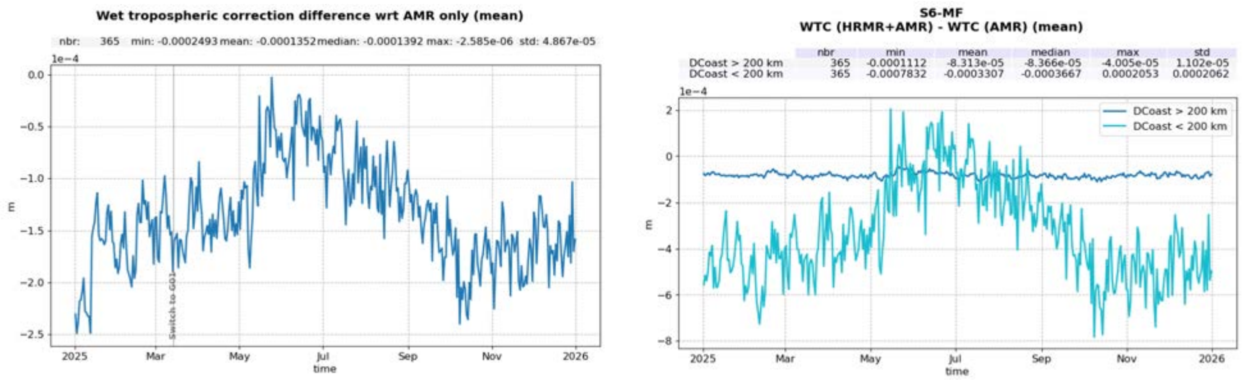

Figure 96: Mean (HRMR+AMR) - AMR wet tropospheric correction difference per day for Sentinel-6 MF in m. Right panel: computed for open ocean (distance to coast larger than 200 km) in dark blue, and for coastal measurement (distance to coast smaller than 200 km) in light blue.

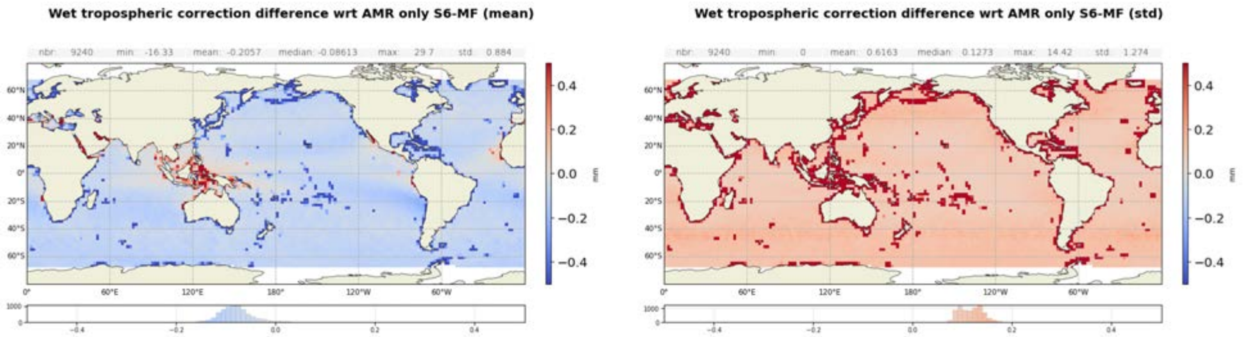

Figure 97: Map of the mean (left panel) and standard deviation (right panel) of the (HRMR + AMR) - AMR wet tropospheric correction differences for Sentinel-6 MF (mm).

Figure 98 shows the difference in the variance of SSHA computed with combined HRMR+AMR WTC and the variance of SSHA computed with AMR only WTC as a function of the distance from coast. Variance reduction ranges between 0.02 mm^2 and -0.02 mm^2 when the coast is within a radius of 100 km, and near zero beyond. A slight increase is observed within the first few kilometers from the coastline, with its origin currently under investigation.

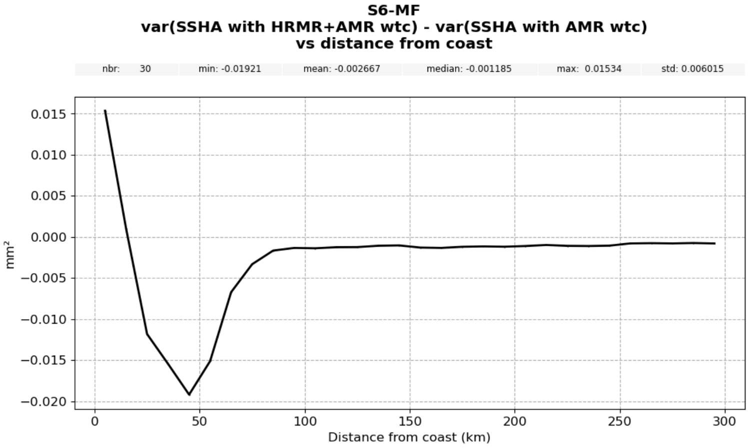

Figure 98: Variance of SSHA computed with HRMR+AMR derived WTC minus variance of SSHA computed with AMR derived WTC, as a function of the distance from the coast for Sentinel-6 MF in mm^2.

6 SSH crossover analysis

6.1. Overview

Sea Surface Height crossover differences are the SSH differences between ascending and descending passes where they cross each other. Sea Surface Heights are computed as follow :

$$SSH = Orbit - AltimeterRange - \sum(GeophysicalCorrections)$$

Crossover differences are systematically analysed to estimate data quality and the Sea Surface Height (SSH) performance. SSH crossover differences are computed from the valid data set on a one cycle basis, with a maximum time lag of 10 days, in order to limit the effects of ocean variability which are a source of error in the performance estimation. The mean SSH crossover differences should ideally be close to zero and standard deviation should ideally be small.

Nevertheless, SLA varies also within 10 days, especially in high variability areas. Therefore, an additional geographical selection - removing shallow waters, areas of high oceanic variability and high latitudes ($> |50|$ deg) - is applied.

6.2. Mono-mission SSH crossovers

The cycle by cycle mean of SSH crossover differences is plotted in figure 99. All curves follow similar variations and average close to zero, Sentinel-6 MF HR retrackers and Jason-3 having a slightly higher mean at 0.8 mm and 0.6 mm respectively, compared to Sentinel-6 MF LR MLE4 and LR NR (-0.02 mm and -0.01 mm respectively). This bias is currently under investigation; it might be related to the wind-speed direction effect in the HR retrackers.

SSH difference at crossover (mean)

	nbr	min	mean	median	max	std
LR_MLE4	38	-0.3136	-0.001573	-0.02144	0.3472	0.1599
LR_NR	38	-0.3114	-0.001476	-0.04348	0.3552	0.162
HR_SAMOSA	38	-0.3601	0.08163	0.07892	0.41	0.1702
HR_NR	38	-0.3808	0.08126	0.08014	0.3802	0.1718
J3	37	-0.5282	0.06373	0.02474	2.132	0.4244

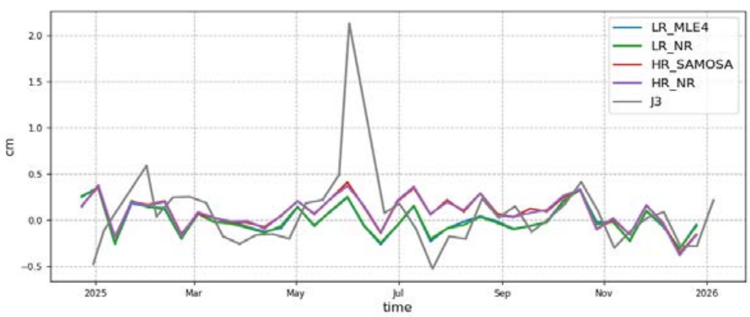

Figure 99: Mean SSH differences at crossovers by cycle for Sentinel-6 MF LR MLE4 (blue), LR NR (green), HR SAMOSA (red) and HR NR (purple) and Jason-3 (black). Computed over 2025.

Figure 100 presents the monitoring of the error of crossover SSH differences, for Sentinel-6 MF LR, HR, and Jason-3, computed as the standard deviation divided by $\sqrt{2}$. Indeed we consider the error to be measured twice, both on ascending and descending arcs, with supposedly decorrelated differences.

All datasets show very good performance, very similar and stable in time. Sentinel-6 MF LR MLE4 and LR NR have similar errors, at 3.3 cm in average, while Sentinel-6 MF HR SAMOSA and HR NR error is slightly lower at 3.2 cm, partially due to lower noise in HR retrievals. Jason-3 error is slightly higher than Sentinel-6 MF, with a mean value of 3.4 cm. These results are summarized in table 6.

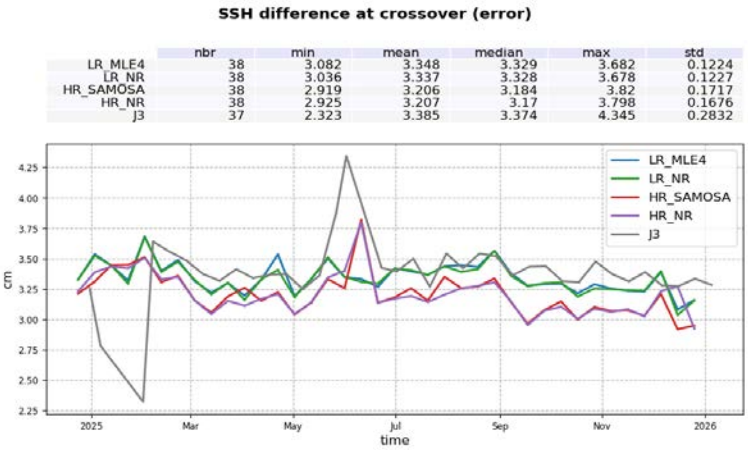

	nbr	min	mean	median	max	std
LR_MLE4	38	3.082	3.348	3.329	3.682	0.1224
LR_NR	38	3.036	3.337	3.328	3.678	0.1227
HR_SAMOSA	38	2.919	3.206	3.184	3.82	0.1717
HR_NR	38	2.925	3.207	3.17	3.798	0.1676
J3	37	2.323	3.385	3.374	4.345	0.2832

Figure 100: Error of SSH differences at crossovers by cycle for Sentinel-6 MF LR MLE4 (blue), LR NR (green), HR SAMOSA (red) and HR NR (purple) and Jason-3 (black). Computed over 2025.

The cyclic monitoring of the crossover differences of the SSH using model wet tropospheric correction is plotted on figure 101. The means of the Sentinel-6 MF LR MLE4, LR NR, HR NR, HR SAMOSA and Jason-3 datasets with model WTC are slightly improved than with radiometer derived WTC, with respective differences not exceeding 0.1mm.

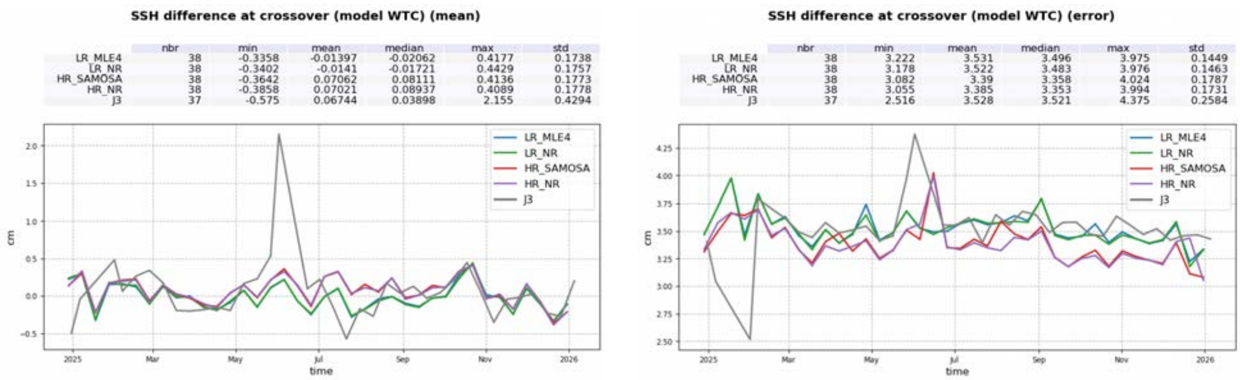

	nbr	min	mean	median	max	std
LR_MLE4	38	-0.3358	-0.01397	-0.02062	0.4177	0.1738
LR_NR	38	-0.3402	-0.0141	-0.01721	0.4429	0.1757
HR_SAMOSA	38	-0.3642	0.07062	0.08111	0.4136	0.1773
HR_NR	38	-0.3858	0.07021	0.08937	0.4089	0.1778
J3	37	-0.575	0.06744	0.03898	2.155	0.4294

	nbr	min	mean	median	max	std
LR_MLE4	38	3.222	3.531	3.496	3.975	0.1449
LR_NR	38	3.178	3.522	3.483	3.976	0.1463
HR_SAMOSA	38	3.082	3.39	3.358	4.024	0.1787
HR_NR	38	3.055	3.385	3.353	3.994	0.1731
J3	37	2.516	3.528	3.521	4.375	0.2584

Figure 101: Mean (left) and error (right) SSH differences at crossovers by cycle for Sentinel-6 MF LR MLE4 (blue), LR NR (green), HR SAMOSA (red) and HR NR (purple) and Jason-3 (black), using model wet tropospheric correction. Computed over 2025.

The differences in errors are slightly higher than with radiometer derived WTC, by about 1.8 mm for all Sentinel-6 MF retrackers and 1.4 mm for Jason-3. This is expected as the radiometer allows for better restitution of the wet path delay in comparison to the model that is often too smooth. These results are summarized in table 6.

Mission	Mean (mm)		Error (cm)	
	Rad. WTC	Model WTC	Rad. WTC	Model WTC
Sentinel-6 MF LR MLE4	-0.02	-0.1	3.3	3.5
Sentinel-6 MF LR NR	-0.01	-0.1	3.3	3.5
Sentinel-6 MF HR SAMOSA	0.8	0.7	3.2	3.4
Sentinel-6 MF HR NR	0.8	0.7	3.2	3.4
Jason-3	0.6	0.7	3.4	3.5

Table 6: Mean and error of mono-mission SSH crossover differences for Sentinel-6 MF LR and HR and Jason-3

The maps of LR and HR SSH differences at crossovers are smooth and do not highlight any strong discrepancies between ascending and descending tracks in terms of SSH (figure 102 top panels).

The map of HR SSH difference at crossover highlights patterns correlated to along-track wind (bottom panel). It is linked to the impact of along-track wind on HR data and more particularly on HR range (see section 5.3.).

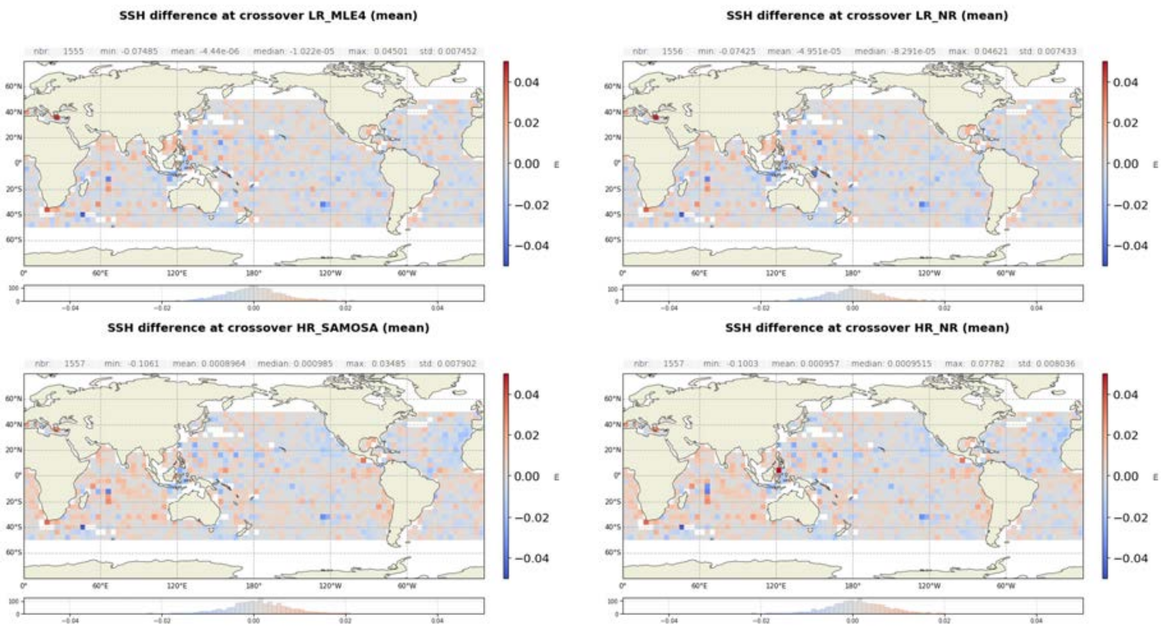

Figure 102: Maps of mean SSH differences at mono-mission crossovers in m for LR MLE4 (top left), LR NR (top right), HR SAMOSA (bottom left) and HR NR (bottom right) computed over 2025.

6.3. Multi-mission SSH crossovers

Multi-mission crossover analysis is also performed between Sentinel-6MF and Jason-3. The corresponding SSH difference is plotted on figure 103. All four cases, LR MLE4/Jason-3, LR NR/Jason-3, HR SAMOSA/Jason-3 and HR NR/Jason-3, follow the same variations, with means of -0.07 cm, -0.03 cm, 1.34 cm and -0.32 cm respectively. A jump is observed after the PB G01 update, bringing the mean differences closer to zero, except for HR SAMOSA/Jason-3 due to the skewness not being applied in HR SAMOSA retracking.

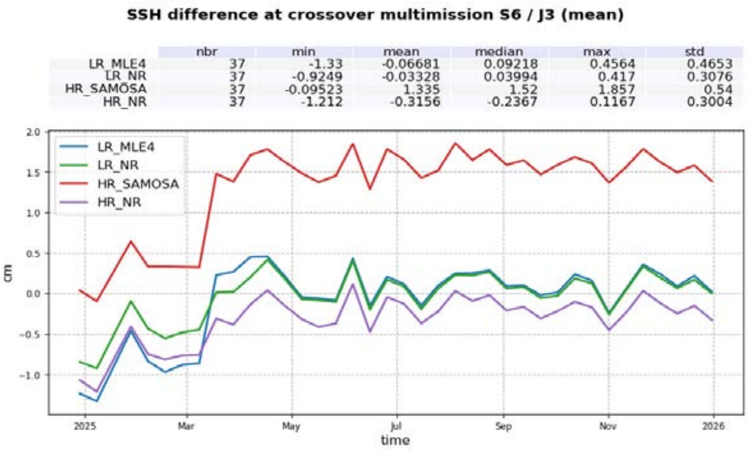

Figure 103: Mean multi-mission SSH differences at crossovers by cycle for Sentinel-6 MF LR MLE4/Jason-3 (blue), LR NR/Jason-3 (green), HR SAMOSA/Jason-3 (red) and HR NR/Jason-3 (purple). Computed over 2025.

Figure 104 presents the monitoring of the standard deviation of multi-mission crossover SSH. All datasets show very good performance at 4.9 cm for LR retrackers and 4.8 cm for HR ones.

A peak is observed in the first half of June, coinciding with the end of the second tandem phase, during which the availability of Jason-3 data decreases as a result of its orbit transition.

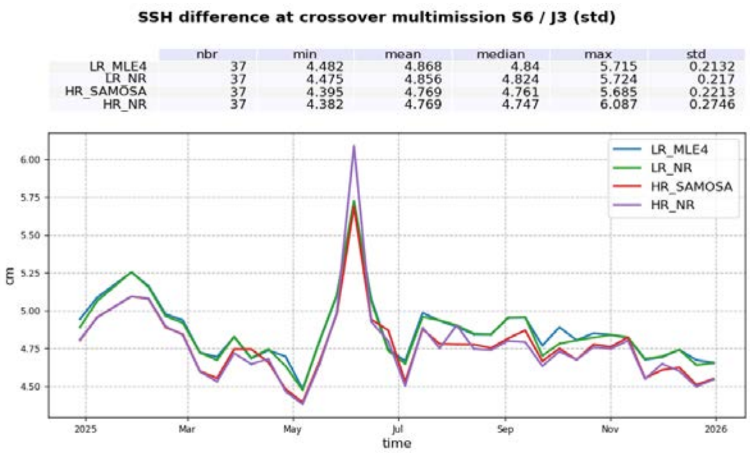

Figure 104: STD multi-mission SSH differences at crossovers by cycle for Sentinel-6 MF LR MLE4/Jason-3 (blue), LR NR/Jason-3 (green), HR SAMOSA/Jason-3 (red) and HR NR/Jason-3 (purple). Computed over 2025.

The cyclic monitoring of the multi-mission crossover differences of the SSH using model wet tropospheric correction is plotted on figure 105. The average SSH crossover difference per cycle follows the same variation as the crossover SSH with radiometer-derived WTC, with only minor value differences.

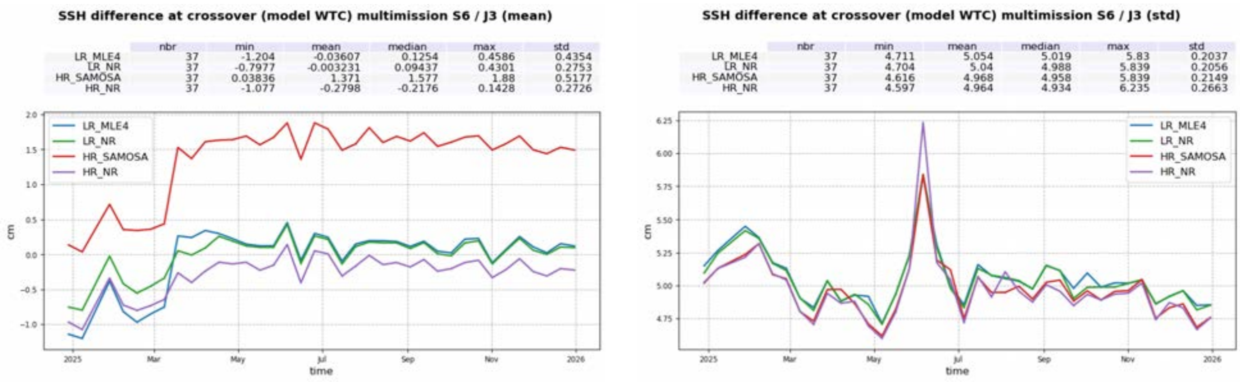

Figure 105: Mean (left) and standard deviation (right) of multi-mission SSH differences at crossovers by cycle for Sentinel-6 MF LR MLE4 / Jason-3 (blue), LR NR / Jason-3 (green), HR SAMOSA/Jason-3 (red) and HR NR/Jason-3 (purple). Computed over 2025 using model WTC for SSH.

The corresponding geographical distributions and their differences are presented in figure 106. While no significant regional pattern can be seen in the Sentinel-6 MF LR/Jason-3 SSH crossovers differences, Sentinel-6 MF HR SAMOSA/Jason-3 SSH crossovers differences are higher at high latitudes. This difference in geographical pattern is clearly visible in the bottom panel, with differences up to about 2 cm at high latitudes, while it is around 0 cm in the equatorial regions. This is expected as no skewness is used in HR SAMOSA processing, unlike LR, HR NR and Jason-3 processing, leading to a residual correlation of the range to sea state conditions (see section 5.3.).

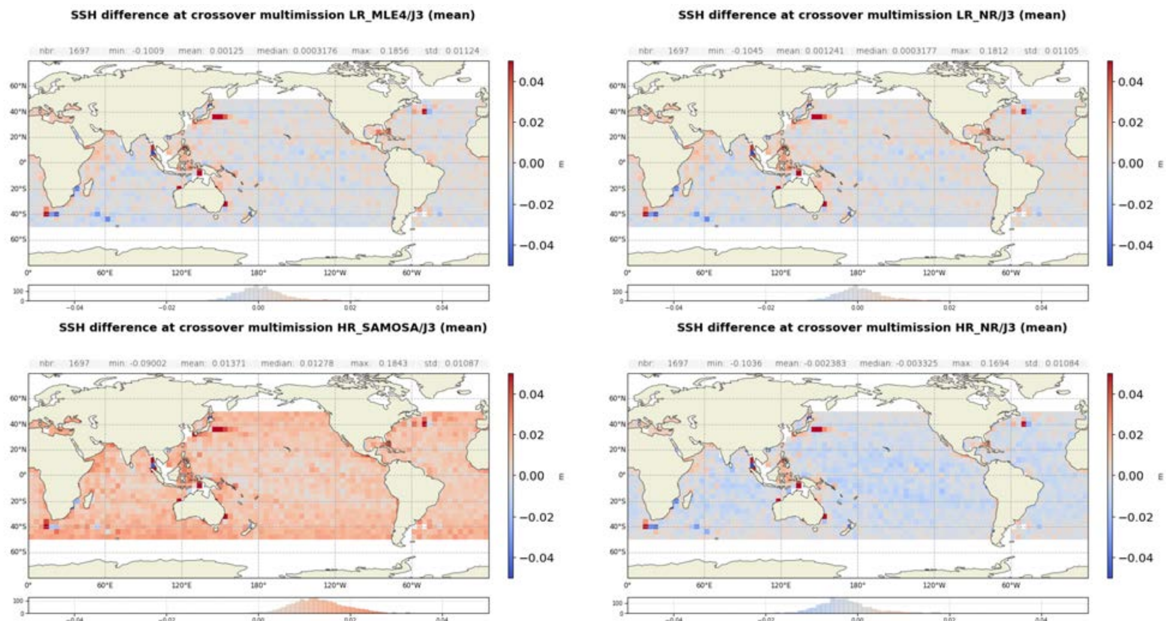

Figure 106: Maps of multi-mission mean SSH differences at crossovers for LR MLE4/Jason-3 (top left), LR NR/Jason-3 (top right), HR SAMOSA (bottom left) and HR NR (bottom right) computed over 2025.

6.4. Pseudo time tag bias

The pseudo time tag bias (α) is found by computing at mono-mission SSH crossovers a regression between SSH and orbital altitude rate ($\dot{H}$), also called satellite radial speed: SSH = $\alpha\dot{H}$. This empirical method allows us to estimate the potential real time tag bias but it can also absorb other errors correlated with $\dot{H}$. Therefore it is called “pseudo” time tag bias. The monitoring of this coefficient estimated at each cycle is performed for Sentinel-6 LR and HR in figure 107.

Its mean is -45 μs for LR MLE4, -45 μs for LR NR, -29 μs for HR SAMOSA and -29 μs for HR NR mode, and never exceeds a few hundred microseconds. Mean values and variations are consistent across all four retrackers and with previous years ([9]).

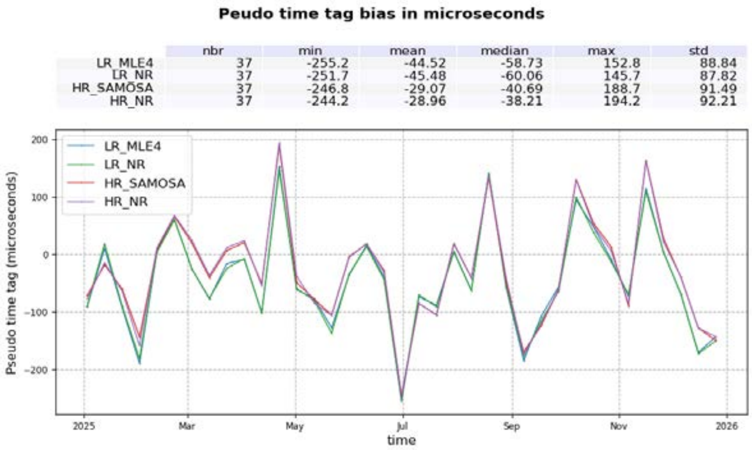

Figure 107: Pseudo time tag bias by cycle for LR MLE4 (blue), LR NR (green), HR SAMOSA (red) and HR NR (purple). Computed over 2025.

6.5. Transponder analysis

An absolute calibration of the Poseidon-4 altimeter is performed over the CDN1 transponder in West Crete mountains for each descending Sentinel-6 MF pass number 18.

The range bias (see figure 108) is calculated for each waveform seeing the Cal/Val site by taking the difference between the transponder-altimeter distance (accurately determined using a precise positioning of the satellite and of the transponder site) and the altimeter range derived from the retracking (based on a sinc-function fit) of the transponder-generated waveform. Note that the altimeter bias is further corrected for transponder and altimeter related errors, the Doppler range shift, and delays through the atmosphere.

The datation bias is also computed and presented in figure 109.

No clear trend is observed but there is remaining significant variability from one cycle to another.

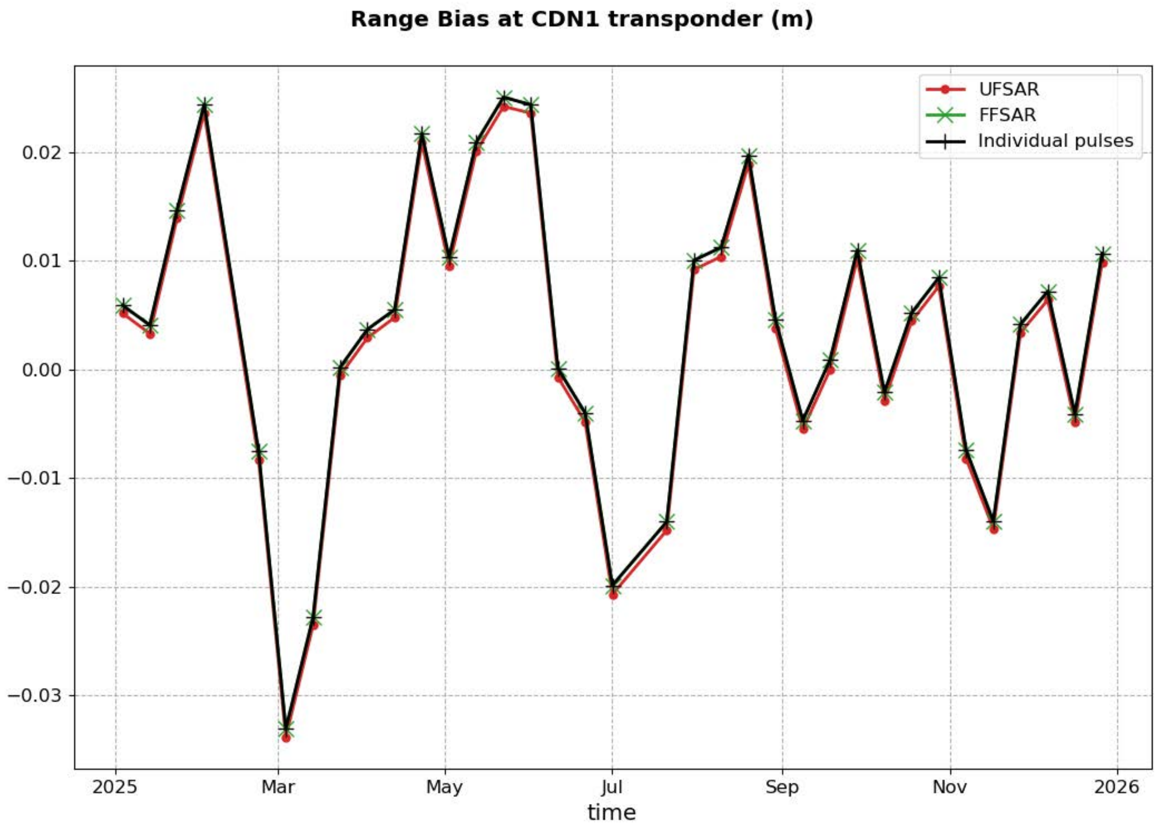

Figure 108: Monitoring of the range bias at CDN1 transponder, computed per cycle for the year 2025.

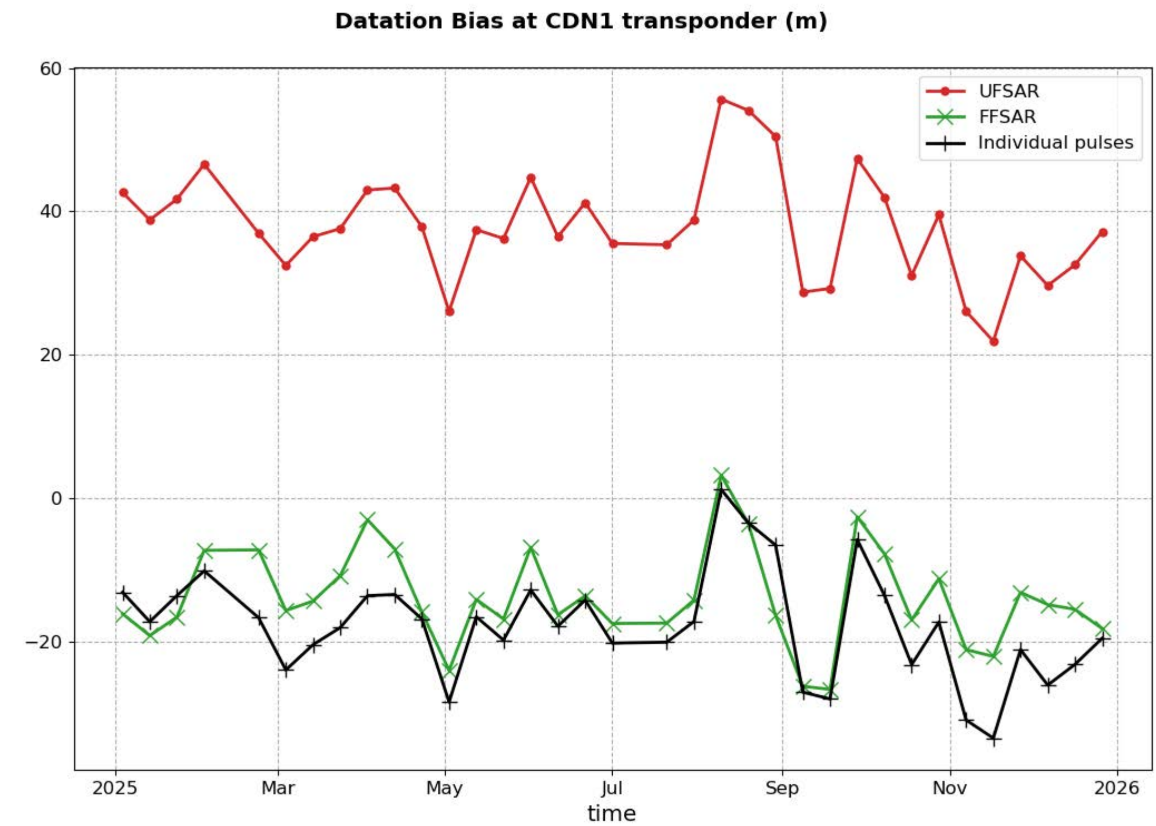

Figure 109: Monitoring of the datation bias at CDN1 transponder, computed per cycle for the year 2025.

7 SSHA along-track analysis

7.1. Overview

The Sea Surface Height Anomaly (SSHA) is the most well-known parameter estimated from altimetry. It corresponds to the elevation of sea surface, with respect to a reference called Mean Sea Surface (MSS), generated by oceanic variability and climatic phenomena (such as Gulf stream current, El Nino, ...). It is computed as follow:

$$SSHA = Orbit - AltimeterRange - \sum(GeophysicalCorrections) - MeanSeaSurface$$

The details of the geophysical corrections can be found in Sentinel-6 ALT Level 2 Product Generation Specification [3].

SSHA analysis is a complementary indicator to estimate the altimetry system performance. It enables the study of the evolution of the SSHA mean (detection of jump, abnormal trend or geographical correlated biases), and also the evolution of the SSHA variance highlighting the long-term stability of the altimetry system performance.

The SSHA distributions are plotted on figure 110 for Sentinel-6 MF LR MLE4, LR NR, HR SAMOSA and HR NR as well as Jason-3. Mean values are 5.3 cm for Sentinel-6 MF LR MLE4, 5.3 cm for LR NR, 3.9 cm for HR SAMOSA and 5.5 cm for HR NR. Sentinel-6 LR MF retrackers are very close to Jason-3 mean value (5.3 cm).

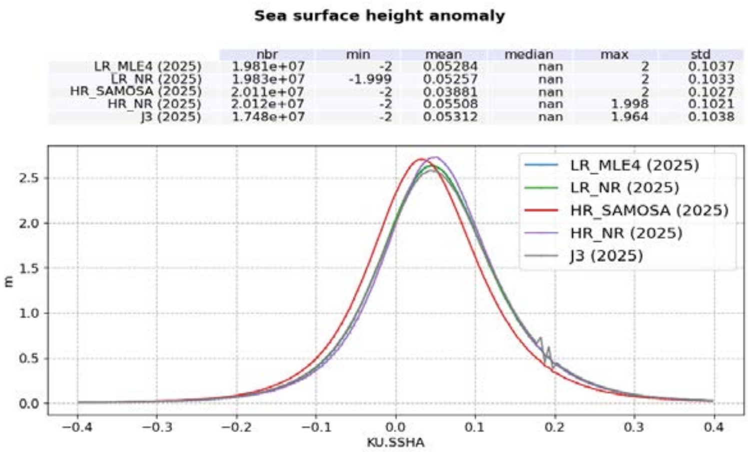

Figure 110: Histograms of SSHA in m for Sentinel-6 MF LR MLE4 (blue), LR NR (green), HR SAMOSA (red), HR NR (purple) and Jason-3 (black).

The monitoring of the SSHA daily mean is presented on figure 111, left panel. With the exception of HR SAMOSA retracker, Sentinel-6 MF and Jason-3 SSHA are very close. Sentinel-6 MF HR SAMOSA SSHA curve is slightly lower due to its skewness correction being set to zero, with an additional drop of about 1 cm after the PB G01 update, increasing its bias relative to the other retrackers. All curves follow similar seasonal cycles and variations.

On figure 111, right panel, is plotted the daily monitoring of the SSHA standard deviation. The Caspian Sea has been excluded from this monitoring as it creates spikes in the standard deviation on days that this region is observed, reducing the readability of the figure. All curves present similar variations, averaging at 10.3 cm for Sentinel-6 MF LR and Jason-3 and 10.2 cm for Sentinel-6 MF HR.

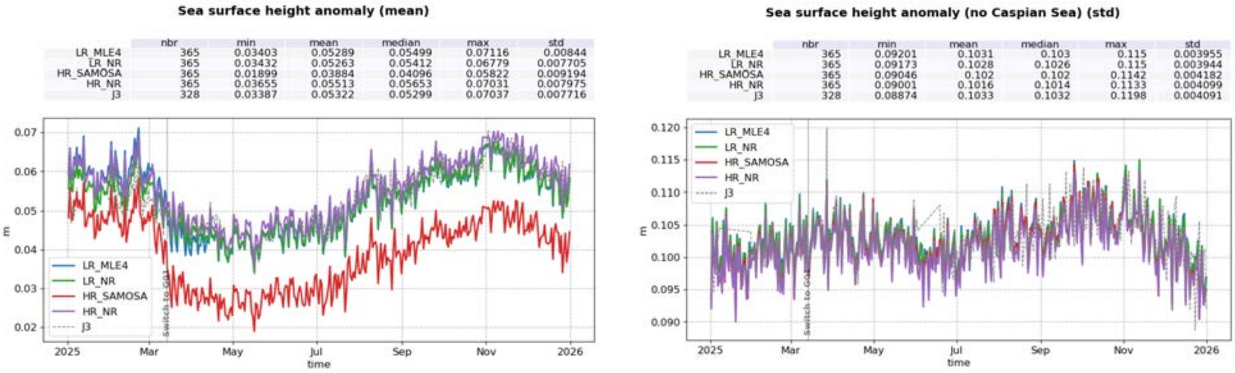

Figure 111: Mean (left) and standard deviation (right) SSHA by day for LR MLE4 (blue), LR NR (green), HR SAMOSA (red), HR NR (purple) and Jason-3 (black).

Figure 112 presents the monitoring of the SSHA computed with model WTC, both in mean (left panel), and standard deviation (right). The use of the model wet tropospheric correction has little impact on the SSHA mean (about 1 mm).
The standard deviation of the SSHA is slightly impacted as well, and increases about 0.4 mm for all datasets when using the model WTC.

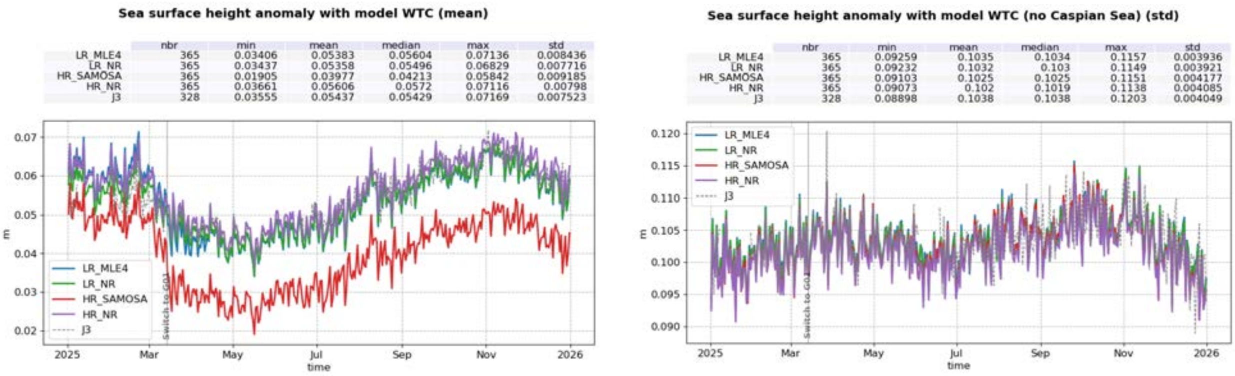

Figure 112: Mean (left) and standard deviation (right) SSHA with wet tropospheric correction from model by day for LR MLE4 (blue), LR NR (green), HR (red) and Jason-3 (black).

7.2. SSHA differences between LR MLE4 and NR

The LR NR - LR MLE4 differences monitoring in figure 113 shows an about 6.5 mm jump at PB G01 update, and another -2 mm jump at the LR MLE4 LUT update. The SSHA series provided by LR retrackers are now in good agreement, with a mean difference under 1 mm and a reduced standard deviation of these differences. This monitoring does not allow to observe the improvement brought by the numerical retracker on the long-term stability of the sea level (no drift observed and occurrence of multiple jumps). A longer and homogenous time series will be studied in the PB G01 full mission reprocessing planned for 2026.

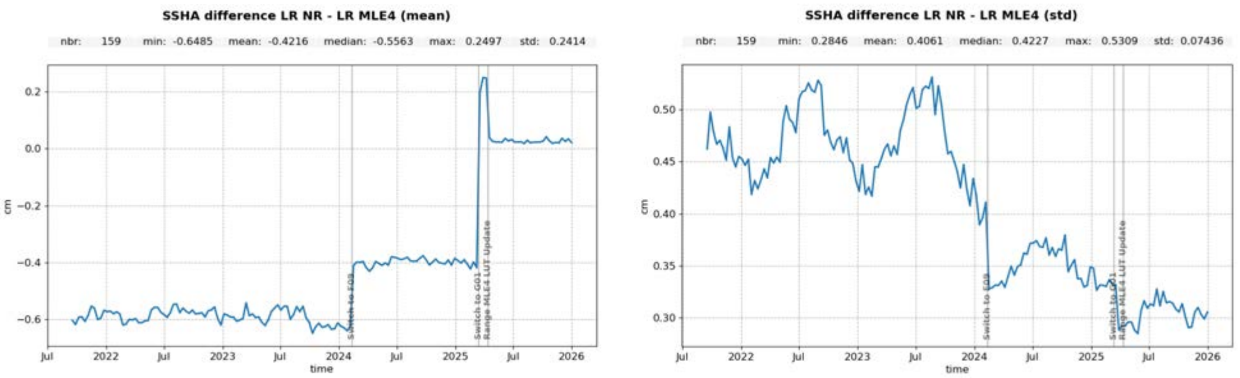

Figure 113: Time monitoring of Sentinel-6 MF LR NR - LR MLE4 SSHA in meters, without the Caspian Sea. Left: mean per cycle, Right: standard deviation per cycle.

The corresponding map on figure 114 highlights a small correlation to SWH of about -1.5 mm between 1 and 7 m SWH. This residual dependency on sea state mainly originates from the PB F09 data contribution, as it was significantly reduced following the MLE4 LUT update implemented in PB G01 (Please refer to Section **5** for more details).

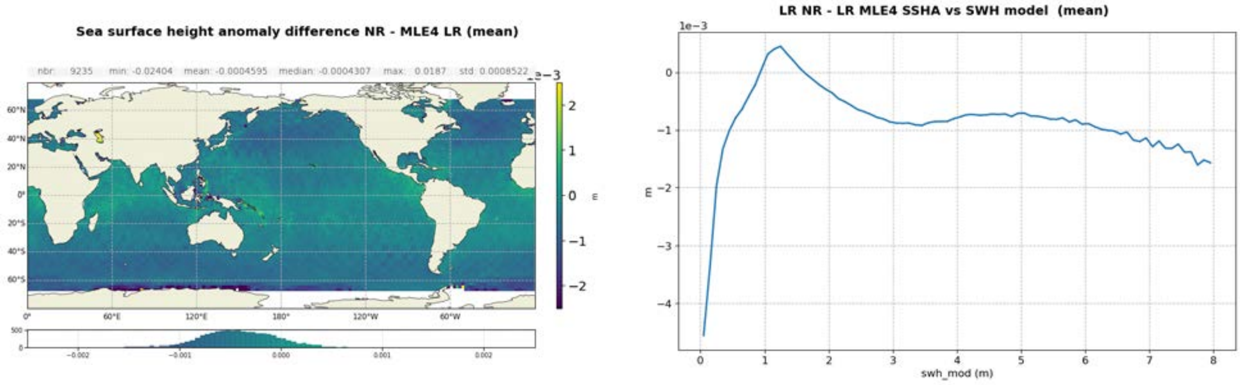

Figure 114: Map of Sentinel-6 MF LR NR - LR MLE4 SSHA in meters (left), and its mean as a function of ERA 5 model SWH (right).

The distribution of SSHA difference is presented on figure 115 for side B. LR SSHA are consistent between retrackers, with only a 0.5 mm bias between LR NR and LR MLE4.

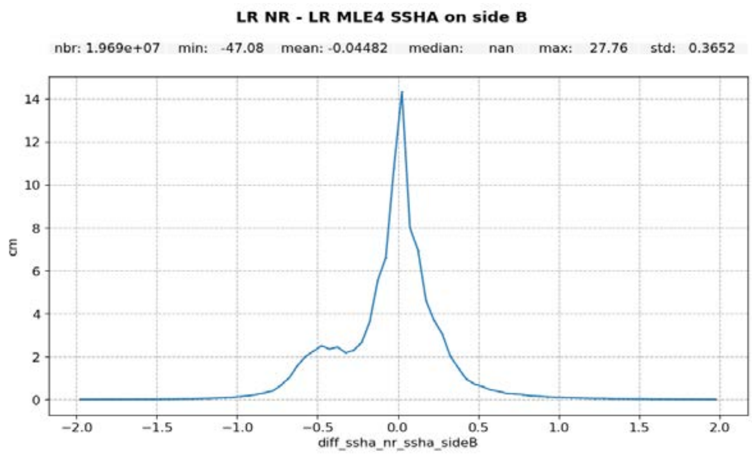

Figure 115: Distributions of Sentinel-6 MF LR NR - LR MLE4 SSHA difference for side B.

7.3. SSHA differences between HR SAMOSA and NR

Figures 116 and 117 show the map, correlation to SWH and distribution respectively of HR NR - HR SAMOSA SSHA differences. The bias (1.6 cm) and correlation to SWH (+1.4 cm between 1 and 7m SWH) are higher than in LR. This is due to the skewness difference between SAMOSA and NR.

The time monitoring (computed 11 months of available F09 data, not shown) are too short to observe any impact of the numerical retracker on the long-term stability of the HR sea level. Further analysis will be conducted with the PB G01 full mission reprocessing (2026).

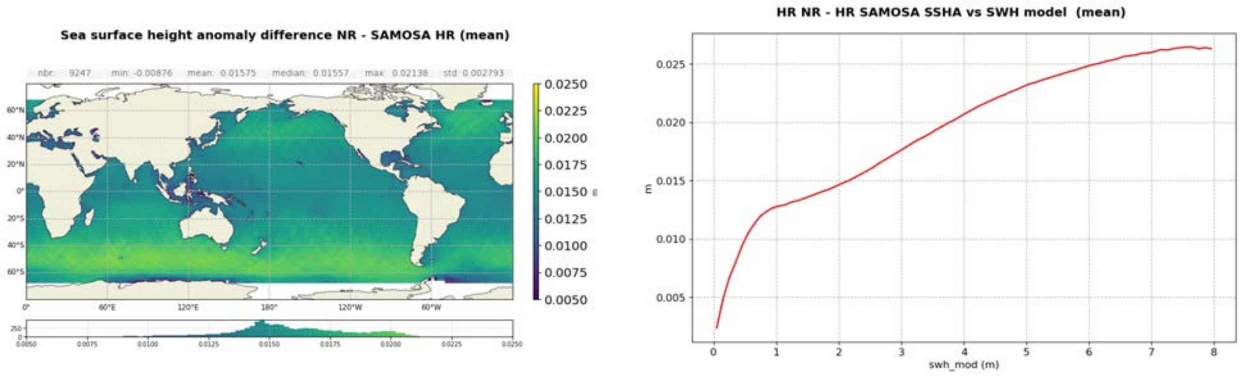

Figure 116: Map of Sentinel-6 MF HR NR - HR SAMOSA SSHA in meters (left), and its mean as a function of ERA 5 model SWH (right).

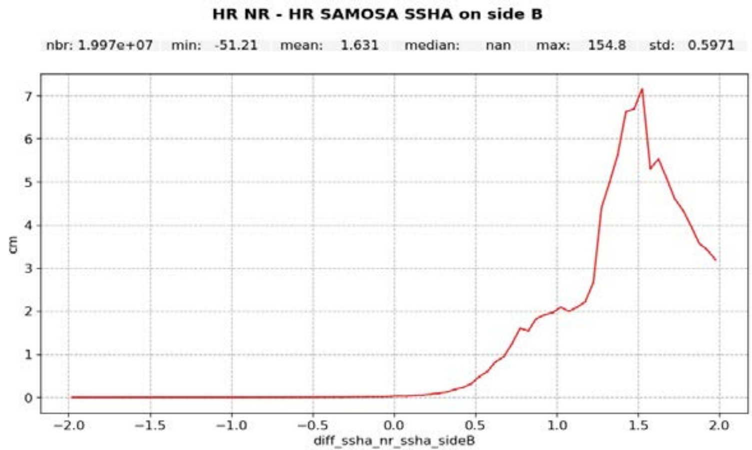

Figure 117: Distributions of Sentinel-6 MF HR NR - HR SAMOSA SSHA difference for side B.

7.4. SSHA differences between HR and LR

Figure 118 presents the monitoring of the HR SAMOSA - LR MLE4 (black) and HR NR - LR NR (grey) SSHA differences. These differences are centered around 1.4 cm and 0.2 cm over 2025 respectively. In the HR SAMOSA - LR MLE4 difference, a smooth shift of about -3 mm is visible after the PB G01 update.

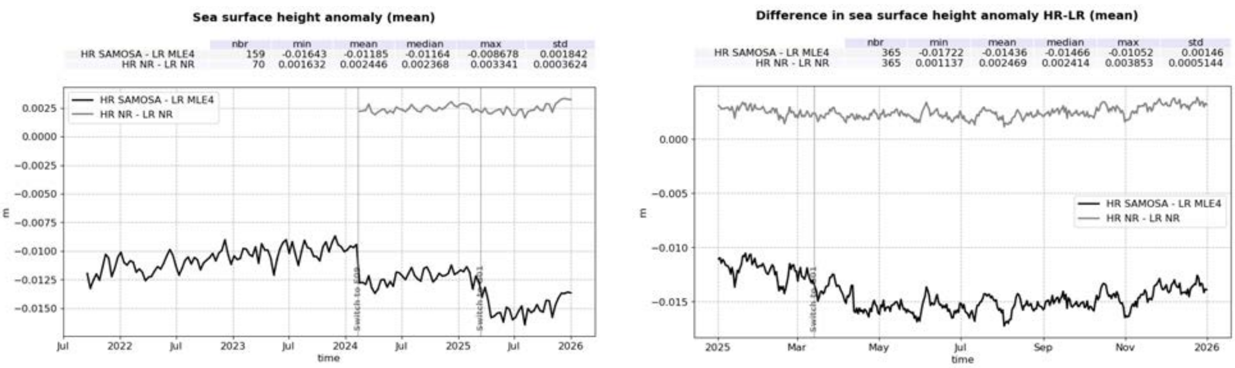

Figure 118: Mean per cycle over side B (left) and per day over 2025 (right) of the HR SAMOSA - LR MLE4 (black) and HR NR - LR NR (grey) SSHA difference.

The geographical distributions of both HR-LR SSHA differences are represented in figure 119. As expected from section 5.3., the HR SAMOSA - LR MLE4 differences are highly correlated with SWH and are mainly due to the absence of skewness parameters in the SAMOSA processing. This correlation is strongly reduced for the HR NR - LR NR difference but not null. The remaining correlation is partly due to the pulse-to-pulse correlation effect impacting LR data.

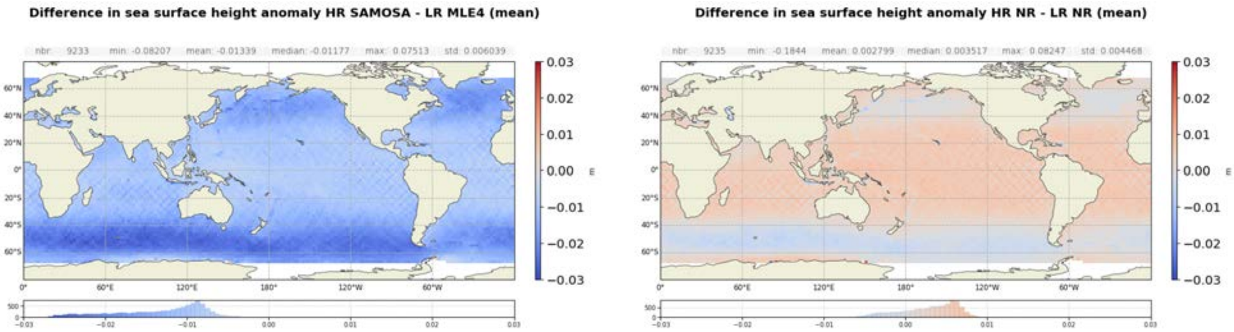

Figure 119: Maps of mean SSHA HR SAMOSA - LR MLE4 (left panel) and HR NR - LR NR (right panel) difference in meters. Computed over 2025.

8 Mean Sea Level trends

8.1. Computation of the Mean Sea Level

The Global Mean Sea Level (GMSL) is one of the most important indicators of climate change. In the past two decades, sea level has been routinely measured from space using satellite altimetry techniques. Since April 2022, Sentinel-6 MF satellite has taken over the responsibility as the reference mission to continue the long-term record of sea-surface height measurements. The role of Copernicus Sentinel-6 MF is not only to extend the GMSL climate record, but also to monitor the changing height of the sea surface with greater precision than before.

Over the tandem phase of Sentinel-6 MF (till cycle 051), both Jason-3 and Sentinel-6 MF satellites flew on the same ground track, only 30s apart. They therefore measured the same ocean, allowing to calibrate Sentinel-6 MF. This allowed linking precisely the MSL time series of Jason-3 and Sentinel-6 MF. The uncertainty of the bias value between the two time series is less than 1 mm. The evolution of the ocean MSL can therefore be precisely observed on a continuous basis since 1993 thanks to the 5 reference missions: TOPEX/Poseidon, Jason-1 (from May 2002 to October 2008), Jason-2 (from October 2008 to May 2016), Jason-3 (from May 2016 to April 2022) and now Sentinel-6 MF (from April 2022 onwards).

Please note that the GMSL presented on figure 120 is computed using DT2024 L2P standards, which uses LR NR data for S6-MF.

Wet troposphere correction, inverse barometer correction, Glacial Isostatic Adjustment are applied to calculate the MSL and the data series are linked together accurately thanks to the tandem flying phases.

For more details about Mean Sea Level (MSL) estimation method, see the dedicated report on the MSL Aviso Website: http://www.aviso.altimetry.fr/msl. This report includes the description of the Mean Sea Level indicator, the comparisons between altimetry and tide gauges measurements, the comparisons between altimetry and ARGO+GRACE measurements and specific studies linked to MSL activities. An exhaustive overview of possible errors impacting the MSL evolution is given in [21]. Furthermore, annual and semi-annual signals are removed from the time series and a 2-month filter is applied.

Though mean sea level trend is globally positive, it is heterogeneously distributed over the ocean: locally, sea level rise or decline up to ± 10 mm/yr are observed as shown on the right panel of figure 120 (note that this map of regional MSL trends is estimated from multi-mission grids (Copernicus Climate Change Service products) in order to improve spatial resolution).

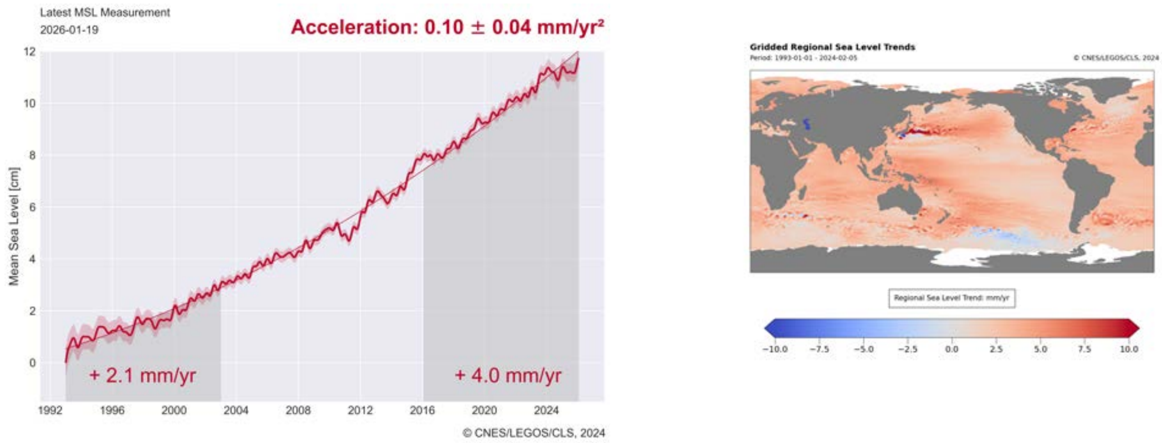

Figure 120: Global (left) and regional (right) MSL trends from 1993 onwards.

8.2. Comparison of LR MLE4, LR NR and HR GMSL

This section focusses on GMSL derived from Sentinel-6 MF from the switch to POS4-B to the end of 2025. The GMSL for LR (MLE4 and NR) and HR SAMOSA are plotted on figure 121, along with Jason-3 estimate over the same period. Due to its shorter time series, GMSL for HR NR is not presented here. This GMSL is computed on a 2-months low-pass filtered data, after having removed the seasonal signals. Such computation is performed with an Ordinary Least Square (OLS) approach, using SSHA from L2 products as input. The details on the computation of the GMSL and its uncertainties are described in Guerou et al. (2022) [21].

Sentinel-6 MF LR MLE4 show lower trends than LR NR with slopes at 1.62 $\pm$ 0.78 mm/yr and 3.51 $\pm$ 0.77 mm/yr respectively. Over the period available here, the improvement brought by the numerical retracker in terms of long term stability cannot be demonstrated. It rather shows the stability of POS-4B retrievals. HR SAMOSA trend is lower than both LR retrackers, at 0.64 $\pm$ 0.77 mm/yr. Over the same time period, Jason-3 GMSL trend is globally higher than for Sentinel-6 MF with 4.91 $\pm$ 0.77 mm/yr. These trends do not significantly change when using model wet tropospheric correction, as shown on the dashed curves of figure 121 and in table 7, suggesting a good stability of the radiometer-derived wet tropospheric correction. Uncertainties are given at the 1.645 sigma confidence level. From mid-2023 to mid-2024, oscillations can be seen on all GMSL curves. This is linked to the El Niño phenomenon occurring during this period.

Please note that the side B GMSL presented here are computed on a small timescale (less than 28 months) and therefore are impacted by correlated noise leading to significant uncertainties.

Mission/mode	**Trend with Rad WTC (mm/yr)**	**Trend with model WTC (mm/yr)**
Sentinel-6 MF LR MLE4	1.62 $\pm$ 0.78	1.74 $\pm$ 0.78
Sentinel-6 MF LR NR	3.51 $\pm$ 0.77	3.63 $\pm$ 0.78
Sentinel-6 MF HR SAMOSA	0.64 $\pm$ 0.77	0.76 $\pm$ 0.78
Jason-3 MLE4	4.91 $\pm$ 0.77	4.84 $\pm$ 0.77

Table 7: GMSL trend values and corresponding 1.645 sigma uncertainties for Sentinel-6 MF LR, HR and Jason-3 (on the Sentinel-6 MF period), with radiometer and model wet tropospheric corrections. Computed over POS4-B period, i.e. from cycle 32 onwards.

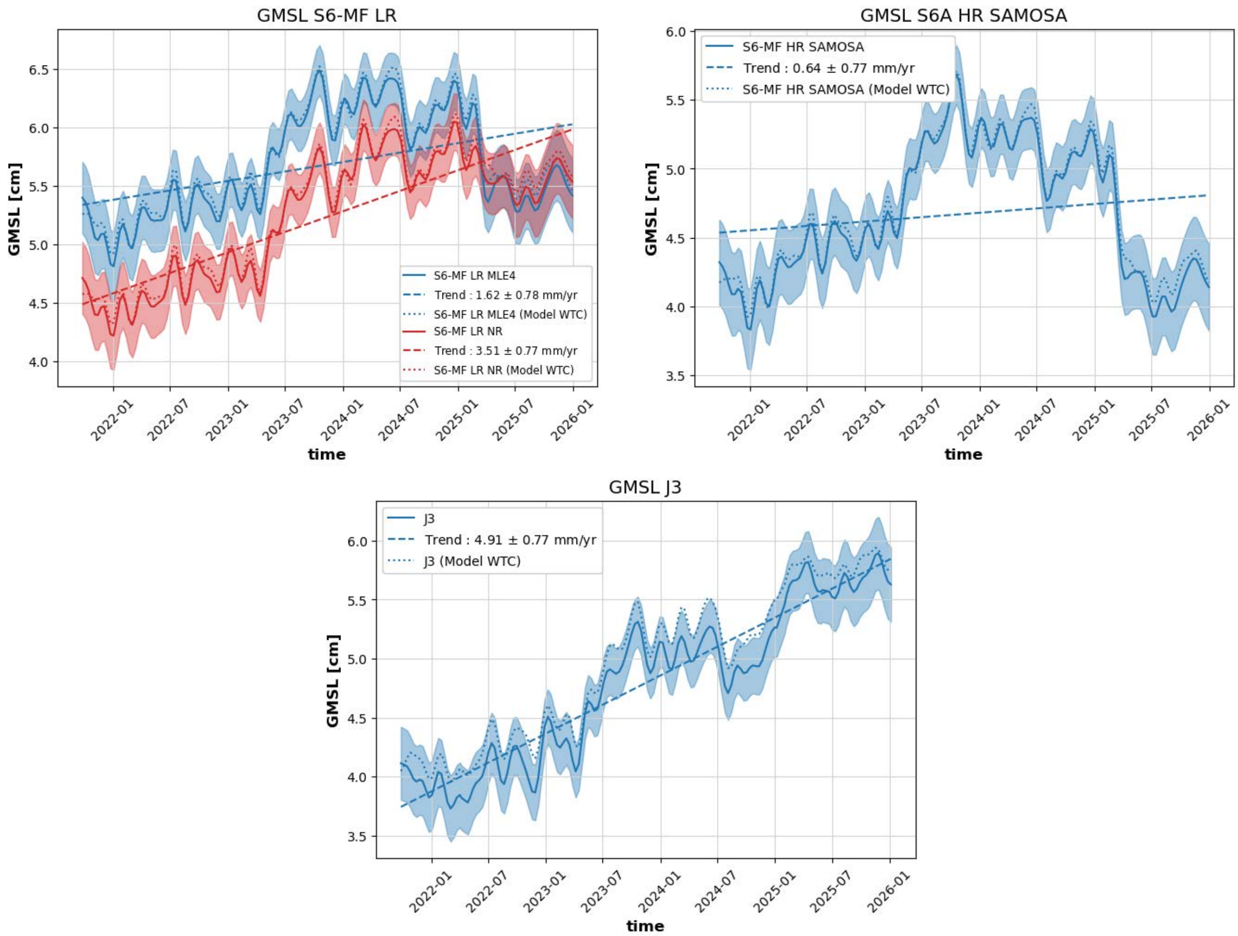

Figure 121: GMSL from Sentinel-6 MF LR data (top left), Sentinel-6 MF HR data (top right) and from Jason-3 GDR-F data with a 1.645 sigma confidence interval. Computed over Sentinel-6 MF POS4-B period, i.e. from cycle 32 onwards.

Sentinel-6 MF GMSL may be impacted by two known effects, none of which are taken into account in the uncertainty computation:

- the evolution of the PTR (Point Target Response) shape in the range direction. It impacts range (PTR dissymmetry) and SWH estimates (main lobe width) both in LR MLE4 and HR SAMOSA. Numerical retracker allows accounting for the PTR shape evolution thanks to the use of in-flight PTRs.
- the evolution of the PTR shape in the azimuth direction, impacting HR range only. It is corrected thanks to the range walk correction, that is available in PB F09. The impact of this correction has been estimated at 3.1 mm/yr, based on Dinardo 2022 study [14]. Please note that the Dinardo 2022 study only covers the first 9 months of side B, from September 2021 to June 2022, and that values may be different after the second half of 2022 because of an expected ongoing stabilization.

It is important to note that these results cover a period with several version changes in the data processing (F08 patch version in October 2023, F09 update in February 2024 and G01 update in March 2025), and therefore must be considered carefully.

9 Particular points and investigations

Within the framework of a CNES R&D project, an in-depth analysis of the Sentinel-6MF altimeter data (including Sentinel-3 data when relevant) is being conducted, along with the development of improved data processing methods. The objective is to optimize the exploitation of the mission capabilities and ultimately enhance the operational use of these data in marine applications. Within this project, three main tasks are addressed:

- a study to analyze and improve the quality of the S6-MF data over transponders and corner reflectors, including an assessment of S3 data over CNES-deployed corner reflectors,
- a study to improve the quality of the sea surface height measurements from the S6-MF mission,
- a study to improve the quality of the wave height measurements from the S6-MF mission.

This chapter presents the latest and most significant results obtained from this project, which was partly carried out using the CNES Sentinel Processing Prototype (SPP). It is organized into three sections corresponding to the aforementioned tasks, as detailed below.

9.1. Calibration of operational altimeter missions using external sites

Sentinel-6 MF (S6-MF) altimeter system calibration activities can be performed using ground-based external reflectors. These activities are of two main types:

The first activity focuses on producing and analysing long-term time series acquired over the active calibration devices located in Crete (CDN1) and Gavdos (GVD). The objective is to monitor both the range bias and the datation bias throughout the mission. The resulting measurements and trends are then reviewed and discussed within the Transponder Working Group, contributing to the overall assessment of the instrument calibration performance. Those results are shown for the CDN1 transponder in the section 6.5.

Various processing approaches show good consistency for range bias monitoring. For the datation bias, the UFSAR method yields an overestimation, a behaviour that is also observed by other teams. Regarding the range bias estimation, the results are very similar for the descending Track 018, which overflies both CDN1 and GVD. In contrast, for Track 109, a systematic offset is observed. This offset is likely related to an asymmetry of the calibration device and requires further confirmation by the TPX group.

The second activity concerns the characterization of the altimeter response over the Uscla corner reflector and the assessment of its performance for calibration purposes. Over this target, both the power (sigma-nought) and the range bias have been successfully monitored for most cycles from launch up to September 2025, despite the high clutter in the area. The range bias time series is well centered around zero, which is not the case for the transponder-based series. This discrepancy may be explained by the fact that such active devices require regular calibration of their internal path delay in order to accurately retrieve the true range bias. Regarding the power, the results are still calibrated as it also depends on the ground reflectivity. The time series becomes more chaotic and less reliable during autumn and winter due to heavy rainfall and the formation of water pools on the ground. These results however demonstrate the suitability of the corner reflector for long-term calibration monitoring and have led to recommendations for the development and deployment of enhanced, high-performance calibration facilities based on corner reflector, such as the one recently established by CNES in Grasse.

This study was carried out using the CNES/CLS transponder processing chain developed during the S6-MF commissioning phase and subsequently updated through more recent research efforts, including the implementation of a standalone processor capable of providing the geophysical and meteorological corrections computed at the corner reflector location

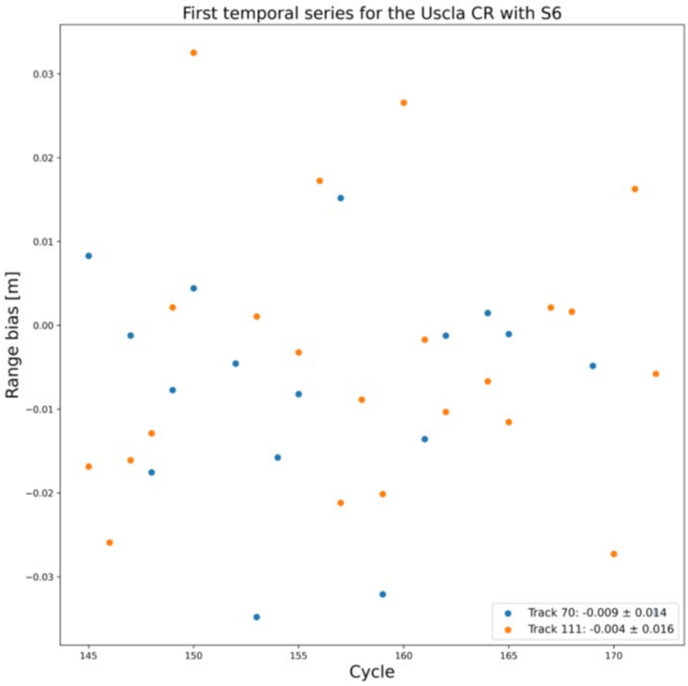

Figure 122: Time serie of the range bias over Uscla corner reflector. From the poster presented in the CalVal conference

9.2. Optimal estimator for LR mode data retracking

An optimal retracking estimator, hereafter referred to as the Weighted Least Square Estimator (WLS) [34], has been implemented in the Sentinel Processing Prototype (SPP). This approach leverages the methodology to provide unbiased estimates of Sentinel-6 LRM Ku-band altimeter parameters, while significantly reducing the variance of the retracked data: up to 60% for SWH, 12% for SSH and up to 50% for σ_0. The method requires an accurate characterization of the waveform noise statistics. This is challenging, as the waveform noise is a Gamma distributed multiplicative, thus model dependent, noise. In the case of onboard averaging enough number of echoes, the noise can be approximated to a Gaussian distribution. In this case, it can be demonstrated that a Weighted Least Squares estimator, with weights defined as the inverse of the data variance (i.e., the waveform noise), is equivalent to a Maximum Likelihood estimator, thereby guaranteeing optimal and unbiased parameter estimation. In the Gaussian approximation, the noise matrix can be expressed analytically as the squared waveform model divided by the Equivalent Number of Looks (ENL) function. For the Sentinel-6 mission, due to the 9 kHz Pulse Repetition Frequency, the ENL varies with range gate and depends on the model parameters, in particular SWH.

By accounting for a realistic characterization of the waveform noise, the WLS estimator provides unbiased estimates of the geophysical parameters (SWH, range, σ_0, and mispointing in the case of the numerical Brown–Hayne waveform model), with parameter uncertainties consistent with the Cramér–Rao lower bound of minimum variance.

Once implemented in the SPP, estimates of the geophysical parameters obtained with the WLS estimator and the unweighted numerical Ordinary Least Square (OLS), which is statistically equivalent to the operational Numerical Retracker, were generated from one Sentinel-6 data cycle (Cycle 24). Temporal and spectral analyses were performed, and 20-Hz noise levels were compared. The agreement with results in [34] validates the integration of the WLS method into the SPP.

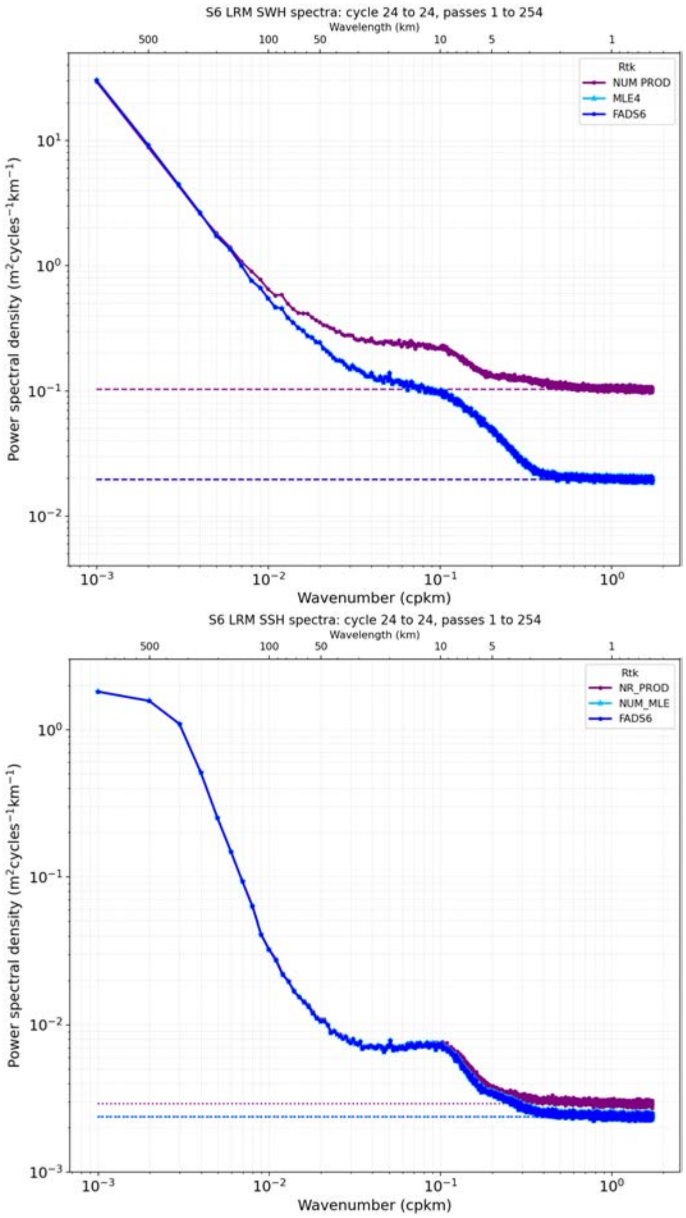

Figure 123: Sentinel-6 LRM spectra of SWH (top) and SSH (bottom) from one data cycle of 20 Hz measurements. The purple lines refer to the operational unweighted Numerical Retracker of the PDAP products, the blue lines to the weighted WLS retracker run with the Adaptive waveform model (dark blue) and the numerical Brown-Hayne model (cyan).

The resulting improvements in geophysical parameter estimation obtained with the WLS estimator, with respect to the unweighted operational Numerical Retracking solution are illustrated in Fig. 123, which shows SWH and SSH spectra computed for one data cycle.

Considering that an iterative estimation is required to robustly characterize the model-dependent multiplicative noise [34], the WLS estimation process takes approximately two to three times longer than the operational unweighted Numerical Retracking, depending on whether a preliminary L2 SWH estimate is available.

Following the application of WLS to LR Ku-band data, the same methodology was implemented in the numerical retracking of the C-band data processing, with the objective of improving C-band data quality compared with the current least-squares approach. The noise level affecting a mean waveform, built from the arithmetic mean of 7 independent pulses, closely follows a Gamma-law distribution, implying that C-band processing can theoretically benefit from WLS. A bias of 8.1 cm was identified between WLS and OLS range estimates, which is close to the 9.5 cm bias applied by [15] in numerical retracking (inherited from the range LUT used for C-band MLE3 data induced by the high speckle noise). This bias is consistent with the differences observed when comparing Ku- and C-band range estimates corrected for SSB and ionospheric delays. This preliminary result further suggests that WLS C-band range estimates would require a dedicated correction to be aligned with corrected C-band OLS estimates. Additional work is needed to confirm this bias, assess its dependence on sea state, and numerically determine the minimal number of averaged pulses required to obtain unbiased WLS estimates.

9.3. Analysis of the 140Hz USAR capability

We have processed Sentinel-6 and Sentinel-3 unfocused SAR altimetry data at increased posting rates to develop and validate an optimal filtering scheme that allows to properly compress the data back to 20 Hz [26]. This filter does not change the shape of the SLA and SWH power spectra (or alternatively their along track autocorrelation) at the highest frequencies—as would be the case when using a mean filter as in [27]—but reduces only the white noise floor over the entire spectrum.

We find that the effective precision gain in SLA and SWH from increased posting rates—averaged over all sea states in a cycle of data—actually reaches from only 9-19 percent. Only for low sea states of SWH< 1 m, the improvements exceed 20–25 %. We conclude that prior publications using a mean filter [27] overestimated the gains, due to the way in which the 20-Hz noise metric is calculated—a result which is affirmed by both the before-developed noise model [25] on the one hand and the optimally filtered data on the other hand, see Table 8 from [26]. Furthermore, it is shown by means of the noise model, that the results are closely tied to the Level-1b processing choices, primarily the number of looks used to average the waveforms.

average 20-Hz noise reduction in percentage points

	Sentinel-3			**Sentinel-6**		
	OF	HFA	mean filter	OF	HFA	mean filter
SLA	14.2 *(14.8)*	7.2 *(7.3)*	26.5 *(26.2)*	9.4 *(11.0)*	9.5 *(7.7)*	21.1 *(22.8)*
SWH	17.3 *(19.0)*	7.0 *(7.3)*	28.1 *(29.6)*	11.4 *(13.7)*	9.0 *(7.7)*	21.5 *(24.6)*

Table 8: Average noise reduction of the different methods in %, formatted as 'from data (from model)', each for ten days of data. ***Only the reduction by Optimal Filtering (OF) represents a true white noise floor improvement****, contrary to mean filter and HFA, which both introduce spectral artifacts.*

For more details, see the corresponding publication in [26].

Note with regard to the section on partially-focused SAR (PFSAR): From the noise model, it can also be anticipated that the precision improvements from relative oversampling are a peculiarity of unfocused SAR only. The effect is suppressed, as the azimuth resolution itself improves.

9.4. Application of LRRMC processing to Sentinel-6 data

The low resolution with range migration correction (LRRMC) processing, introduced by [35], is in many aspects like unfocused SAR (USAR), in that it includes Doppler beam forming, Doppler correction, and range migration correction. However, whereas in USAR the Doppler beam stacks are built from beams that point towards the same ground location, in LRRMC the stacks are made of beams from individual bursts. Hence, both use the same number of looks, but the LRRMC footprint is coarser, effectively smoothing surface waves and attenuating correlated errors at sub-mesoscales. As a result, the LRRMC noise levels have a negligible dependency on sea state. This was illustrated by [36] using Sentinel-3 data. Furthermore, [26] indicate that the performance of the LRRMC processing can be fully explained by speckle noise, while USAR suffers from an additional component pertaining to small-scale variability, whose importance increases with sea state.

We applied the LRRMC processing to Sentinel-6 MF and found an average improvement of 35 % on sea surface height noise and 50 % on significant wave height noise, at 3 m waves, compared to USAR. This is overall better than what was obtained with Sentinel-3A ([36]). The LRRMC and USAR sea level anomaly power spectra, shown in Figure 124, are similar down to scales of around 50 km. At scales lower than 10 km, the LRRMC spectrum is rather flat, consistent with white noise, whereas the USAR spectrum presents a red-noise slope. In between these scales, the LRRMC spectrum shows a slope that is less steep than the geostrophic slope, and also less steep than that obtained with Sentinel-3A ([36]).

We are currently looking into enhancing the outputs of the LRRMC processing by applying two-dimensional retracking models that include the effect of surface motions ([37], [31]). Indeed, as USAR, LRRMC exploits Doppler shifts and is consequently sensitive to sea-surface dynamics, which can distort the Doppler spectrum and ultimately limit the accuracy of geophysical retrievals. We are also investigating the application of the weighted least-squared retracking (, [34]), which according to [26] should yield the best currently attainable performance for a SAR-based processing.

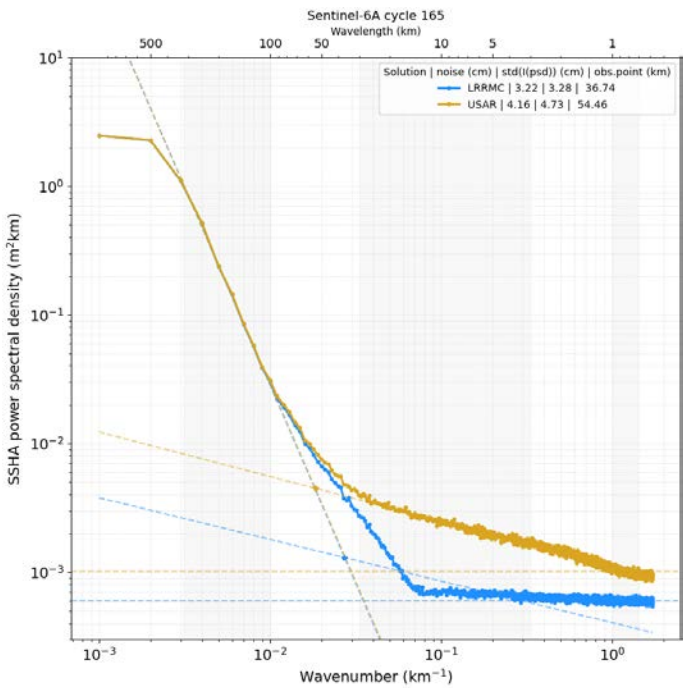

Figure 124: Sea level anomaly power spectra for LRRMC and USAR applied to Sentinel-6 MF data from cycle 165. The geostrophic slope, mesoscale slope, and noise level are estimated within the corresponding gray areas. The noise levels along with the observability points (smallest wavelength at which the dynamical structures can be observed from along-track data) are given in the labels.

9.5. Partially-Focused SAR (PFSAR) processing approach

The idea behind this research is to use neither unfocused SAR processing (coherent integration over a single burst duration) nor fully-focused SAR (coherent integration over all bursts) processing over ocean or coasts, but the “best” trade-off in between. Considering the resolution limits dictated by the sea state [28, 31, 32], the azimuth cut-off for the Sentinel-6 mission is almost always larger than 50 meters. A coherent integration over segments of 7 consecutive Sentinel-6 bursts increases the azimuth resolution to approximately 40 meters and, therefore, can capture all physically resolvable detail—as in FFSAR—while retaining a Doppler stack—as in USAR—that is compatible with the state-of-the-art 2D stack retrackers [30, 29]. To stay in line with previous nomenclature, we call this approach partially-focused SAR, while the general idea is also referred to as sublook processing in [32]. An example of differently processed waveforms is shown in Figure 125.

While an assessment of real data is ongoing, a first retracking study using speckled synthetic Doppler stacks already revealed increased performance across all retracked parameters, but in particular for the newly introduced wave vertical velocity variance σ_v^2 and u_x parameters, see Figure 126.

Hence, PFSAR is a promising candidate to simultaneously improve

1. the product resolution for optimal swell wave characterization and
2. the sensitivities to the new sea state parameters estimated by the recently developed 2D stack retrackers.

Furthermore, a PFSAR processor allows to emulate both USAR and FFSAR as special cases, therefore benefitting the continuity between processing modes and over different surfaces.

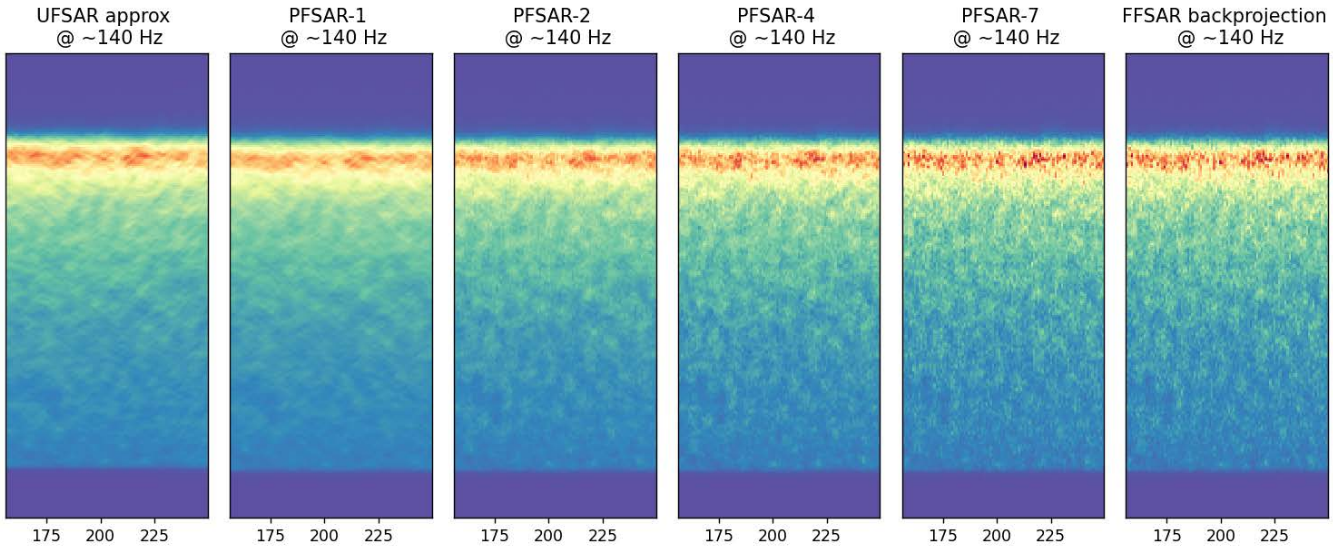

Figure 125: An example of a swell-impacted Sentinel-6 waveform segment of ~ 4.5 km along track distance. The same scene was processed with USAR (left), and FFSAR (right), and with different PFSAR-N configurations in between, where N indicates the number of coherently processed bursts.

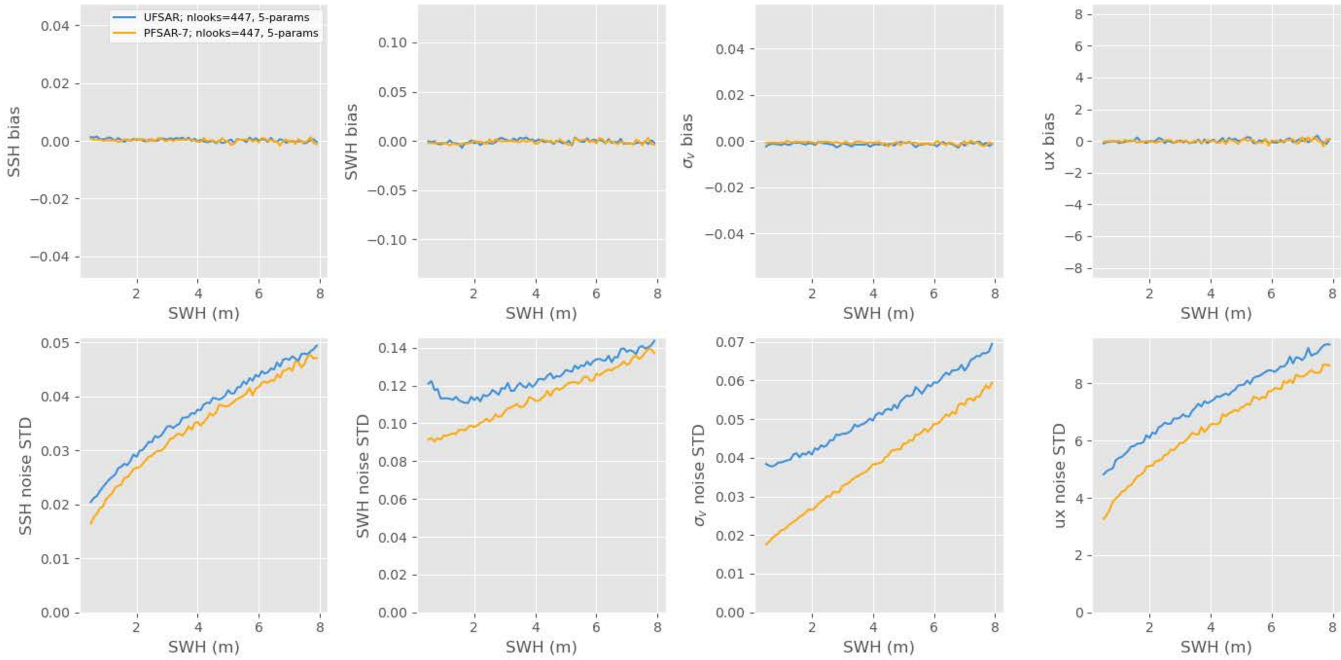

Figure 126: Results of the synthetic performance assessment of PFSAR-7 (yellow) compared to USAR (blue).

9.6. Physics-based EMB correction using wave spectra

The sea state bias (SSB) is made up of three contributions: the electromagnetic bias (EMB), the skewness bias and the processing bias. Today, empirically derived SSB models are commonly used to estimate a net SSB correction. Theoretical models have been developed but they typically involve parameters that cannot be retrieved from altimeter measurements.

CFOSAT mission, which carries SWIM instrument, provides, for the first time, the ability to retrieve surface parameters relevant to SSB models. Amongst the EMB models available in the literature, the one derived by Millet et al. in 2006 [23] provides a relatively simple and tractable relationship involving parameters that can be retrieved from SWIM spectra. In the present study, Millet's model was further developed to (i) match the Ku band of CFOSAT mission, (ii) apply the model to SWIM spectra extended beyond SWIM's wavenumber range using Elfouhaily theoretical spectra (see Figure 127 (a)), (iii) account for a "dynamic" WS-dependent two-scale separation wavenumber k_{sep}, and (iv) account for WS-dependent (rather than constant) γ and τ short-wave-related parameter values.

The upgraded EMB model shows improved performance compared with the 2D Jason-3 GDR-F table applied to CFOSAT nadir (SWH, WS): it reduces (on average) the variance at SSH cross-over points and in direct SLA measurements by 2.7 cm^2 compared with the 2D correction (see Figure 127 (b)). These unprecedented results pave the way for the use of wave spectra in deriving model-based EMB corrections and offer perspectives in reconciling empirical and theoretical SSB studies.

In the future, we could envisage using Sentinel-6 wave spectra [24] to describe the swell part of wave spectra, while Elfouhaily theoretical spectra would cover the wind sea part. We could then compute again the EMB model parameters retrieved from such spectra, apply to Sentinel-6 data, and compare results with the present study.

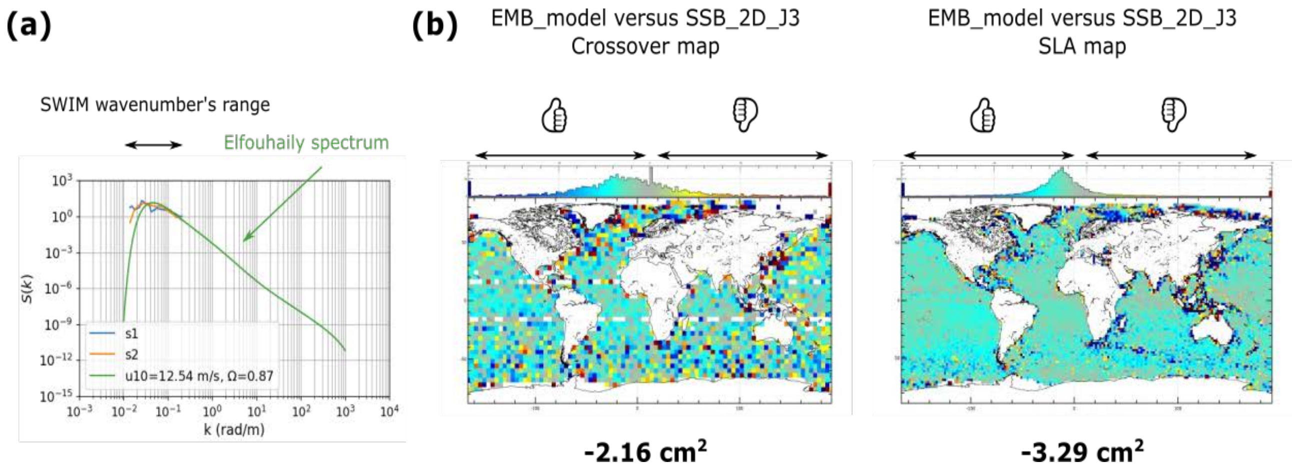

Figure 127: (a) Example of SWIM side 1 (s1) and side 2 (s2) wave spectra extended using a theoretical Elfouhaily spectrum. (b) Comparison of the physics-based EMB correction against 2D Jason-3 GDR-F table applied to CFOSAT nadir (SWH, WS): left on crossover dataset, right on SLA dataset.

9.7. Doppler ambiguities

When the altimeter pulse repetition frequency is not high enough to sample the Doppler bandwidth with respect to the Nyquist criterion, Doppler ambiguities appear, causing energy from out-of-band frequencies to fold back onto the edges of the Doppler spectrum and thereby degrade retracking performance. To mitigate this, Doppler ambiguity masking can be applied to suppress the ambiguous signals. This strategy is used in the Sentinel-6 operational processing chain, though it inevitably removes part of useful signal. Previous work showed that the two processing configurations (i.e. with and without masking) yield globally comparable performance over the open ocean. However, that analysis did not specifically investigate which sea surface conditions or geographic areas might locally introduce retracking errors when Doppler ambiguities are left unmasked.

To address this question, we compared the two processing configurations over atypical ocean areas (such as internal solitary waves, long-period swell, or coastal zones) where strong spatial variations in backscatter can induce asymmetries between the forward and backward Doppler ambiguity returns. Geometrically, these ambiguities correspond to signals originating several kilometres away from the focused surface point. When inhomogeneities occur over such distances, the power contained in the two folded Doppler-range samples can differ, as illustrated in Figure 128, which may in turn degrade retracking accuracy. These differences are observed only in a limited number of areas, for which applying Doppler ambiguities masking is recommended. Interestingly, the inconsistencies detected between forward/backward Doppler ambiguities could also be exploited to identify large-scale sea surface heterogeneities along the satellite track.

9.8. Spectral swell characterization

The modulation of CryoSat-2, Sentinel-3, and Sentinel-6 Fully-Focused SAR radargrams can be related to the swell spectral properties. Long swell wavelengths (> 200 m) can be reliably retrieved in a favorable sea state, although wave-direction estimates remain affected by left-right and 180° ambiguities.

By sublooking the FF-SAR illumination time, we can correlate sea states separated by ~ 1 s with cross-spectra, observed with the same instrument, with a slightly different along-track look angle. This technique gives us improved signal-to-noise ratio, as well as information about the swell direction of propagation

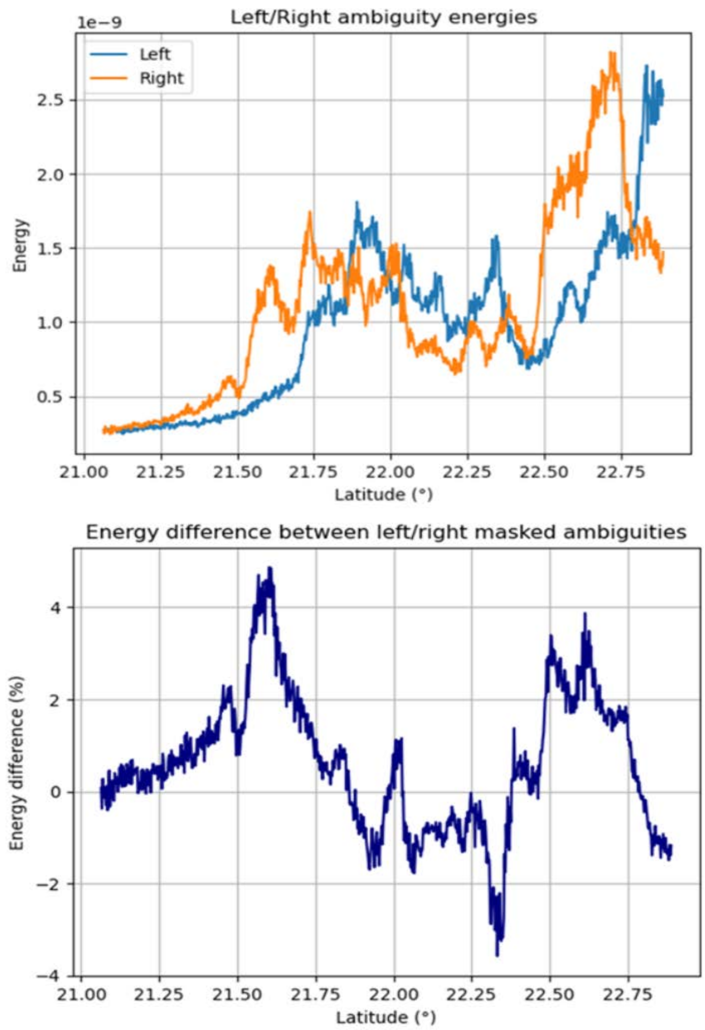

Figure 128: Top : Energy in left/right Doppler ambiguities in the DDM. Bottom : Energy difference between the left and right ambiguities, normalized by the energy of the masked stack.

through the imaginary part, and disambiguates the 180° uncertainty (see Figure 129).

On the other hand, using the Sentinel-6 tandem phase one can correlate sea states separated by ~ 30 s. This time difference, typically exceeding a full swell period, allows for a more accurate estimation of swell wavelength and significantly reduces speckle noise, as has been demonstrated using power density spectra of the Sea Level Anomaly during the Sentinel-3 tandem phase. The tandem configuration also opens sensitivity to longer-scale wave phenomena, such as wave groups. Additionally, the ~ 800 m cross-track offset between the platforms theoretically disambiguates the left-right symmetry inherent to nadir altimetry.

9.9. 2D retracking of SAR altimeter data

In the operational chain, SAR retracking models still rely on a “frozen sea” assumption that neglects the impact of ocean dynamics on Doppler frequencies, introducing biases in the estimated sea-state parameters. Recent advances have introduced more complete formalisms that incorporate both the standard deviation of the waves’ vertical velocity and the along-track component of the Geophysical Doppler vector. Estimating these quantities requires retracking the full two-dimensional unfocused SAR Delay–Doppler maps (stacks), rather than summing Doppler beams and retracking a one-dimensional multilooked waveform as currently

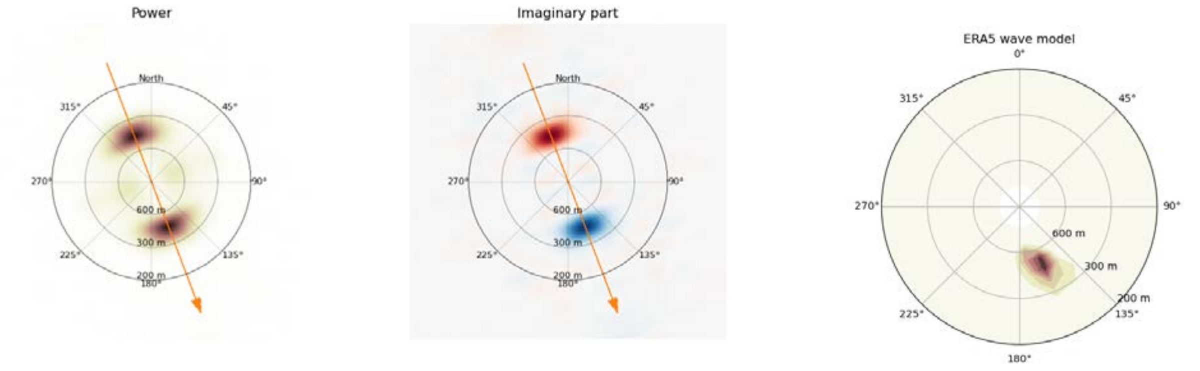

Figure 129: Wave spectrum derived from S6-MF FF-SAR data in the Atlantic ocean (2022-03-13T10:38). From left to right: power, imaginary part, ERA5 model. The spectrum derives from S6-MF data matches very well the prediction from the ERA5 wave model. The left-right ambiguity is irrelevant when the waves propagate along-track.

done. The modifications to the processing are minimal in terms of implementation and computational time, as the full model stack is already computed prior to summation in current L2 processing.

Reprocessing a year of data, we demonstrated that the new product is consistent with conventional altimetry, both in sea surface height (SSH) and significant wave height (SWH) as can be seen in Figure 130, while providing reduced noise and enhanced along-track resolution. The main improvements are the following:

- Characterization of azimuth smearing due to vertical wave motion, enabling retrieval of the standard deviation of vertical wave velocity (see Figure 130). This quantity relates to the mean zero up-crossing wave period and offers new insights into surface wave dynamics. Its inclusion in the SAR model corrects the SWH bias caused by the sea-state. The velocity variance estimate shows good agreement with the ERA5 wave model, without relying on look up tables or external corrections.

- Estimation of the along-track projection of the geophysical Doppler vector, related to wind direction and magnitude and/or total or part of the surface current (such as the Stokes drift). Including this term removes the wind-dependent SSH bias that impacts SAR altimetry (see Figures 62 and 63), particularly between ascending and descending passes, without altering large-scale spectral content.

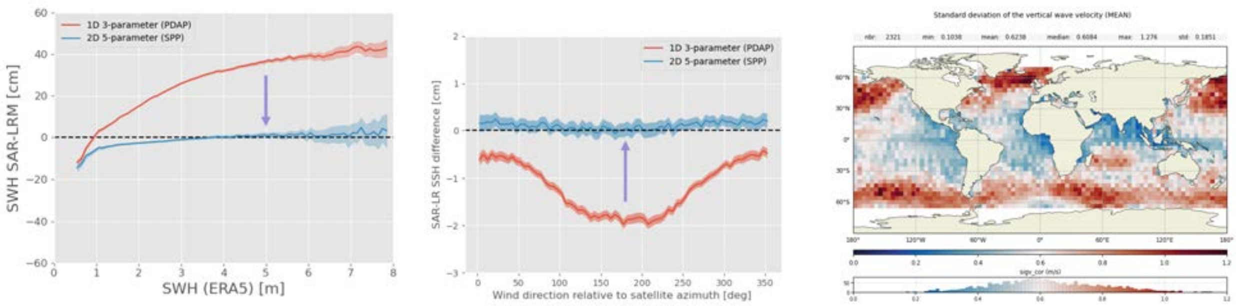

Figure 130: Output of the 2D 5-parameter retracker (cycle 45): from left to right, reduction of the SWH and SSH bias versus LRM compared to the current 1D 3-parameter retracker, and derivation of the standard deviation of the wave vertical velocity.

9.10. Wave-induced Small Scale Variability study

The nadir SAR altimetry signals suffer from the impact of long waves. However, their impact is often overshadowed or distorted by the left-right ambiguity, the poor cross-track resolution, and the wind sea. The latter inherently limits the achievable cross-track and azimuth resolutions through wave-field dependent cut-offs [see 31, 32]. Therefore, a good agreement between ocean wave spectra and projected altimetry signal spectra (see above) is only observed in the minority of cases.

We therefore propose an alternative theoretical framework that describes the wave-induced small scale variability in the altimetry signal through range-gate-dependent perturbations (statistical fluctuations) to the mean and standard deviation of the scattering facet surface elevation distribution $p_z(r)$—which is a slightly more general approach as taken for conventional altimetry in [33]. The new approach appears suitable to parametrize the statistics of SAR altimetry signal perturbations—see Figures 131 & 132— arising from resolved, partially-resolved, as well as unresolved waves, when the speckle is accounted for as in [26]. As the wave imprints in SAR waveforms primarily act as increased noise, a combined model of both speckle and wave-induced SSV autocovariance such as presented in Fig. 132 is crucial to generalize the optimal estimator [see 34, & previous section] to SAR altimetry.

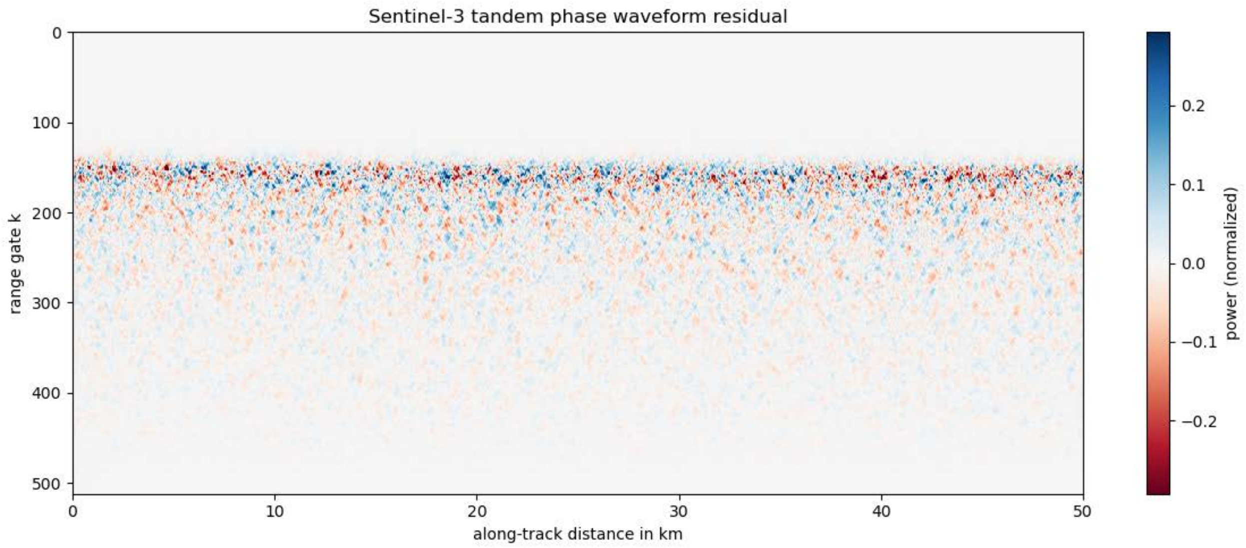

Figure 131: Sentinel-3 tandem phase waveform residuals, which should almost exclusively consist of differences in speckle and changes in the wave field, due to the 30 s time delay between the observations.

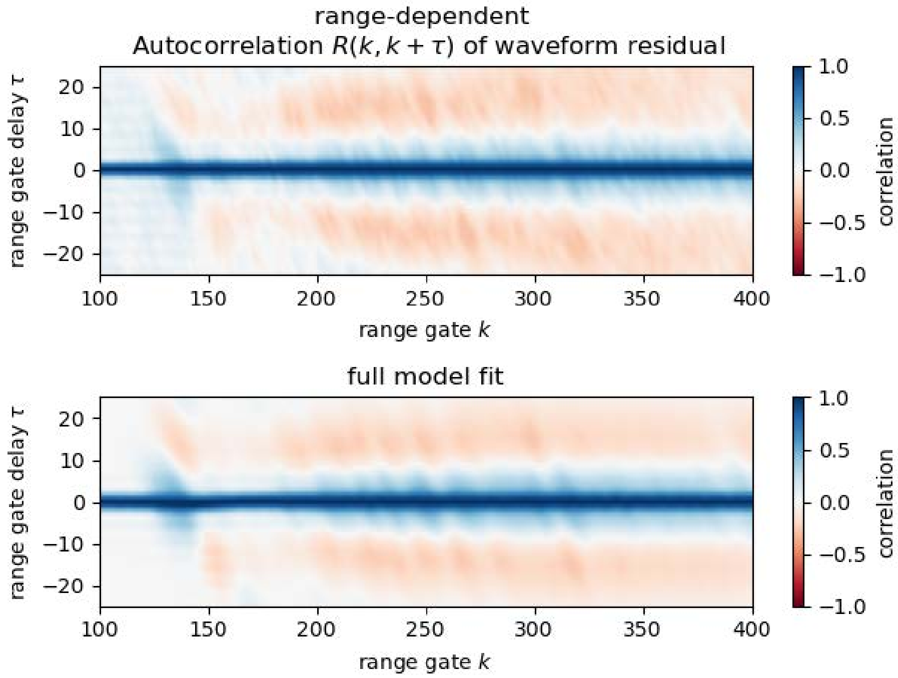

Figure 132: Empirical range autocorrelation of the waveform residual in Fig. 131 (top) and the fit of the analytical model including both speckle and SSV contributions (bottom).

10 Conclusions

Sentinel-6 MF was launched on November 21th, 2020 and reaches its operational orbit on December 17th 2020. From this date until April 7th, 2022, Jason-3 and Sentinel-6 MF were flying in tandem formation, with only 30 seconds delay, before Jason-3 was moved to the interleaved orbit. On April 7th 2022, Sentinel-6 MF became the reference altimetry mission, taking on the responsibility to extend the global sea level record on the reference ground track started in 1992 by Topex/Poseidon and continued by the Jason's series.

The main points of the present performance assessment are summarized below:

- Ocean data availability is excellent with a percentage above 99% in both LR and HR modes.
- Data quality is also very good with 6.4 %, 6.3 %, 4.8 % and 4.9 % of measurements not consistent with altimeter and radiometer parameters threshold criterion in LR MLE4, LR NR, HR SAMOSA and HR NR respectively.
- HR SAMOSA measurements were improved thanks to the correction of ocean vertical velocity applied with the PB G01 update. The absence of skewness parameter in the SAMOSA processing does not allow to properly compare HR range derived parameter to LR or HR NR or Jason-3 data.
- At crossovers, Sentinel-6 MF shows very good performance with errors on SSH differences of 3.3 cm for LR retrackers and 3.2 cm for HR retrackers. Jason-3 standard deviation is similar to HR.
- At crossovers between Sentinel-6 MF and Jason-3, SSH performance presents excellent results with an SLA bias of about -0.07 cm, -0.03 cm, 1.34 cm and -0.32 cm for LR MLE4, LR NR, HR SAMOSA and HR NR respectively.
- Improvements thanks to PB G01 update:
  - Significantly better consistency and lower correlation to SWH between retrackers, thanks to the LUTs update in LR MLE4, the correction of the small waves anomaly in LR NR and the 20Hz VWM application on HR SAMOSA and HR NR. This last correction also signicantly improves the 1Hz SWH noise.

Finally, several recommendations can be made to further refine Sentinel-6 MF data consistency and stability :

- Compute an ice flag from Sentinel-6 MF AMR and altimeter parameters as done for Jason-3.
- Implement a skewness correction in the HR SAMOSA processing.
- Implement a P2P effect correction derived from S6B commissioning data.
- Compute WVM correction from Sentinel-6 MF parameters instead of using model.
- Compute dedicated SSB parametrizations for each retracker, especially SAMOSA.

11 References

References

[1] Sentinel-6A user handbook available at https://user.eumetsat.int/resources/user-guides/sentinel-6-altimetry-level-2-data-guide

[2] Jason-3 product handbook available at https://www.aviso.altimetry.fr/fileadmin/documents/data/tools/hdbk_j3.pdf

[3] Sentinel-6 ALT Level 2 Product Generation Specification available at https://user.eumetsat.int/s3/eup-strapi-media/Sentinel_6_Jason_CS_ALT_Level_2_Product_Generation_Specification_L2_ALT_PGS_V5_09f3679da5.pdf

[4] Product notice for Sentinel-6 MF Processing Baseline F08 available at : https://www.eumetsat.int/media/50743

[5] Sentinel-6 MF F08 Reprocessing Calval Assessment available at : https://user.eumetsat.int/s3/eup-strapi-media/S6_A_F08_Reprocessing_Calval_Assessment_v2_1_c6273b0e23.pdf

[6] Product notice for Sentinel-6 MF Processing Baseline F09 available at : https://user.eumetsat.int/s3/eup-strapi-media/Copernicus_Sentinel_6_Michael_Freilich_Product_Notice_Altimetry_V9_a5ee70077d.pdf

[7] Product notice for Sentinel-6 MF Processing Baseline G01 available at : https://user.eumetsat.int/s3/eup-strapi-media/Copernicus_Sentinel_6_Michael_Freilich_Product_Notice_Altimetry_v10_B_68a7c5ecb4.pdf

[8] Sentinel-6 MF G01 Reprocessing Calval Assessment available at : https://user.eumetsat.int/s3/ope-eup-strapi-media/Sentinel_6_MF_G01_Reprocessing_Calval_Assessment_7e75a56d93.pdf

[9] 2024 Sentinel-6MF annual validation report available at : https://www.aviso.altimetry.fr/fileadmin/documents/calval/validation_report/S6A/S6MF_2024_annual_report_v1_3.pdf

[10] 2023 Jason-3 annual validation report available at :

[11] Brown G.S., "The average impulse response of a rough surface and its application", IEEE Transactions on Antenna and Propagation, Vol. AP 25, N1, pp. 67-74, Jan. 1977.

[12] Thibaut, P. O.Z. Zanif´e, J.P. Dumont, J. Dorandeu, N. Picot, and P. Vincent, 2002. Data editing: The MQE criterion. Paper presented at the Jason-1 and TOPEX/Poseidon Science Working Team Meeting, NewOrleans (USA), 21-23 October.

[13] Raynal et al, Lessons learned from Sentinel SARM missions in preparation of Jason-CS. Oral Presentation, Ocean Surface Topography Science Team Meeting 2019, Chicago

[14] Dinardo S. poster, Sentinel 6 MF Poseidon 4 main results from the first year of mission from the S6PP LRM and UF SAR chain , OSTST 2022

[15] Dinardo S. et al., Sentinel6-MF Poseidon-4: Last Evolutions and Findings from the CLS-CNES S6PP, 4TH S6VT 2022

[16] Boy F., Callahan P., Desjonqueres J. D., Egido A., Smith W. H. F., Fornari M., Martin-Puig C. (2022): High-Level Instrument Processing Summary for Jason 3 and Sentinel-6 Michael Freilich Tandem Phase. Oral Presentation, Ocean Surface Topography Science Team Meeting(Virtual). Available on-line at https://ostst.aviso.altimetry.fr/fileadmin/user_upload/OSTST2022/presentations_mars2022/01-Jason3andSentinel-6MFTandemPhaseInstrumentProcessing_20220321.pdf

[17] Emeline Cadier, Bastien Courcol, Pierre Prandi, Victor Quet, Thomas Moreau, Claire Maraldi, François Bignalet-Cazalet, Salvatore Dinardo, Cristina Martin-Puig, Craig Donlon : Assessment of Sentinel-6MF low resolution numerical retracker over ocean: continuity on reference orbit and improvements, Advances in Space Research, Volume 75, Issue 1, 1 January 2025, Pages 30-52

[18] Collard, F., 2005. "Algorithmes de vent et période moyenne des vagues jason à base de réseaux de neurones." Boost Technologies, BO-021-CLS-0407-RF, 33 pp.

[19] Nencioli Francesco, Roinard Hélène, Bignalet-Cazalet Francois. 2021. Filtering ionospheric correction from altimetry dual-frequencies solutions. DOI 10.24400/527896/a02- 2021.001. Available at https://www.aviso.altimetry.fr/fileadmin/documents/data/tools/NT-Nencioli_FilteredIonosphericCorrection.pdf

[20] Obligis, E., L. Eymard, M. Ablain, B. Picard, J.F. Legeais, Y. Faugere and N. Picot, 2010. The wet tropospheric correction for altimetry missions: A mean sea level issue. Oral presentation at OSTST meeting, Lisbon, Portugal.

[21] Guérou, A., Meyssignac, B., Prandi, P., Ablain, M., Ribes, A., and Bignalet-Cazalet, F.: Current observed global mean sea level rise and acceleration estimated from satellite altimetry and the associated uncertainty, EGUsphere [preprint], https://doi.org/10.5194/egusphere-2022-330, 2022.

[22] Laloue, A., Schaeffer, P., Pujol, M.-I., Veillard, P., Andersen, O., Sandwell, D., Delepoulle, A., Dibarboure, G and Faugère, Y.: Merging Recent Mean Sea Surface Into a 2023 Hybrid Model (From Scripps, DTU, CLS, and CNES), https://agupubs.onlinelibrary.wiley.com/doi/full/10.1029/2024EA003836, 2025.

[23] Millet, F. W., Warnick, K. F., Nagel, J. R., and Arnold, D. V.: Physical Optics-Based Electromagnetic Bias Theory With Surface Height-Slope Cross-Correlation and Hydrodynamic Modulation, IEEE Transactions on Geoscience and Remote Sensing, 44(6), https://doi.org/10.1109/TGRS.2005.863852, 2006.

[24] Altiparmaki, O., Kleinherenbrink, M., Naeije, M., Slobbe, C., and Visser, P.: SAR Altimetry Data as a New Source for Swell Monitoring, Geophysical Research Letters, 49(7), https://doi.org/10.1029/2021GL096224, 2022.

[25] Ehlers, F., Slobbe, D.C., Verlaan, M., Kleinherenbrink, M., A noise autocovariance model for SAR altimeter measurements with implications for optimal sampling, Advances in Space Research, Volume 71, Issue 10, 2023, Pages 3951-3967, https://doi.org/10.1016/j.asr.2023.02.043.

[26] Ehlers, F., Rodet, L., Alves, M., Moreau, T., Slobbe, D.C., Verlaan, M., Maraldi, C., Borde, F., 2025. Modeling the SAR Altimetry Noise: From High Posting Rates to Precision Gains. Advances in Space Research, in Press. https://doi.org/10.1016/j.asr.2025.11.103

[27] Egido, A., Dinardo, S., Ray, C., The case for increasing the posting rate in delay/Doppler altimeters, Advances in Space Research, Volume 68, Issue 2, 2021, Pages 930-936, https://doi.org/10.1016/j.asr.2020.03.014.

[28] Buchhaupt, Christopher, Luciana Fenoglio, Matthias Becker, and Jürgen Kusche. “Impact of Vertical Water Particle Motions on Focused SAR Altimetry.” Advances in Space Research, 25 Years of Progress in Radar Altimetry, 68, no. 2 (July 15, 2021): 853–74. https://doi.org/10.1016/j.asr.2020.07.015.

[29] Buchhaupt, C., Egido, A., Smith, W., Fenoglio, L. (2022). Conditional Sea Surface Statistics and Their Impact on Geophysical Sea Surface Parameters Retrieved From SAR Altimetry Signals, Adv. Space Research, https://doi.org/10.1016/j.asr.2022.12.034.

[30] Buchhaupt C., Fenoglio-Marc L., Dinardo S., Scharroo R., Becker M. (2018): A fast convolution-based waveform model for conventional and unfocused SAR altimetry. Advances in Space Research, Volume 62, Issue 6, 2018, Pages 1445-1463, ISSN 0273-1177. https://doi.org/10.1016/j.asr.2017.11.039.

[31] L. Marie et al., On the Effects of Ocean Surface Motion on Delay-Doppler Altimetry, Remote Sensing, Volume 62, 2024, Pages 1-25. https://doi.org/10.1109/TGRS.2024.3387667.

[32] M. Kleinherenbrink et al., Cross-Spectral Analysis of SAR Altimetry Waveform Tails, Remote Sensing, Volume 62, 2024. https://doi.org/10.1109/TGRS.2024.3402390.

[33] De Carlo, M., Ardhuin, F., Ollivier, A., Nigou, A., 2023. Wave Groups and Small Scale Variability of Wave Heights Observed by Altimeters. Journal of Geophysical Research: Oceans 128, e2023JC019740. https://doi.org/10.1029/2023JC019740.

[34] Mangilli, A. et al, 2025. Optimal Estimation of the Geophysical Parameters Over Ocean for the Sentinel-6MF Reference Mission. IEEE Transactions on Geoscience and Remote Sensing, vol. 63, pp. 1-25, 2025, Art no. 5108925,https://doi.org/10.1109/TGRS.2025.3625270.

[35] Phalippou, L., Demeestere, F., 2011. Optimal retracking of SAR altimeter echoes over Open Ocean: Theory versus results for SIRAL2 data. OSTST Meeting 2011, San Diego, California, United States, Oct. 19-21..

[36] Moreau,T. et al., 2021. High-performance altimeter Doppler processing for measuring sea level height under varying sea state conditions. Advances in Space Research, Volume 67(6), 1870-1886. .

[37] Buchhaupt, C. et al., 2023. Towards the Mitigation of Discrepancies in Sea Surface Parameters estimated from Low- and High-Resolution Satellite Altimetry. Remote Sensing, 15, 4206..